

TOWARDS WELL-DEFINED GOLD NANOMATERIALS VIA DIAFILTRATION
AND APTAMER MEDIATED SYNTHESIS

by

SCOTT FRANCIS SWEENEY

A DISSERTATION

Presented to the Department of Chemistry
and the Graduate School of the University of Oregon
in partial fulfillment of the requirements
for the degree of
Doctor of Philosophy

December 2007

“Towards Well-Defined Gold Nanomaterials via Diafiltration and Aptamer Mediated Synthesis,” a dissertation prepared by Scott F. Sweeney in partial fulfillment of the requirements for the Doctor of Philosophy degree in the Department of Chemistry. This dissertation has been approved and accepted by:

Dr. Mark C. Lonerger, Chair of the Examining Committee

11/26/07
Date

Committee in Charge: Dr. Mark C. Lonerger, Chair
 Dr. James E. Hutchison, Advisor
 Dr. Michael M. Haley
 Dr. J. Andrew Berglund
 Dr. Stephen D. Kevan

Accepted by:

Dean of the Graduate School

An Abstract of the Dissertation of
Scott Francis Sweeney for the degree of Doctor of Philosophy
in the Department of Chemistry to be taken December 2007
Title: TOWARDS WELL-DEFINED GOLD NANOMATERIALS VIA
DIAFILTRATION AND APTAMER MEDIATED SYNTHESIS

Approved: _____
Prof. James E. Hutchison

Gold nanoparticles have garnered recent attention due to their intriguing size- and shape-dependent properties. Routine access to well-defined gold nanoparticle samples in terms of core diameter, shape, peripheral functionality and purity is required in order to carry out fundamental studies of their properties and to utilize these properties in future applications. For this reason, the development of methods for preparing well-defined gold nanoparticle samples remains an area of active research in materials science. In this dissertation, two methods, diafiltration and aptamer mediated synthesis, are explored as possible routes towards well-defined gold nanoparticle samples.

It is shown that diafiltration has considerable potential for the efficient and convenient purification and size separation of water-soluble nanoparticles. The suitability of diafiltration for (i) the purification of water-soluble gold nanoparticles, (ii) the separation of a bimodal distribution of nanoparticles into fractions, (iii) the fractionation

of a polydisperse sample and (iv) the isolation of trimers from monomers and aggregates is studied. NMR, thermogravimetric analysis (TGA), and X-ray photoelectron spectroscopy (XPS) measurements demonstrate that diafiltration produces highly pure nanoparticles. UV-visible spectroscopic and transmission electron microscopic analyses show that diafiltration offers the ability to separate nanoparticles of disparate core size, including linked nanoparticles. These results demonstrate the applicability of diafiltration for the rapid and green preparation of high-purity gold nanoparticle samples and the size separation of heterogeneous nanoparticle samples.

In the second half of the dissertation, the identification of materials specific aptamers and their use to synthesize shaped gold nanoparticles is explored. The use of in vitro selection for identifying materials specific peptide and oligonucleotide aptamers is reviewed, outlining the specific requirements of in vitro selection for materials and the ways in which the field can be advanced. A promising new technique, in vitro selection on surfaces (ISOS), is developed and the discovery using ISOS of RNA aptamers that bind to evaporated gold is discussed. Analysis of the isolated gold binding RNA aptamers indicates that they are highly structured with single-stranded polyadenosine binding motifs. These aptamers, and similarly isolated peptide aptamers, are briefly explored for their ability to synthesize gold nanoparticles.

This dissertation contains both previously published and unpublished co-authored material.

CURRICULUM VITAE

NAME OF AUTHOR: Scott Francis Sweeney

PLACE OF BIRTH: Lowell, Massachusetts

DATE OF BIRTH: October 2, 1977

GRADUATE AND UNDERGRADUATE SCHOOLS ATTENDED:

University of Oregon, Eugene, OR
Univeristy of Southern Maine, Portland, ME
Beloit College

DEGREES AWARDED:

Doctor of Philosophy in Chemistry, 2007, University of Oregon
Bachelor of Arts with Honors in Chemistry, 2000, University of Southern Maine

AREAS OF SPECIAL INTEREST:

Materials and nanomaterials, surface science, green chemistry, microreactor design, bioinspired synthesis

PROFESSIONAL EXPERIENCE:

Graduate Research Assistant, Department of Chemistry, University of Oregon,
Eugene, OR, 2002-2007

Research Intern, Air Force Research Labs, Wright-Patterson AFB, Dayton, OH,
2006

Graduate Teaching Assistant, Department of Chemistry, University of Oregon,
Eugene, OR, 2002-2003

Research Assistant, Cabot Corporation, Inkjet Colorants Division, Billerica, MA
2000-2002

Undergraduate Research Assistant, Department of Chemistry, University of
Southern Maine, Portland, ME, 1998-2000

Undergraduate Teaching Assistant, Department of Chemistry, University of
Southern Maine, Portland, ME, 1998-1999

GRANTS, AWARDS AND HONORS:

Chemistry Department Senior Service Award, University of Southern Maine,
2000

PUBLICATIONS:

Sweeney, S. F.; Woehrle, G. H.; Hutchison, J. E. Rapid purification and size
separation of gold nanoparticles via diafiltration. *J. Am. Chem. Soc.* **2006**, *128*,
(10), 3190-3197.

ACKNOWLEDGMENTS

Graduate school is a wild and bumpy ride without a seatbelt, but there were a few people who made it a little smoother. Dr. Gerd Woehrle, provided me with lots of advice. His help during my first year made my work possible, and a subsequent visit with him in Germany was great. Others in the Hutchison Lab, including Dr. Greg Kearns, Mike Jespersen, Lallie McKenzie, Dr. Bevin Parks, Jenny Dahl, and my undergrad Carly Corrado all gave me good advice, or assisted me in some way at some point. To all of you, thanks! Outside of the Hutchison Lab, there was Dr. Nathaniel Szymczak who helped a lot during my advancement to candidacy. Thanks to Kurt Langworthy for TEM and SEM assistance and Stephen Golledge for XPS assistance. Dr. Sasha D. T. Kruger, who taught me that the synthesis of CdSe nanoparticles was not very much fun. Matthew O'Conner assisted in getting some ligands synthesized. And finally, and most importantly, Amy Mahady from the Berglund lab who worked with me so much over the past couple of years trying to get ISOS to work. I don't think I'd be getting my Ph.D. if it weren't for her help.

Many thanks to my thesis committee: Professors Lonergan, Berglund, Kevan and Haley – for asking me tough questions and giving me valuable advice. Thank you to Jim Hutchison, my esteemed advisor, for being skeptical about everything I proposed using my “creative problem-solving,” being supportive when it all worked out, giving me the opportunity to address the many challenges of nanotech research and for giving me the tools to be an independent scientist.

Thank you to Rajesh Naik and the rest of the Naik laboratory and the Air Force Research labs for hosting me as an intern and giving me the opportunity to further develop the ISOS technique with phage display.

I'd further like to thank Matt O'Conner, Benjamin Schmid and Dr. Dave Walker for keeping me sane and getting me into a lot of trouble. Y'all have been great friends. Further thanks to a lot of other people, too numerous to name individually, whom I have skied, biked, hiked, backpacked, kited, walked, eaten, snowshoed, sledged or snowforted with in the last five years. Let's keep it up!

Finally to my parents, grandparents and family for being so proud and encouraging me. And Emily, who has seen me through the last few years and many more to come. Thank you.

Dedicated to Mount Martha for teaching me never to give up and to my grandfather for watching over me and keeping me in line.

TABLE OF CONTENTS

Chapter	Page
I. INTRODUCTION TO WELL-DEFINED NANOMATERIALS	1
Introduction	1
Well-Defined Nanomaterials	5
Well-Defined Gold Nanomaterials	7
Electronic Structure and Properties of Gold Nanoparticles	9
Optical Properties of Gold Nanoparticles	13
Gold Nanoparticle Preparation	16
Non-Specific Ligands	19
Phosphine-Stabilized Nanoparticles	21
Thiol-Stabilized Nanoparticles	23
Nonspherical Gold Nanoparticles	24
Nanoparticle Functionalization	28
Post-Synthetic Modification	28
Ligand Exchange	29
Purification	33
Characterization	35
¹ H-NMR	36
TGA	37
XPS	38
UV-Vis	38
TEM	39
Overview of Dissertation	41
II. PURIFICATION AND SIZE SEPARATION OF WATER-SOLUBLE GOLD NANOPARTICLES VIA DIAFILTRATION	44
Introduction	44
Experimental Section	48
Results and Discussion.....	53
Traditional Methods of Purification	54

Chapter	Page
Diafiltration as an Approach to Nanoparticle Purification	55
Diafiltration vs. Conventional Methods for Nanoparticle Purification ...	56
Size Separation of 1.5 and 3-nm Nanoparticles	59
Fractionation of Nanoparticles	62
Conclusion	64
Bridge	66
III. ISOLATION OF LINKED GOLD NANOPARTICLES VIA DIAFILTRATION	67
Introduction	67
Experimental Section	70
Results and Discussion	76
Linker Synthesis	77
Linked Nanoparticle Preparation	79
Ligand Exchange and Diafiltration	81
Ligand Exchange / Linking Dynamics	82
Conclusion	85
Bridge	86
IV. ADVANCING IN VITRO SELECTION FOR MATERIALS APPLICATIONS	87
Introduction	87
Introduction to In Vitro Selection	90
In Vitro Selection For Materials	94
Elements of In Vitro Selection	97
The Library	97
The Target	98
Incubation	100
Washes / Elution	102
Amplification	103
Characterization	106
Peptide / Phage Display	108

Chapter	Page
Introduction to Phage Display	108
Introduction to Bacteriophages	109
Peptide / Phage Display for Materials	112
Peptide / Phage Display Wrap-Up	118
SELEX	120
Introduction to SELEX	120
SELEX for Materials	123
Comparison of SELEX to Peptide Display	127
Summary and Paths for Advancement.....	127
Bridge.....	133
V. IDENTIFICATION OF GOLD BINDING RNA APTAMERS VIA IN VITRO SELECTION ON SURFACES (ISOS)	134
Introduction	134
In Vitro Selection on Surfaces	137
Sequence and Structural Analysis	140
Gold Dot Assay	142
Conclusion	145
Experimental	146
Bridge	149
VI. SCREENING OF GOLD BINDING RNA AND PEPTIDE APTAMERS FOR GOLD NANOPARTICLE FORMATION	150
Introduction	150
Results and Discussion	154
RNA Mediated Gold Nanocrystal Synthesis	154
Peptide Mediated Gold Nanocrystal Synthesis	158
Conclusions and Future Directions	160
Experimental	161
VII. CONCLUDING SUMMARY	164
Diafiltration.....	164

Chapter	Page
Aptamer Mediated Synthesis.....	166
APPENDICES	168
A. SUPPORTING INFORMATION TO CHAPTER II	168
B. SYNTHETIC SCHEMES FOR CHAPTER III	174
C. PHAGE DISPLAY USING IN VITRO SELECTION ON SURFACES	176
REFERENCES	186

LIST OF FIGURES

Figure	Page
1.1. Schematic of the Water-Gas Shift Reaction Catalyzed by Nanoparticles	3
1.2. Schematic of the Density of States of Gold From Bulk to Atomic	10
1.3. Schematic of Nanoparticle Single Electron Transistor	11
1.4. Graph of Ideal Functioning of Nanoparticle Single Electron Transistor	12
1.5. Schematic of Plasmon Resonance and UV-vis of Plasmon Resonance	14
1.6. UV-vis Spectrum of Bimodal Plasmon Resonance of Gold Nanorods	15
1.7. Illustration Describing the Important Aspects of a Gold Nanoparticle	16
1.8. Schematic of Gold Nanoparticle Growth and Graph of LaMer Theory	17
1.9. Preparation of Citrate- and TOAB-Stabilized Nanoparticles	20
1.10. Various Routes to Triphenyl Phosphine-Stabilized Nanoparticles	21
1.11. Various Routes to Thiol-Stabilized Nanoparticles	23
1.12. Hypothesized Mechanism of Nanorod Growth	25
1.13. Synthetic Steps for the Preparation of Gold Nanorods and Expected Products	27
1.14. Routes to Functionalized Gold Nanoparticles	28
1.15. Stripping Process to Remove Citrate Allowing Thiol Functionalization	30
1.16. Various Methods for Purifying Water-Soluble Gold Nanoparticles	35
1.17. Schematic of the Diafiltration Process	41
1.18. Illustration of the Synthesis of Hexagonal Material Using RNA	43
2.1. Schematic of the Diafiltration Setup Used in this Study	47
2.2. ¹ H-NMR Spectra of Ligand and Nanoparticles Au _{2.9} -Crude, Au _{2.7} -D, Au _{2.8} -ECC and Au _{2.9} -70R	57
2.3. UV-vis Spectra, TEM Histograms and TEM Images of Separated Fractions Au _{2.9} -50R and Au _{1.5} -50P	61
2.4. Diafiltration Scheme Used for Obtaining Nanoparticle Fractions	63
3.1. Illustration of Diafiltration	69

Figure	Page
3.2. Structure of the Three-Fold Linkers 1 and 2 Used in this Study.....	78
3.3. Trimer Formation Scheme	80
3.4. TEM Images of Ligand Exchanged and Diafiltered Linked Structures.....	82
3.5. Scheme for Ligand Exchange, Hypothesized Structure of Nanoparticle and Exchange Rates for Different Sites on Gold Nanoparticle.....	84
4.1. Schematic of the In Vitro Selection Cycle	92
4.2. Synthesis and Assembly Using a Bifunctional Aptamer	95
4.3. Schematic of Release of Phage Using a Protease.....	103
4.4. Probing of Sequence Space Using Mutations	105
4.5. Gold Dot Assay Used to Quantify RNA Binding to Gold.....	107
4.6. Diagram of the M13 Filamentous Bacteriophage.....	109
4.7. Chemical Structures of Modified Alanine for Phage Display.....	111
4.8. Selected, Wild-Type Phage Have Identical Specificity for GaAs (100)	114
4.9. PCR Driven Phage Display as Described by Naik	116
4.10. Example SELEX Templates.....	121
4.11. Schematic of SELEX Utilizing Post-Synthetic Modification	123
4.12. SELEX Scheme Used by Gugglioti to Identify RNA for Pd Crystals.....	124
4.13. ISOS Microreactor, ISOS Inserts and Comparison of ISOS to Traditional Selection.....	126
4.14. Use of Structure-Activity Relationships to Guide In Vitro Selectons.....	128
5.1. Prototype ISOS Microreactor, Kel-F Inserts and Selection for Traditional “3D” and ISOS “2D” Target Substrates	138
5.2. Representative Sequences, Predicted Structure and Nucleotide Content	141
5.3. Schematic of the Gold Dot Assay and Assay Results.....	143
6.1. Schematic of the In Vitro Selection Cycle.....	152
6.2. Synthetic Method for Nanocrystals Using RNA and Resultant Products.....	156
6.3. SEM Images of Gold Island Growth on Surfaces	157
6.4. Two Gold Binding Peptides Isolated Using Phage Display.....	159
6.5. TEM Image of Small Nanoparticles and a Nanocube	160
A.1. TGA for Sample Au _{2,9} -Crude.....	168

Figure	Page
A.2. TGA for Sample Au _{2.8} -ECC.....	169
A.3. TGA for Sample Au _{2.7} -D.....	170
A.4. TGA for Sample Au _{2.9} -70R.....	171
A.5. UV/vis for Retentate Fractions.....	172
A.6. TEM Images from Fractionation.....	173
B.1. Synthesis of Trifold Symmetrical TMS-ethynyl Preligands.....	174
B.2. Synthesis of Protected Thiol Capped Ligands.....	175
C.1. Schematic of the ISOS Microreactor.....	177

LIST OF TABLES

Table	Page
2.1. TGA, XPS and TEM Results for Different Purification Methods	58
4.1. Selection Criteria and Considerations	93
5.1. Summary of ISOS Conditions	139

CHAPTER I

INTRODUCTION TO WELL-DEFINED NANOMATERIALS

Introduction

At a recent invited lecture, Prof. George Whitesides of Harvard University said of technology, and nanotechnology specifically “If it is interesting science then it’s probably premature for commercialization.” What he was talking about is our ability to produce nanomaterials quickly, efficiently and reproducibly. In essence, we need to have a high degree of control over the size, shape, morphology and composition of nanomaterials using, in his words, “dumb science.”

Recent years have seen the emergence of a nanotechnological revolution, grand in its promise but minute in its constituents. Chemists and materials scientists have synthesized nanoscale building blocks from carbon, organics and polymers, transition metals and oxide materials, among others. Physicists, physical chemists and biologists have set about assessing the properties of nanomaterials, e.g. their strength, electronic, optical, and toxicological properties. The proponents of nanotechnology tout the advantages of incorporating nanoscale materials in everything from electronic and optical applications, to sensing and diagnostics, and on to therapeutics and cosmetics. What makes nanomaterials so exciting are the unique properties that arise as a material is

shrunk down to dimensions between 1 and 100 nanometers. In addition to size, the shape and surface functionality of nanomaterials play significant roles in the properties and behavior of such materials, as well as their interactions with other materials, the environment and themselves. It is clear that nanotechnology is poised to play a major, economic role in the future of our society. Our ability to transition from lab-scale, proof-of-concept research to reproducible, high-yielding production of useful or commercial nanomaterials is less clear.

As an example, carbon nanotubes have been targeted for a number of applications owing to their expected high electrical and heat conductivity, as well as their mechanical strength. In addition, the ability to easily draw upon organic chemistry for their functionalization makes them particularly attractive. Potential applications include field emission light sources,¹ conductive plastics,² fuel cell components³ and as the structural component in diverse technologies ranging from a supposed space elevator to bicycle frames. Despite their great promise, the syntheses of carbon nanotubes often lead to ill-defined products. Recent studies by NIST indicate that up to 60% of the atoms by mass in commercially available carbon nanotube samples are the metal catalysts used to synthesize them. In addition, the samples contained other allotropes of carbon including buckyballs and graphite.⁴ These recent findings have very clear implications for the future of carbon nanotube research, as the properties of nanomaterials depend very strongly on the purity and composition of the material.

Another example comes from the field of nanoparticle based heterogeneous catalysis. As the search for alternative energy sources continues, hydrogen has become a

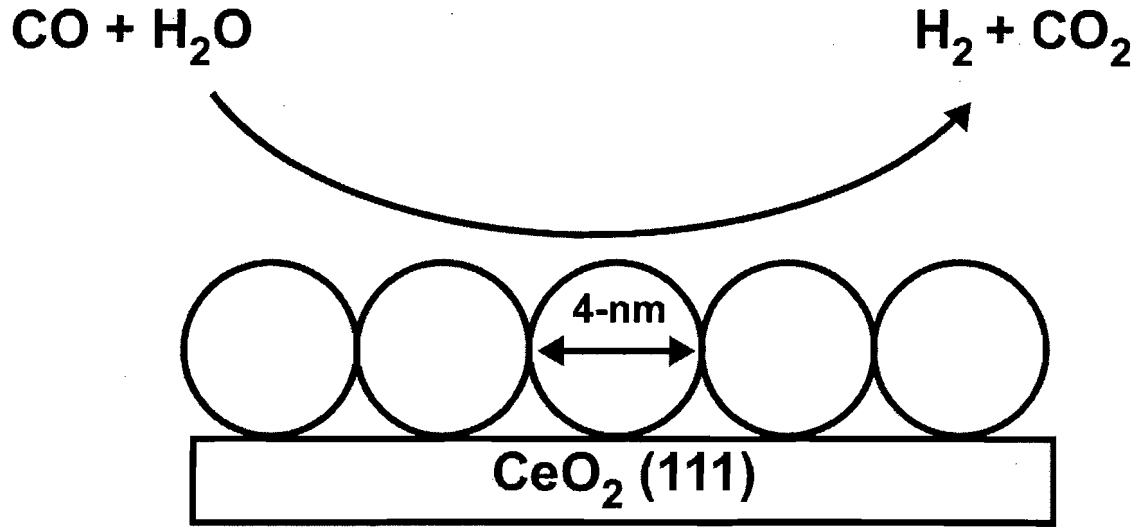


Figure 1.1. Schematic of the water-gas shift reaction catalyzed via 4-nm copper nanoparticles on a $\text{CeO}_2 (111)$ support.

promising fuel source. Unfortunately CO, which is a byproduct of hydrogen generation via steam reforming of hydrocarbons, will poison the expensive Pt catalysts that are used to split hydrogen in proton exchange membrane fuel cells.⁵ Supported copper nanoparticles (Figure 1.1) that catalyze a low temperature water gas shift reaction ($\text{CO} + \text{H}_2\text{O} \rightarrow \text{H}_2 + \text{CO}_2$) are being investigated for the removal of CO poisons, while generating an equivalent of H_2 gas.⁶ Recent evidence suggests that Cu nanoparticles < 4-nm in diameter are crucial for the efficient function of these heterogenous catalysts, and furthermore Cu (100) is the preferred active site on the nanoparticle.⁷ Clearly, synthetic methods that allow access to well-defined copper nanoparticles in terms of size and morphology will be of importance for future hydrogen fuel-cell needs.

A final example comes from the rapidly developing field of nanomedicine, wherein nanoscale materials are being developed for use as imaging agents or for drug delivery vectors. For drug delivery applications, the current paradigm is to encapsulate

therapeutics within an organic or polymeric shell such as supramolecular aggregates (liposomes),⁸ polymeric nanoparticles⁹ or dendrimers.¹⁰ Although the use of organic nanoparticles allows for easy tailoring of peripheral functionalities for greater *in vivo* stability and targeting, significant challenges remain in the preparation of well-defined organic nanomaterials in terms of size and shape. Significantly, these factors play a role in therapeutic loading, as well as in the mobility of the nanomaterial *in vivo*. Recent studies have shown that both the size and shape of organic nanomaterials play a crucial role in the bioavailability nanotherapeutics.¹¹ To this end, much work is currently focused on imparting greater control over these properties in order to gain access to well-defined materials.¹²

What these examples demonstrate is that there is no shortage of possible applications for nanomaterials and in fact the majority of research in the field of nanoscience is focused entirely upon answering the question “What do we do with nanomaterials?” An unfortunate consequence of this thinking has been the assumption that there is the capability for nanomaterials to be synthesized routinely, in high yields and with a high degree of control over the key properties that make them appealing. Except in a few cases, *we do not have this capability*. As a result, our ability to accurately and consistently measure the properties of nanomaterials have been hindered. To remedy this, there needs to be a significant shift from the traditional thinking, and more focus spent on the question “How do we prepare well-defined nanomaterials?” Within the ability to accurately control and assess the properties of nanomaterials lies the promise of

nanotechnology. Only very recently has this shift of focus to the preparation of well-defined nanomaterials occurred.

Well-Defined Nanomaterials

In a sense, the idea well-defined nanomaterials, aside from a few truly molecular species, is a contradiction due to the intrinsic variability of nanomaterials. For example, when discussing a 10-nm +/- 3-nm cadmium selenide / zinc sulfide (CdSe/ZnS) nanoparticle with a surfactant ligand shell one can *describe* the material, however truly *defining* it is difficult. Based upon TEM and spectroscopic measurements or other techniques, an average core size can be surmised. However, techniques to isolate *discrete* core sizes are unavailable and our ability to determine exactly how many atoms constitute the core remains limited to theoretical calculations based upon average core size. In addition, we have limited knowledge about the crystallinity and surface chemistry of a CdSe/ZnS nanoparticle, and batch-to-batch variations make the task even more difficult. As the luminescent properties of CdSe/ZnS nanoparticles can be affected by the crystallinity of the surface and sensitive to surface defects, knowledge about the surface or even precise control over the surface morphology can be quite useful. The ligand shell, in this case a surfactant, is another gray area - we can estimate how much surfactant is present based upon thermogravimetric analysis and by IR or NMR techniques, but we don't know precisely what is bound or how it is bound to the surface. Post-synthetic modifications, for example ligand exchange to introduce a functional group to the surface, complicate the issue as it is often unknown to what extent this exchange has occurred. An understanding of this is also crucial, since the peripheral functionality of the

nanoparticle is what mediates its interactions with the environment. Finally, the identity and quantity of impurities within the sample is often poorly understood, and the effects are often underestimated. Following synthesis and even after purification, there may be significant highly toxic byproducts, salts and free ligand that are loosely associated with the nanoparticle, and may further affect its interactions with the environment. There are now several examples where the observed properties of nanomaterials aren't due to the material itself, but due to associated impurities that result from insufficient purification.¹³ Size, shape, surface chemistry and crystallinity, ligand shell and impurity profile differences exist amongst 10-nm +/- 3-nm CdSe/ZnS nanoparticles prepared using a *single* synthetic method. Additionally, it should be noted that *several* syntheses exist for this "same" material.¹⁴ The case is the same amongst virtually all nanomaterials, and this intrinsic variability remains one of the greatest challenges in nanoscience.

Given an inability to obtain truly uniform, absolutely characterized nanomaterials, what does it mean to have a well-defined nanomaterial? To be well-defined, a nanomaterial must be sufficiently uniform in terms of size, shape, crystallinity, surface chemistry, peripheral functionality and impurity profile that the desired property or properties to be measured or utilized or intended applications for the nanomaterial are not adversely affected. In addition, the preparations of such a nanomaterial should be robust enough to minimize or eliminate batch-to-batch variability. Inherent to the idea of well-defined nanomaterials is the idea of limits or the degree to which a particular nanomaterial meets the ideal for each of the criteria outlined and can be thought of as the percent purity typically associated with chemicals. The percent purity required often will

be dictated by the application or particular property for which the material has been synthesized. Clearly, a carbon nanotube used for strengthening the frame of a racing bike will not be bound by the same limits on purity as a nanotube used for nanoelectronics applications or for the assessment of toxicological properties. Nevertheless, the promise of nanotechnology depends on our ability to fully understand the materials being used.

In the next section, a particular class of nanomaterials - gold nanoparticles - will be discussed. Electronic and optical properties, as well as the preparation and functionalization of gold nanoparticles, will be considered with regards to factors such as size, shape, ligand shell and purity.

Well-Defined Gold Nanomaterials

The optical properties of colloidal gold have long been known, and perhaps the most commonly cited and dramatic example is the Lycurgus Cup from the 4th century C.E., whose glass turns red in transmitted light and green in reflected light. The use of gold colloids for colorants and in drinkable form as a cure all continues to this day. It was Faraday in the mid-19th century who began formal investigations of the interactions between gold colloids and light¹⁵ and in the 20th century, physical descriptions, such as Mie theory¹⁶ (and later Gans theory¹⁷), were able to describe and predict the optical properties of gold nanoparticles. In addition, descriptions of very small gold colloids or *nanoparticles* as zero-dimensional quantum wells and the theory of Coulomb blockade¹⁸⁻²¹ has opened up the study of their electronic properties, and the hope that nanoparticles (gold and otherwise) may provide solutions to the limits of Moore's law. Due to their

unique size-dependent optical, electronic and catalytic properties, spherical and shaped gold nanoparticles are being investigated for a number of applications.

In the latter half of the 20th century, a number of syntheses were developed that allowed for the routine synthesis of what are now known as gold nanoparticles. Synthetic methods have been developed that allow for the preparation of nanoparticles in a range of sizes from below one nanometer to 100-nm or more. Methods have been developed for the tuning of the interactions of gold nanoparticles with their environment through functionalization or derivativization of the ligand shell that surround the gold core. Recent progress has shown that not only can the size be tuned, but also the shape, yielding diverse gold nanoparticle morphologies including rods,²² prisms,²³ cubes,²⁴ stars²⁵ and other shapes. This convenient access to gold nanomaterials has led to preliminary studies of their electronic, optical and catalytic properties and hints at their promise for applications ranging from single-electron transistors^{18,26} and optical waveguides,²⁷ to sensors²⁸ and drug delivery vehicles.²⁹

Despite recent progress, there remain significant challenges in the consistent preparation of well-defined gold nanomaterials. For example the average core diameter of as-prepared nanoparticles typically varies by 30 percent or more. In the synthesis of gold nanorods, other shapes such as prisms are also obtained. It can be difficult to separate dimers and trimers from monomers and aggregates during the preparation of linked gold-nanoparticle oligomeric structures. Methods that allow for convenient access to well-defined samples with greater control over size, shape and purity will have significant, long lasting positive impacts on the study and applications of not only gold nanoparticles,

but other nanomaterials as well. The following sections summarize: (i) the electronic and optical properties of gold nanomaterials, (ii) recent progress in the preparation of gold nanomaterials, (iii) characterization with regards to how well-defined a gold nanoparticle sample is and (iv) how diafiltration and aptamer mediated synthesis may be used to achieve the goals of well-defined gold nanomaterials.

Electronic Structure and Properties of Gold Nanoparticles

Gold nanoparticles are a unique class of materials whose size and properties lie in an area between the bulk metal and molecular species. Gold nanoparticles are comprised of tens to thousands of gold atoms and as such have an electronic structure that contains aspects of both the discrete energy levels found in atoms and molecules and the band structure seen in extended metallic materials. Shown in Figure 1.2. is a qualitative picture of the changes in electronic structure as gold is shrunk from its bulk state, through the nanoscale, and on to molecular species. In bulk, metallic gold, the electronic properties are characterized by the valence and conductance bands, comprised of an infinite number of bonding and antibonding orbitals respectively. The Fermi level lies within the conductance band, allowing the metal to conduct using only thermal energy. As the dimensions of the metal are diminished to just a few tens of nanometers, some discrete energy levels begin to show up at the band edges. Although the properties of the gold nanoparticle remain largely metallic, some molecular transitions can be observed under certain conditions (such as low T). As the size is further decreased to below ~ 2 -nm, further intercalation of discrete energy levels within the band structure can be observed. As a result, the nanoparticle loses the majority of its metallic character and there is an

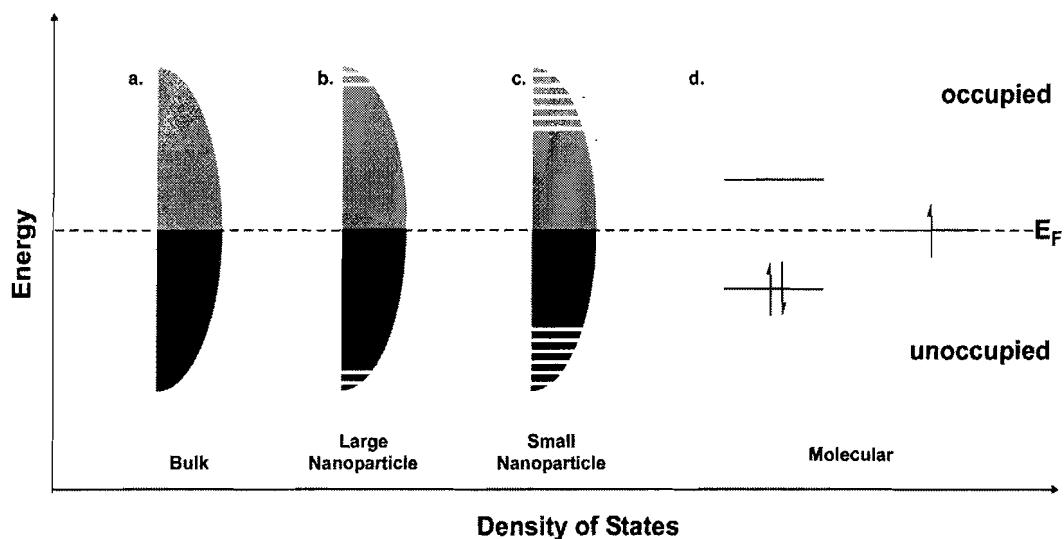


Figure 1.2. Schematic of the density of states for gold moving from the bulk state to the atomic state.

increased likelihood of observing molecular transitions under ambient conditions. Further decreases in size to small clusters and molecular species see the electronic properties become dominated by molecular transitions. These changes in the electronic structure with size underscore the need for access to well-defined gold nanoparticles with respect to the core diameter.¹⁸

Because very small gold nanoparticles (< 2-nm) do not possess the continuous band structure of large gold nanoparticles and bulk gold, they have intriguing electronic properties that make them of utility in the emerging field of nanoelectronics. Of particular interest is single electron transfer onto and off of the particle. The energy required to add an electron to a system, E_C , is ~ 0 for bulk gold. However, in small gold nanoparticles, electrons are subject to considerable confinement leading to strong Coulombic repulsion and an increase in E_C as a result. When E_C is much greater than the available thermal energy ($k_B T$), single electron transfer events may be observed. As core diameter decreases to less than 2-nm, $E_C \gg k_B T$ at room temperature.^{20,30} Aside from tuning the

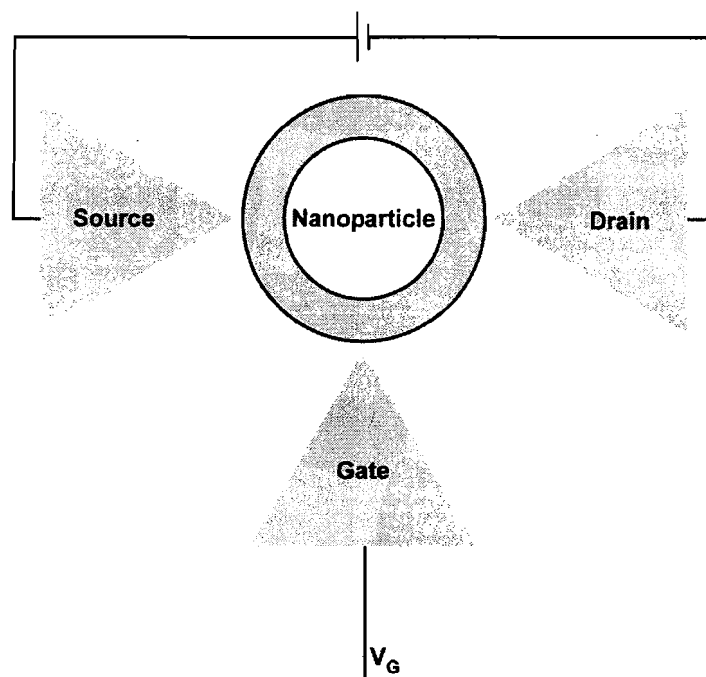


Figure 1.3. Schematic of a nanoparticle based single electron transistor, containing a gate electrode.

electronic properties via changes in core dimensions, changes in the ligand shell may also be used to tune the properties. Changes in the length of the ligand surrounding the core, which acts as a tunnel barrier, can affect the single electron transfer. Brust³¹ and Murray³² have both shown that changes in interparticle spacing will affect the electron transfer properties between adjacent nanoparticles.

One interesting application that has been developed around the electronic properties of small gold nanoparticles is the single electron transistor (SET) (Figure 1.3).^{18,26,32} If an electron tunnels onto a gold nanoparticle from the source, the potential of the nanoparticle is increased by e/C , where C is the capacitance of that particle. This is due to the considerable Coulombic repulsion felt by the electron as a result of being confined on the nanoparticle.^{21,33} In order for electrons to tunnel between the source and the drain

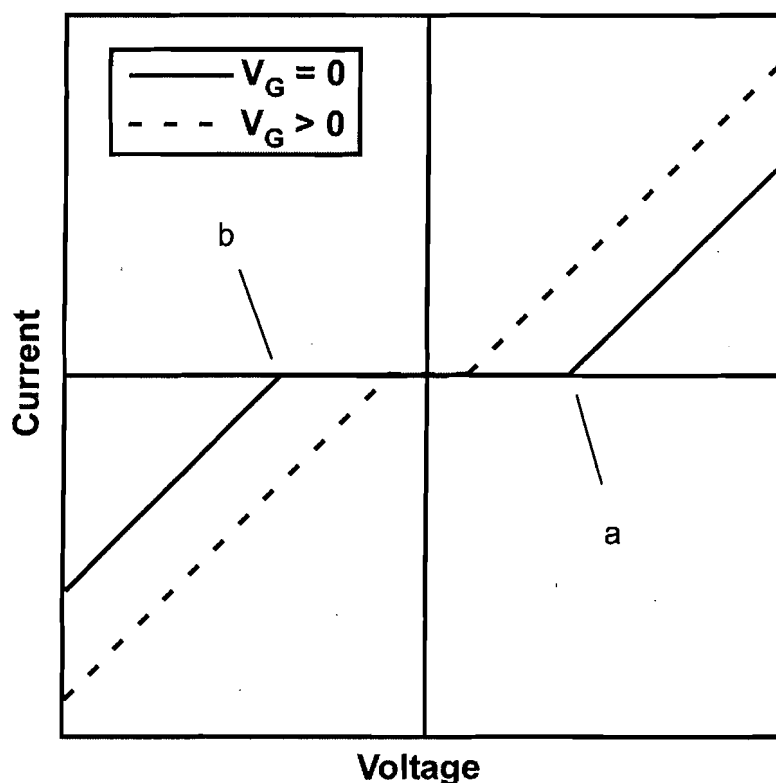


Figure 1.4. Graph showing ideal functioning of a nanoparticle based single electron transistor within the Coulomb blockade region under both 0 and applied gate bias, V_G .

through the nanoparticle, a minimum energy known as the charging energy ($E_C = e^2/2C$) must be applied. For gold nanoparticles below 2 nm, $E_C > k_B T$, i.e. there isn't enough thermal energy available under zero applied bias for current to flow.²⁴ Only when the applied bias between the source and the drain passes a certain threshold value (labeled a and b on the solid trace, Figure 1.4) will current flow. This threshold voltage can be decreased by increasing the core size (thus increasing the capacitance) or by applying a gate voltage, as shown in Figure 1.4.

In an SET with a variable gate voltage, the energy of the nanoparticle is given by

the equation $E = \frac{Q^2}{2C} - QV_g$, where Q is a charge placed on the nanoparticle with

capacitance C and applied gate voltage V_g .^{18,34} Again, for a gold nanoparticle < 2 -nm, if this energy is greater than the thermal energy available at room temperature, electrons will not be able to tunnel and Coulomb blockade will be in effect. However, if the gate voltage is made more positive, the threshold voltage will decrease and, at a high enough gate voltage, electron tunneling will occur. Within the Coulomb blockade region, the SET is in the off or “0” state, and at high enough gate voltages, the SET will be in the on or “1” state.^{18,34}

As indicated above, careful control over the size and composition as well as the purity of gold nanoparticles is important for observing and utilizing the unique electronic properties of these materials. Careful control over these parameters will be required to develop gold nanoparticles for nanoelectronic applications.

Optical Properties of Gold Nanoparticles

Because the electronic structure of large (> 2 -nm) gold nanoparticles is dominated by the band structure of bulk gold, they are not useful for room-temperature electronic applications, with the exception as use for interconnect materials. Instead, large gold nanoparticles may play a role in optical applications such as sensors³⁵ and wave-guides.²⁷ Like bulk gold (and other noble metals), large gold nanoparticles exhibit plasmon resonance. Plasmon resonance arises from the coupling of the electromagnetic portion of incoming light to the surface (conduction band) electrons of the metal core. This coupling leads to the collective oscillation of the electrons (Figure 1.5a).³⁶ The plasmon resonance is easily observed for gold nanoparticles as a broad absorption in the UV-visible spectrum at ~ 520 nm (Figure 1.5b). As a general rule, an increase in core size will lead to

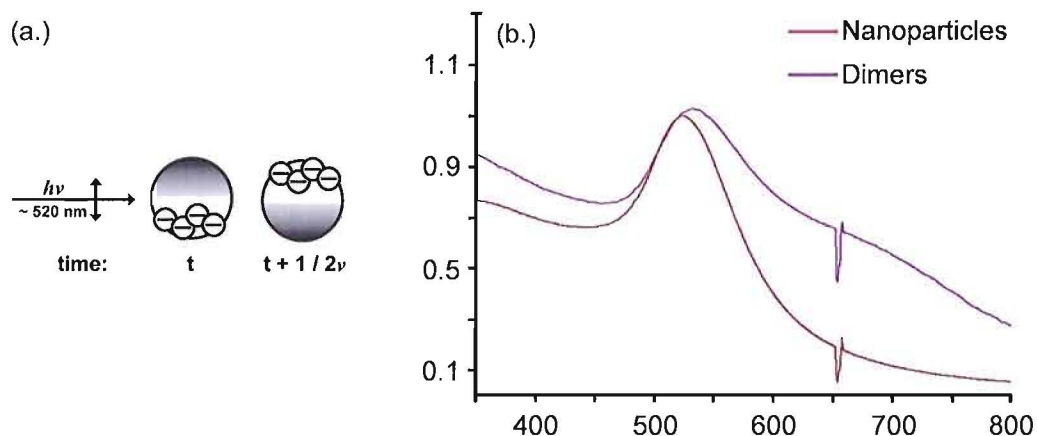


Figure 1.5. (a.) Schematic of plasmon resonance on a gold nanoparticle. (b.) UV-vis spectrum of the plasmon resonance on 8-nm citrates stabilized nanoparticles (orange) and dimers (purple).

a narrowing of the plasmon peak, an increase in intensity and a redshift of the plasmon peak in the UV-vis.³⁶

Plasmonic coupling can occur between two or more adjacent nanoparticles, leading to a redshift in the absorption spectrum (Figure 1.5b, purple trace). The extent of plasmonic coupling is dependent upon the interparticle spacing. Because it leads to an easily observed spectral shift, plasmonic coupling is being targeted as a method for rapid diagnostics and sensors.³⁷ Another application of this coupling is that of wave-guides.²⁷ Waveguides are devices that transmit information from light through the solid state, making them useful for opto-electronics. It has been shown that linear arrays of small metal islands can function as wave-guides through the propagation of plasmons of individual particles. Given sufficiently monodisperse gold nanoparticle samples with tunable interparticle spacing, gold nanoparticles may be ideally suited for waveguide applications.

While spherical nanoparticles exhibit a single plasmon resonance mode, shaped, anisotropic nanoparticles may exhibit multiple plasmon modes.^{38,39} In the example of gold nanorods, there are both transverse and longitudinal plasmon resonances, leading to two absorption peaks in the absorption spectrum (Figure 1.6). The transverse plasmon is located at ~ 520 -nm, typical for gold nanoparticles. However, the longitudinal plasmon is dependent upon the aspect ratio of the nanorods (controlled during synthesis) and can be tuned from the far-visible into the near-IR. Because near-IR radiation can penetrate the skin, the optical properties of gold nanorods are anticipated to play a role in medical diagnostics⁴⁰ and for hyperthermic therapies.⁴¹

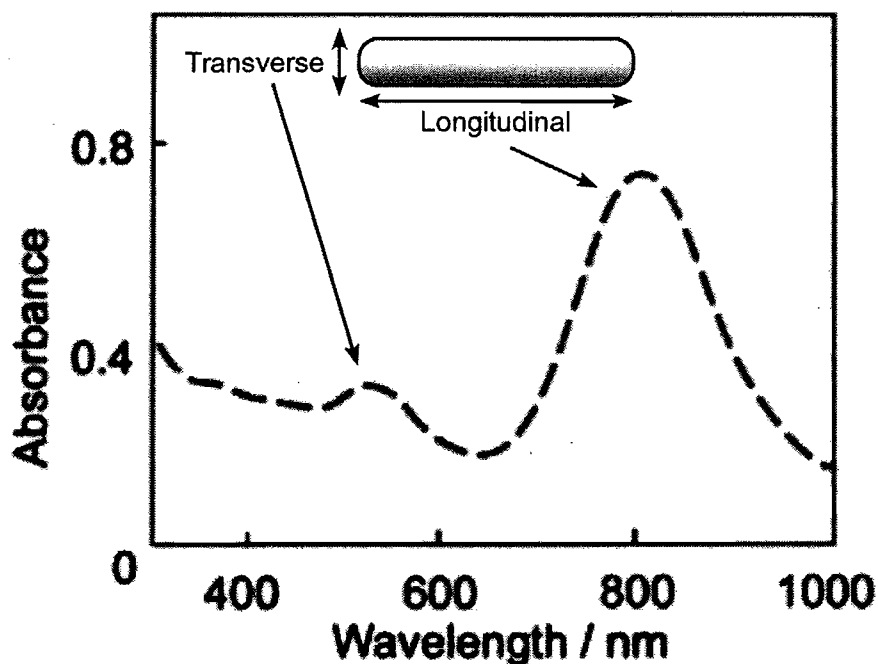


Figure 1.6. UV-vis spectrum of the bimodal plasmon resonance found in gold nanorods.

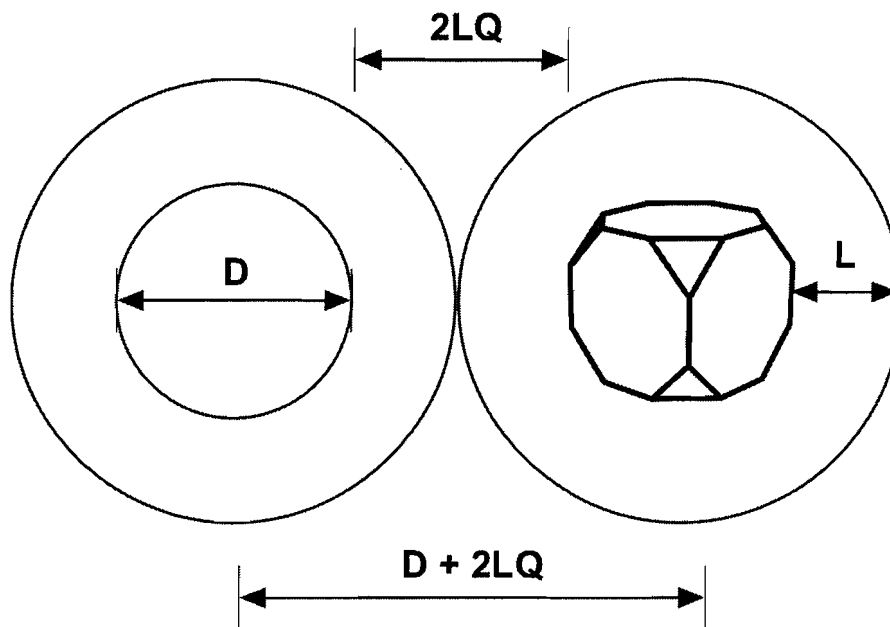


Figure 1.7. Illustration describing the important aspects of a gold nanoparticle, including the diameter (D) and ligand length (L). The interparticle spacing ($2LQ$) is related to the ligand length and the interdigitation factor (Q). On the right is the truncated cube geometry expected for a gold nanoparticle, with the large faces being Au (111) and the smaller faces Au (100).

As with the electronic properties of gold nanoparticles, the optical properties are also affected by the size, shape, composition, assembly and purity of the nanoparticle samples. Careful control of size and shape during synthesis, an attention to the purity of the nanoparticles, and controlled functionalization are all important aspects of preparation that will allow for the realization of potential applications for both large and shaped gold nanoparticles for optical applications.

Gold Nanoparticle Preparation

The goal in preparing spherical gold nanoparticles is to produce a population of narrowly dispersed gold cores passivated and stabilized by an organic ligand shell (Figure 1.7). Most commonly, a Au (III) salt is reduced to Au (0) to form an activated species, either in a single step or via a Au (I) intermediate followed by reduction to Au (0). These

activated Au (0) species are thermodynamically unstable and rapidly aggregate to form nuclei and eventually the desired gold nanoparticle (Figure 1.8a). The most commonly referenced mechanism for this process comes from LaMer theory.⁴² LaMer theory was originally developed to describe the formation of small sulfur clusters; however, it is

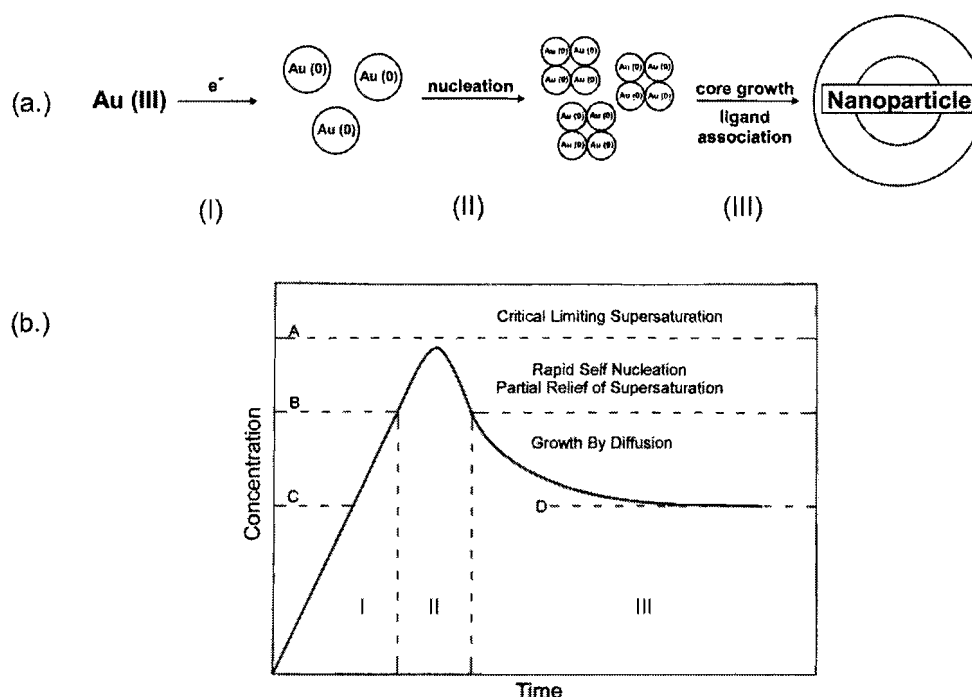


Figure 1.8. (a.) Schematic of gold nanoparticle growth. (b.) Graph depicting the change in Au (0) concentration over time during the synthesis of gold nanoparticles, as predicted by LaMer theory.

broadly applicable to clusters and nanoparticles of other materials. Lamer theory is broken into three stages (Figure 1.8b), (I) precursor addition / formation of the activated species, (II) nucleation and (III) core growth. In Stage I, the precursor (Au (III) or Au (I)) is chemically reduced to form the activated Au (0) species. As the concentration of this activated species increases, the system passes into the supersaturated regime (Stage II) at which point the Au (0) species begin to aggregate and form nuclei. Nucleation continues

until the concentration of Au (0) in solution drops below the supersaturated regime (Stage III), at which point the formed nuclei continue to grow through diffusion. This process typically occurs in the presence of an organic ligands which associate with the surface and eventually passivate it. Although some syntheses have been developed for bare gold particles, these species are typically thermodynamically unstable and decompose to bulk metal.

In order to produce a uniform, narrowly distributed population of gold nanoparticles, the following criteria must be met: (i) the activated species must be homogeneously dissolved throughout the reaction medium, (ii) nucleation events should occur simultaneously, and (iii) the number of initial nuclei should be a constant for a given nanoparticle size. To meet these criteria, reactions are typically carried out in small volumes with millimolar concentrations of reactants using constant, vigorous stirring. The rate of activated species formation, and thus the rate of nucleation, is controlled by choice of reducing agent (thus reduction potential), concentration or temperature. One promising approach that has been recently pioneered is the use of flow-synthesis or microreactors to accurately control reaction conditions.⁴³

Although hundreds of syntheses have now been reported for the preparation of gold nanoparticles, they can generally be categorized by the type of organic ligand they have been prepared with. These categories include (i) non-specific ligands, such as citrate or surfactants, (ii) phosphines, such as triphenyl phosphine and (iii) thiols, such as dodecanethiol or 2,2'-mercaptoethoxyethanol. Syntheses resulting in nanoparticles containing these classes of ligands are discussed below. The discussion is not meant to be

a comprehensive review of all preparative methods but instead covers those most relevant to the work described in this dissertation.

Non-Specific Ligands

The most common method of synthesizing gold nanoparticles is through the use of citrate. (Figure 1.9) Turkevich et al. reported that adding sodium citrate to a boiling solution of chlorauric acid led to the formation of nanoparticles.⁴⁴ Later work showed that variations in temperature and the ratio of reactants allowed for control over the core size from 10 to 100-nm.⁴⁵ More recent work has shown that Au/citrate solutions reduced with NaBH_4 allow for the synthesis of nanoparticles < 10-nm in average core size. Despite being the most common method of producing nanoparticles, citrate-stabilized nanoparticles are disadvantageous for several reasons. First, they cannot be isolated from solution, making it difficult to store or study them in the solid state. Second, their stability with changes in pH or ionic strength is minimal. Finally, and most importantly, their functionalization, either through ligand exchange or via derivitization of carboxylic acids in the ligand shell, is extremely limited. To partially overcome these shortcomings, our lab has recently developed diafiltration methods that may allow for ligand exchange with thiols, thus extending the utility of nanoparticles prepared via the citrate route.⁴⁶

Another common method for the preparation of gold nanoparticles containing non-specific ligand shells is through the use of tetraoctyl ammonium bromide (TOAB), as reported by Brust et al.⁴⁷ In this method, HAuCl_4 is transferred from the aqueous phase to toluene and subsequently reduced by NaBH_4 in the presence of the TOAB to form toluene soluble, 5 to 6-nm gold nanoparticles. Although the ability to synthesize a diverse

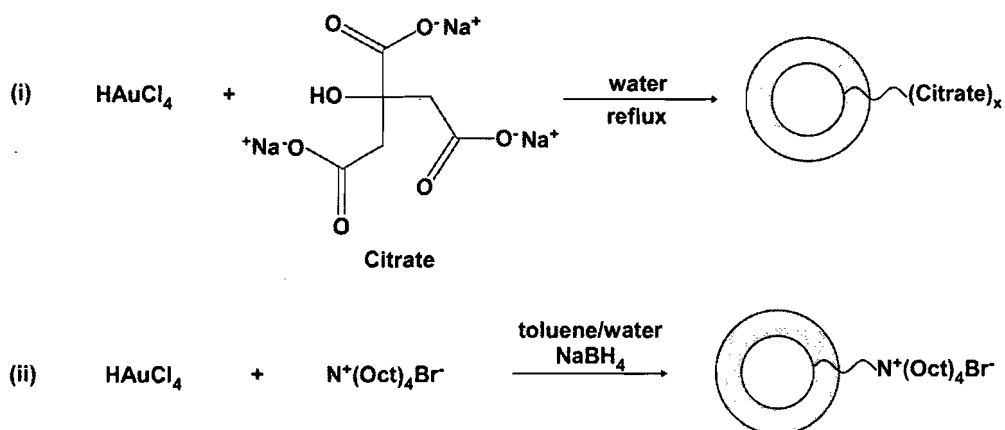


Figure 1.9. (i) Preparation of citrate-stabilized nanoparticles. (ii) Preparation of TOAB-stabilized nanoparticles.

range of core sizes is limited, this method is advantageous in that the resultant nanoparticles can be isolated from solution and the ligand can be exchanged to yield both thiol and amine stabilized nanoparticles.^{48,49}

As noted, the synthesis of gold nanoparticles using non-specific ligand shells typically yields nanoparticles with large (> 5-nm) cores. These particles are useful for optical applications, where the strongly enhanced plasmon resonance of the large nanoparticles is useful, and also as tagging agents for biological applications. Also, the larger nanoparticles produced by these methods have found utility as precursors in seeded growth reactions. Although at very low temperatures interesting electronic properties can be observed, large nanoparticles are not especially suited for electronics applications. For this reason, there has been significant effort put into the synthesis of smaller nanoparticles.

Phosphine-Stabilized Nanoparticles

Though not as common as citrate preparations, another important class of gold nanoparticles are stabilized using phosphine ligands (Figure 1.10). The small size of these particles, typically < 2-nm, makes them particularly attractive for electronics applications which would take advantage of their predicted room-temperature Coulomb blockade properties. One drawback to phosphine-stabilized nanoparticles is the limited functionality available with compatible phosphine ligands and the fact that many phosphine-stabilized nanoparticles are not stable in solution. However, work done in our labs has demonstrated that phosphine-stabilized nanoparticles can undergo ligand

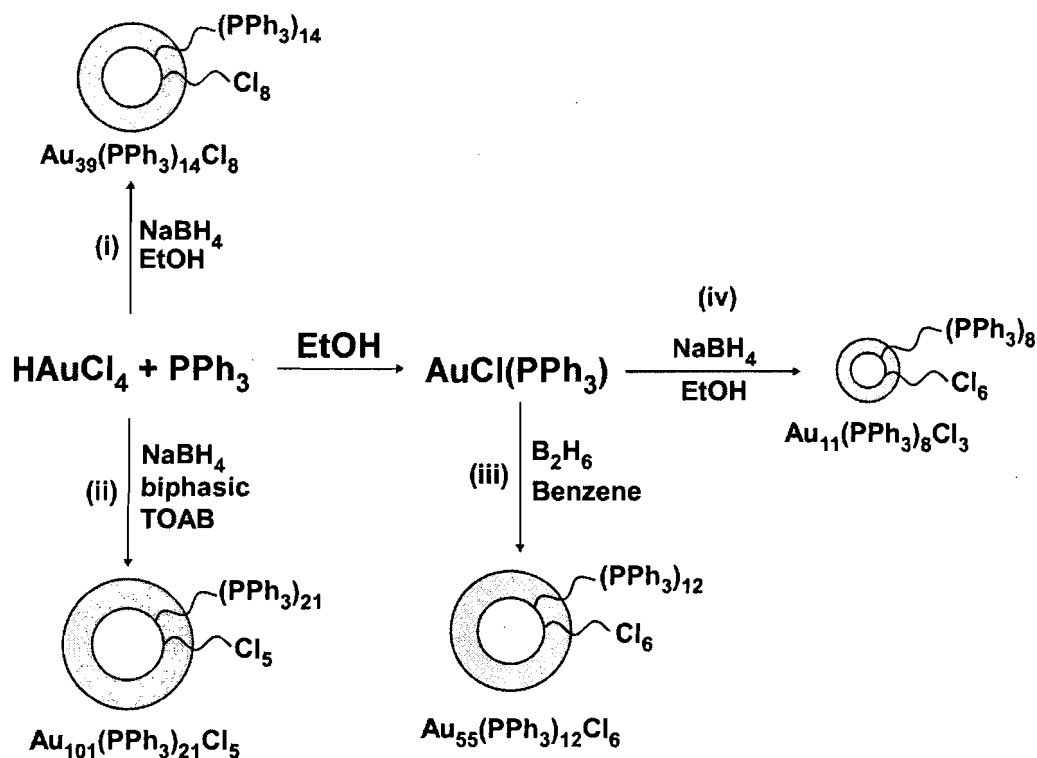


Figure 1.10. Various routes to triphenyl phosphine-stabilized nanoparticles with core diameters from 0.8 to 1.5-nm.

exchange reactions with a wide variety of thiols, giving access to nanoparticles that are stable in solution for extended periods.⁵⁰

The earliest syntheses were borne out of cluster chemistry, and some of the first molecular gold clusters contained just a few gold atoms. Au₅ and Au₁₁ were early reported clusters, and a number of other molecular species up to Au₃₉ have been reported.⁵¹ The move from sub-nanometer cluster chemistry to nanoparticle synthesis began with Schmid's synthesis of Au₅₅ with 1.4-nm average core diameter.⁵² These particles were synthesized by the reduction of a Au (I) compound, Au(PPh₃)Cl with diborane gas in warm benzene. Our group has more recently developed a synthesis of 1.5-nm Au₁₀₁ nanoparticles using a biphasic system similar to that shown for TOAB stabilized particles above.⁵³ This new approach yields nearly the same product as the Schmid synthesis, yet is much safer and more convenient to carry out, making it a much more attractive route to nanoparticles useful for studies of electronic properties.

Nanoparticles synthesized using phosphines and subsequently ligand exchanged are being targeted primarily for electronic and catalytic applications, as the small size precludes any significant optical activity. Ligand exchange can be used to introduce peripheral functionality, but the ability to directly synthesize nanoparticles with the desired functionality would be useful. Direct synthesis using thiols and Bunte salts offer one such solution.

Thiol-Stabilized Nanoparticles

In 1994, Brust et al. reported the direct synthesis of gold nanoparticles containing dodecanethiol ligands using similar phase transfer processes as above for the preparation TOAB and triphenylphosphine-stabilized nanoparticles.^{31,47,54} This preparation led to organic soluble nanoparticles in the 2-nm size regime (Figure 1.11 (i)). Follow-up work showed that a monophasic procedure could be used to prepare alcohol-soluble gold nanoparticles and eventually water-soluble gold nanoparticles.⁵⁵ In 1997, Whetten et al. provided evidence that the direct synthesis of thiol-capped gold nanoparticles may involve the formation of a gold-thiol polymer.⁵⁶ Since these initial reports, syntheses have been developed for a wide variety of organic- and water-soluble nanoparticles containing a number of functional groups. Murray's group has shown that the core size of

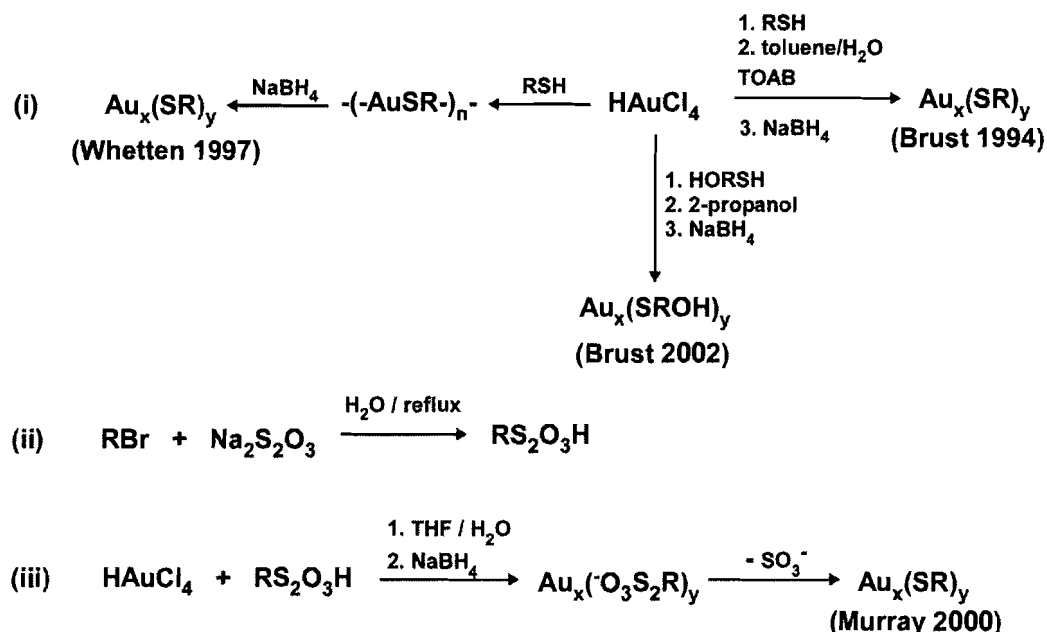


Figure 1.11. Various routes to thiol-stabilized nanoparticles. (i) Traditional, direct synthesis routes involving thiols. (ii-iii.) Synthesis of Bunte salts, and the synthesis of gold nanoparticles using Bunte salts.

nanoparticles prepared in this fashion can be tailored by varying the ligand to gold ratio during the reaction.⁵⁷ In general, the direct synthesis of thiol-capped gold nanoparticles leads to nanoparticles in the 2 to 8-nm size regime and tends to result in a greater degree of size dispersity than, for example, phosphine-stabilized nanoparticles. Another disadvantage of this approach is that the scope of thiol ligands available is limited to the stability of the ligand to the reaction conditions. Furthermore, thiol for thiol ligand exchanges on gold nanoparticles can be difficult.

One recent advancement that avoids these potential issues with the direct use of thiols is through the use of Bunte salts (Figure 1.11 (ii)-(iii)).⁵³ Bunte salts are the thiosulfate analogs of thiols and are easily synthesized using sodium thiosulfate and a brominated precursor.⁵⁸ Synthesis of nanoparticles using Bunte salts is similar to that of direct thiol synthesis. Bunte salts offer several advantages: (i) they can be easily stored for longer periods than the thiol analogs, (ii) they are easier to synthesize than thiols and (iii) they are stable to a wider variety of reaction conditions. Despite several advantages, control over size and size-dispersity remains difficult, however recent work by our lab may lead to greater control over size.⁵⁹

Nonspherical Gold Nanoparticles

Nonspherical or shaped gold nanoparticles have garnered significant attention due to their intriguing shape-dependent properties, including multi-modal plasmon resonance and fluorescence, which make them promising candidates as tagging agents and surface-enhanced Raman scattering substrates, amongst other applications. Preparations for shaped nanoparticles such as rods,²² prisms,^{38,60} hexagonal plates,⁶¹ cubes,^{24,62} and stars²⁵

have been described. A number of methods, such as electrochemical⁶³ or templated growth⁶⁴ have been described for their preparation. However, the most common route to shaped nanoparticles is through seeded-growth methods (Figure 1.12). Here the synthesis and proposed mechanism for nanorod preparation with a seeded growth approach will be described as it is the best understood system, and it is expected that other shaped nanoparticles have similar growth mechanisms.

In seeded growth reactions, a previously synthesized “seed” nanoparticle is introduced to a growth solution containing a Au (III) salt, a weak reducing agent, and a directing agent (most commonly a surfactant). Initially, the seed particles grow through the slow-diffusion of gold atoms onto their surface. After an initial period, the seeds have

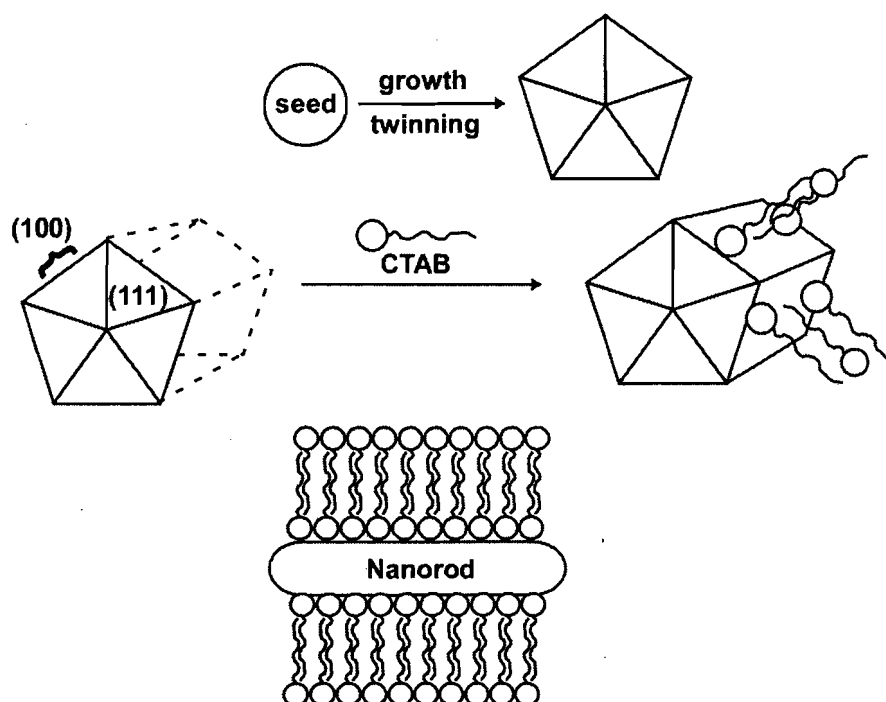


Figure 1.12. Hypothesized mechanism of nanorod growth. The initial seed undergoes growth and twinning. The directing agent, CTAB, assembles on the Au (100) face, leading to growth primarily on the Au (111) faces.

grown into isometric crystals with well-defined Au (111) and Au (100) crystal faces. These enlarged seeds aggregate along these well-defined faces to form pentatwinned species that serve as the starting material for rod growth. Simultaneous with the twinning events, the surfactant begins to associate and assemble on the Au (100) faces acting as a directing agent and preventing further growth on the (100) face. As a result, further growth occurs on the Au (111) faces and along the (110) axis, leading to an elongation of the crystal to form a nanorods.^{22,65,66} Slight changes in reactant ratio, the use of different seeds, variations in pH or the use of dopants can be used to modify the interactions of the directing agent with the growing crystal or otherwise affect the growth, leading to changes in morphology.^{25,38,61}

Among the most studied routes to shaped gold nanoparticles are those for nanorods first reported by Murphy's group.⁶⁵ These preparations use multiple seeded growth steps to give access to gold nanorods of increasing aspect ratio. In the first step, small 4-nm citrate seed nanoparticles are placed into a growth solution containing HAuCl_4 , ascorbic acid as a weak reductant and cetyl-trimethylammonium bromide (CTAB) as the directing agent. If only low aspect ratio rods are desired, the synthesis may be stopped here. However, if longer rods are desired an aliquot of nanoparticles from the first growth solution is added to a second growth solution. This process continues until nanorods of the desired length and aspect ratio have been obtained. As mentioned above, slight changes to this procedure have allowed for the synthesis of nanorods of differing aspect ratio, prisms, hexagonal plates and stars. One draw-back to a multiple step seeded growth process is that populations of differently shaped particles can arise; however, recent work

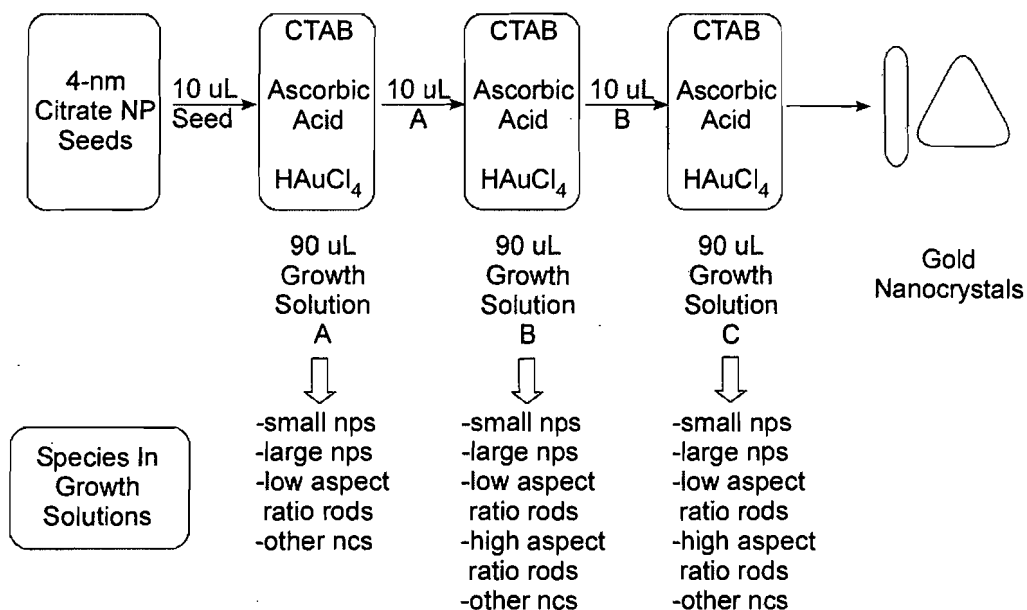


Figure 1.13. Synthetic steps for the preparation of gold nanorods, as reported by Murphy et al.⁶⁵ On the bottom is the expected populations of different nanoparticle products, both spherical and shaped in each growth solution.

has improved this. Mulvaney and el Sayed have both shown that using CTAB as the ligand on the seed particle and the addition of silver salts will improve nanorod yields.^{39,66}

Despite much progress, the ability to obtain uniform shaped nanoparticles in high yields remains elusive. Furthermore, functionalizing these shaped nanoparticles has proven difficult. The development of methods that address these issues would allow for further research into the fundamental properties and applications of shaped gold nanoparticles.

Nanoparticle Functionalization

Upon synthesis, gold nanoparticles often contain an improperly functionalized ligand shell, useful during synthesis but not for assembly, targeting or other applications that require nanoparticles containing specific peripheral functional groups. The presence of peripheral functionality allows for tuning the interactions between the gold nanoparticle and its environment, such as solubility, reactivity and self-assembly. Tailoring the ligand shell also plays a role in controlling nanoparticle-nanoparticle interactions. Two general approaches have been devised for the introduction of functional groups into the periphery of the ligand shell: (i) post-synthetic modification of the existing ligands or (ii) ligand exchange to replace the existing ligands with ligands containing a desired functionality (Figure 1.14).

Post-Synthetic Modification

Post synthetic modifications are used to attach molecules containing a desired functionality to the periphery of the nanoparticle using an existing functional group on

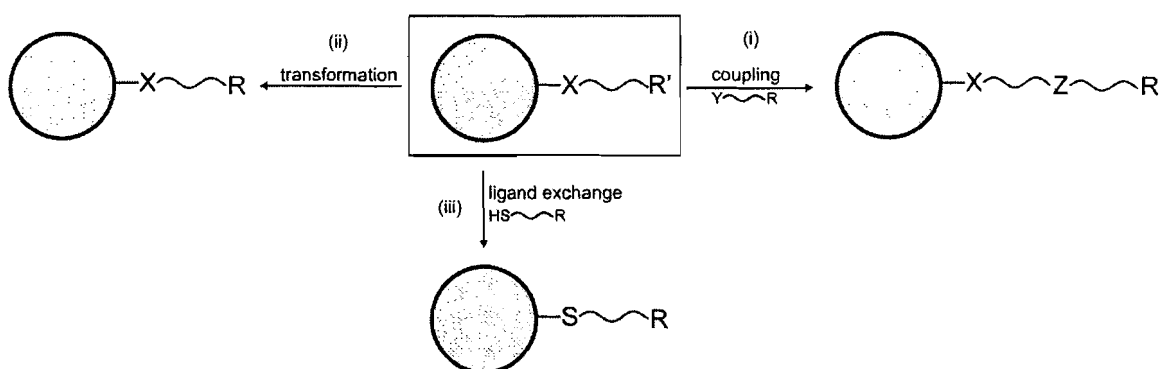


Figure 1.14. Routes to functionalized gold nanoparticles. (i) Coupling of a functional molecule to the ligand shell, (ii) transformation of an endogenous group in the ligand shell, (iii) ligand exchange.

the nanoparticle. For instance, Templeton et al. investigated the S_N2 reactivity of bromo-groups on the periphery of gold nanoparticles.⁶⁷ In particular, the influence of the chain length of the ligand shell (4, 8 and 10 carbons) as well as the bulkiness of the nucleophile were investigated. Subsequent work showed terminal -COOH groups could be modified by alcohols and amines to form the resultant amides and esters.⁶⁸ Other post-synthetic modifications have included coupling reactions,^{67,68} polymerization⁶⁹ and peripheral group transformations.⁷⁰

Post-synthetic modification offers the opportunity to start with a common precursor nanoparticle and, through well-known chemical transformations, obtain functionalized nanoparticles. However, the success of this approach is limited not only by the stability of the gold nanoparticle under the reaction conditions, but also by the reactivity and sterics of the peripheral functionality to be modified. Furthermore, characterization of the resultant product to determine the extent of functionalization is exceedingly difficult. Due to these obstacles, ligand exchange is often employed.

Ligand Exchange

Ligand exchange is the process whereby the existing ligand shell on a gold nanoparticle is either partially or fully displaced by another ligand that contains the desired functionality. Most commonly, the gold nanoparticle is synthesized with a small, labile ligand shell that can be easily displaced in subsequent steps. Generally, the gold nanoparticles are dispersed in a suitable solvent, and then an excess of the incoming ligand, typically a thiol, either under monophasic or biphasic conditions is added. This is allowed to stir for several hours or days either under ambient conditions or at elevated

temperatures. Following the exchange, excess and exchanged ligand are removed via suitable purification methods, yielding the ligand exchanged product. In all cases, removal of the excess ligand is important following ligand exchange because it has been shown that excess ligand will destabilize the nanoparticles over short to medium time scales via an etching process.

For each of the classes of nanoparticles described above, ligand exchange methods have been developed to introduce desired functionality.

Non-Specific ligands. Citrate stabilized nanoparticles, despite their ubiquity, are notoriously difficult to functionalize via ligand exchange. This is due to the complex aggregation of citrate on the surface of the nanoparticle. Some incomplete thiol exchanges onto the surface have been observed, but these reactions have been limited in scope.⁷¹ Ligands bearing two chelating thiols have also been used.⁷² More recently, our group has pioneered the use of diafiltration to “strip” the majority of the citrate from the

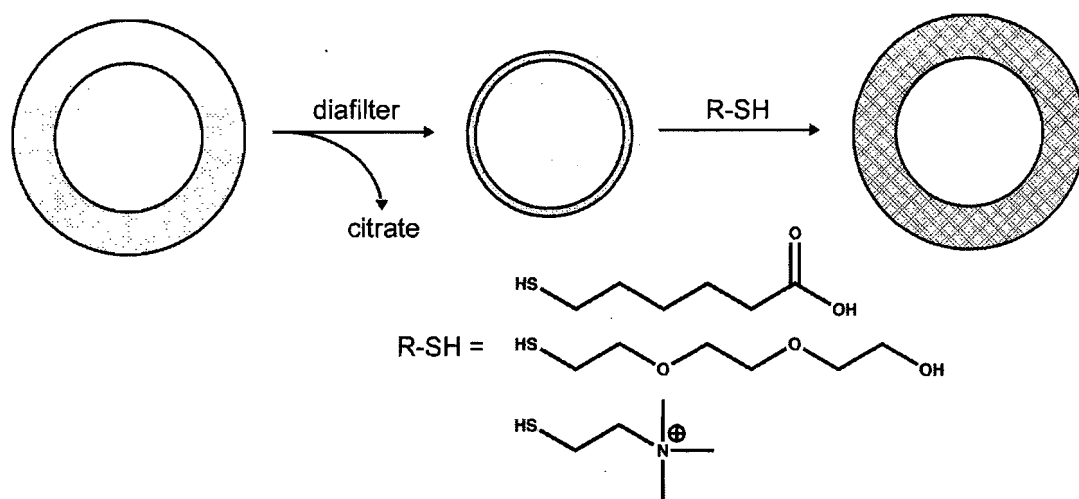


Figure 1.15. Stripping process to remove citrate from the surface of nanoparticles, allowing for thiol functionalization.

surface of the nanoparticle. These bare nanoparticles have been shown to be suitable substrates for ligand exchange of both charged and neutral thiol ligands.⁴⁶

Nanoparticles synthesized via TOAB offer a more versatile route to large, functionalized gold nanoparticles, though the size of the nanoparticle is limited to 5 or 6-nm. TOAB stabilized nanoparticles may be exchanged with 4-dimethylamino pyridine (DMAP) to yield water-soluble nanoparticles.⁴⁸ Both the organic-soluble TOAB and water-soluble DMAP stabilized nanoparticles are versatile substrates for ligand exchange, though the longer alkyl chain length of the TOAB can limit the extent of exchange.^{48,49} Gandubert et al. recently demonstrated the preparation of water, alcohol and organic soluble gold nanoparticles via this multi-step protocol.⁴⁹

Phosphine Ligand Exchange. Triphenyl phosphine (TPP) stabilized nanoparticles, both 0.8 and 1.4-nm, are common gold nanoparticle precursors in our labs and their ligand exchange chemistry was well-described in two papers by Woehrle.⁵⁰ His studies into the ligand exchange of 1.4-nm TPP stabilized nanoparticles, under both single and biphasic conditions, showed that the TPP was displaced as a Au(PPh₃)Cl compound followed by association of the incoming thiol during the ligand exchange process. Though some loss of gold from the surface was observed, reductions in core diameter were negligible. Similarly, undecagold 0.8-nm TPP stabilized nanoparticles have been exchanged with both functionalized phosphines and thiols to yield ligand exchanged products. Because the phosphine exchanged products are often unstable, they have not been studied extensively. On the other hand, thiol exchange provides a versatile route to relatively stable functionalized 0.8-nm gold nanoparticles, despite the fact that these thiol

exchanges often require rigorous conditions (i.e. high temperature) in order to occur. Brown showed that phosphine to amine ligand exchanges led to core growth of the 1.4-nm TPP precursor particles.⁷³ Using this approach allows for access to larger, amine stabilized nanoparticles with control over core size through manipulation of the exchange conditions.

Thiol Ligand Exchange. Nanoparticles synthesized directly with thiol ligands are attractive because they offer the ability to obtain stable nanoparticles containing a functionalized ligand shell in a single step. Unfortunately, the scope of direct thiol-stabilized nanoparticle synthesis is limited by the stability of thiols with respect to disulfide formation. For this reason, thiol-thiol ligand exchange is often required to obtain nanoparticles with the desired functionality. Unfortunately, thiol-thiol ligand exchanges are often more difficult than exchanges on TPP or DMAP-stabilized nanoparticles.

Murray et al. suggested that ligand dissociation and exchange occurs via a concerted mechanism whereby an incoming ligand transfers a proton to the sulfur of an outgoing ligand.⁷⁴ It has been further hypothesized that certain locations on a nanoparticle are more reactive during ligand exchange (refer to Figure 1.7). Vertex sites (areas where gold atoms have few nearest neighbors) are expected to have the highest reactivity, followed by edge sites, near-edge face sites and then interior face sites. It is likely that the vertex sites are the most reactive because (1) the gold atoms at the vertex have the highest potential, and therefore show the highest reactivity (i.e. for redox chemistry) and (2) ligands at these sites are not stabilized by Van der Waals interactions. By similar arguments, interior surface sites show the greatest stability because the gold

surface is more uniform and there is much higher ligand packing density, which increases the stability of the monolayer.⁷⁴

Several other factors have been shown to be important during the ligand exchange process. First, it has been shown that ligand exchange occurs most readily when the precursor particle has a ligand shell that is composed of short chain length and that is labile. Longer chain lengths lead to greater monolayer stability and lower exchange rates. It has also been shown that for the same reasons, incoming ligands that have favorable Van der Waal or hydrogen bonding interactions will show higher exchange rates. The concentration of incoming ligand also plays a large role. Although there is a 1:1 ligand exchange ratio, a high concentration of incoming linker is required to force the ligand exchange reaction to completion. The reason for this is that there is significant equilibrium of thiols on the surface and in solution. As with any equilibrium situation, pushing the reaction towards completion requires a significant excess of the incoming thiol. Additionally, time and temperature also play a role in forcing the reaction.⁷⁵

Purification

One of the most crucial aspects of nanoparticle preparation is purification of the desired product. Following nanoparticle synthesis, the product is often contaminated with precursor molecules, excess free ligand, salts and nanoparticles outside of the desired size range. These impurities will often adversely affect the properties of the gold nanoparticles as well as their interactions with the environment, either for self-assembly or for assessing the toxicology. Interestingly, sufficient purification has only recently

been taken seriously as a step in the preparation of gold nanoparticles, despite the necessity for having pure nanoparticle samples.

The method employed for purifying nanoparticles depends upon the nanoparticle characteristics and the composition of the impurity to be removed, as there are very few “one size fits all” purification methods. As an example, in the preparation of 1.4-nm gold nanoparticles, the material is precipitated and then carried through successive solvent washes to remove excess TPP ligand and phase-transfer catalyst. Due to the biphasic nature of the synthesis, salts are left behind in the aqueous phase.⁵³

Water-soluble, thiol-stabilized nanoparticles can be challenging to purify as the desired material and the impurities, both salts and free ligand, often have similar solubility. Shown in Figure 1.16 are several possible methods for purifying water-soluble, thiol stabilized nanoparticles. Extractions and solvent washes are useful for removing free ligand and other organic impurities, but tend to leave residual salts behind. Dialysis is effective for removing excess salts, but leaves behind free ligand. A combination of these approaches may be useful for removing the majority of impurities, however the combined time and large amount of waste required to carry out these multiple approaches make purification tedious, expensive and wasteful. Size exclusion chromatography is useful for removing both salts and free ligand, however the nanoparticles tend to irreversibly precipitate on the chromatography supports, leading to decreased yields. Centrifugation is another method for removing both types of impurity, but requires a significant amount of time for adequate purification. Diafiltration is a method developed in our lab that overcomes many of these limitations. and yields nanoparticles that are highly pure. The

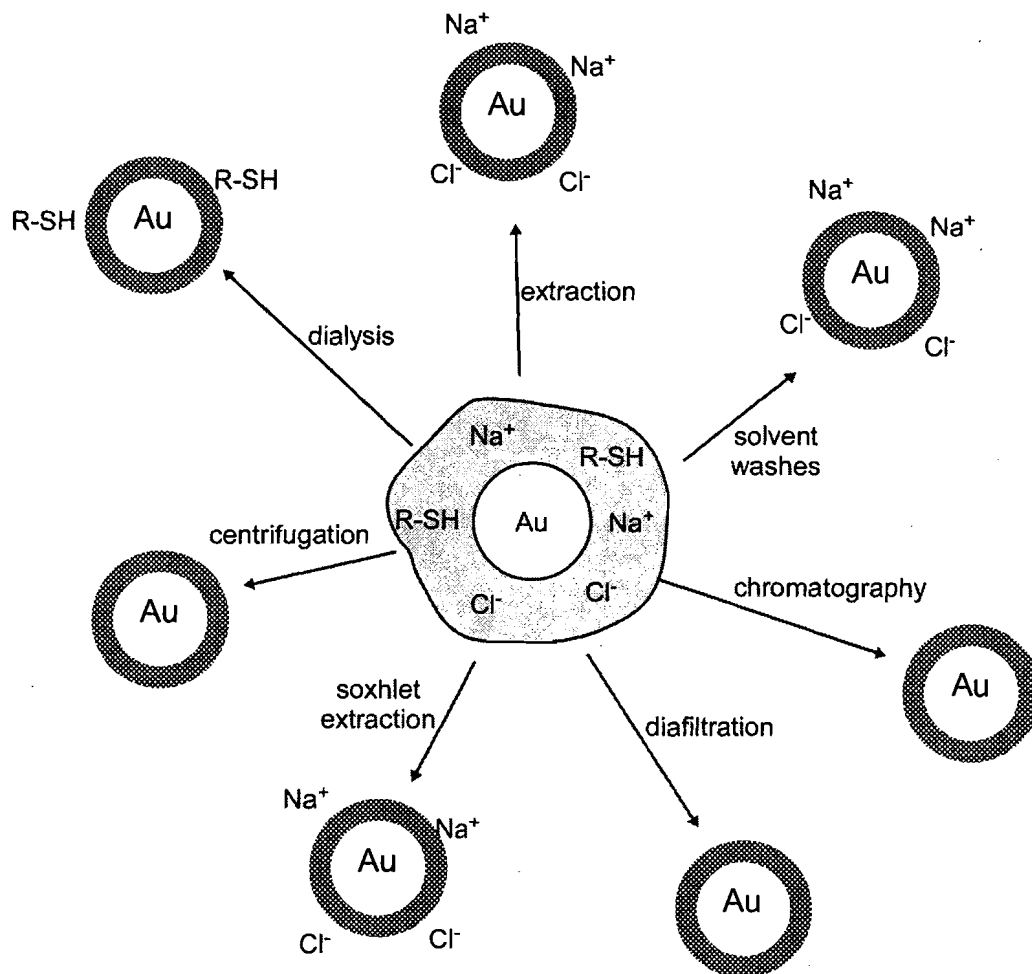


Figure 1.16. Various methods for purifying water-soluble gold nanoparticles and the types of impurities that can be removed using each method.

use of diafiltration for the purification and size separation of gold nanoparticles is discussed extensively in Chapter II.

Characterization

One of the significant challenges in gold nanoparticle synthesis is sufficient characterization in order to establish average core diameter and shape, ligand shell composition and impurity profile of the synthesized material. Developing an accurate picture of the gold nanoparticles allows for a greater understanding of the optical and

electronic properties and assists in the development of structure-function relationships. In order to determine the size and shape of the gold nanoparticle core, transmission electron microscopy (TEM) and UV-Visible spectroscopy (UV-vis) are often used. $^1\text{H-NMR}$ can be used to determine the identity of ligands bound to the surface versus those in solution or weakly bound. TGA offers the ability to determine the percentage of organic material in a nanoparticle sample. Comparison of this value versus an expected percentage allows for a determination of how much organic impurities are present in the material. XPS allows for similar assessments, and also allows for the determination of how much inorganic impurities (e.g. excess salts) are present in the sample. Using this battery of characterization methods, it is possible to develop a fairly accurate picture of the gold nanoparticle sample, though the development of new characterization methods is an active area of research.

$^1\text{H-NMR}$

Nuclear magnetic resonance (NMR) is a widely used technique in both organic and inorganic chemistry for carrying out structural analysis of molecules and assessing the kinetics of reactions, amongst other uses. In the realm of nanoparticle study, NMR is used primarily to confirm the composition of the ligand shell and to identify any impurities in the sample. The resonances of organic ligands bound to the gold nanoparticle core are significantly broadened in comparison to ligand that is free in solution, allowing for easy assessment of bound ligand versus impurities.⁷⁵ The broadening of the bound ligands is due to a number of factors which include a heterogeneous ligand environment on the surface of the nanoparticle, a decrease in the degrees of freedom in the bound state

as well as changes in spin-spin relaxation due to the tumbling of the nanoparticles in solution.⁷⁵ For short chain length molecules bound to the surface, these effects can be quite strong, however as the chain length increases, protons at the periphery show less broadening. Smaller gold clusters also show less of an affect. Due to the effects of the nanoparticle core and the proximity of bound ligands to one another, integration and thus quantification of the relative concentrations of different species associated with the nanoparticle is usually not applicable, thus other methods such as TGA and XPS are used for quantification.

TGA

Thermal gravimetric analysis (TGA) is a method for monitoring mass changes in heated samples and can be used to determine the percentage of volatile organic species in a sample. During a TGA experiment, a lyophilized gold nanoparticle sample is subject to increasing temperatures while the loss in mass is simultaneously recorded. The percent mass loss can be correlated to the amount of organic material associated with the sample. Aside from determining the amount of organic material present, the temperature at which mass loss occurs as well as the mass loss profile can be correlated with the identity of the ligand and the strength of ligand binding. One of the more powerful uses of TGA is as a quantitative measure of the concentration of organic impurities. Using techniques developed by Murray et al., one can calculate the theoretical amount of ligand associated with the surface of a gold nanoparticle.⁵² Comparing this number to the percentage obtained from the TGA measurement allows for an assessment of how much free organic material is in the sample.

XPS

XPS is a useful technique for analyzing solid state samples. In the context of gold nanoparticles, XPS is used to identify elements present within a sample and to determine their relative abundances in relation to each other. In an XPS experiment, X-rays of known energy are focused onto a drop-cast film of gold nanoparticles, stimulating photoelectron emission. The kinetic energy of the photoelectron is dependent upon the energy of the X-ray source and the material it was emitted from and thus can be used to determine the identity of the elements present, the orbital of the element from where the photoelectron originated and in some cases, can be used to characterize the oxidation state of elements present. In the work carried out here, the peak areas for each of the elements to be analyzed are used to determine the atomic concentration relative to the other elements. For example, in Chapter II, the gold to sulfur ratio determined by XPS is used to determine the concentration of thiol ligands bound to the surface of a nanoparticle as well as determine how much free inorganic impurities are associated with the sample. In conjunction with TGA and NMR, XPS can be used to develop a strong understanding of the purity and ligand shell composition of the gold nanoparticle.

UV-Vis

Aside from NMR, another rapid and routine characterization method used for assessing gold nanoparticle samples is UV-vis spectroscopy. UV-vis allows access to the optical properties of gold nanoparticles, primarily through the plasmon resonance exhibited at ~520 nm, however the location may be shifted due to the dielectric constant of the solvent, ligand shell properties, aggregation or core size.²⁹ In the case of

nonspherical nanoparticles, there is typically more than one plasmon resonance peak due to asymmetry, allowing for assessment of shape as well.³⁰ Because of the convenience of the technique, UV-vis allows for rapid, qualitative assessment of the core size and shape.

TEM

While UV-vis allows for a qualitative assessment of core size and shape, transmission electron microscopy (TEM) allows for far more quantitative determination of characteristics as it allows for direct visualization of the metallic core. Additionally, electron diffraction experiments can also be carried out, allowing for an assessment of atomic packing and orientation, which is useful for shaped gold nanoparticles.

While powerful, quantitative assessment of nanoparticle size and shape via TEM can be quite laborious. To determine the average core diameter and size dispersity requires proper sample preparation, microscopy technique and data analysis. Sample preparation consists of depositing the nanoparticles onto a suitable TEM substrate (typically an SiO/Cu or SiO₂ TEM grid). For optimal analysis, a dilute nanoparticle sample is aerosoled onto the grid in order to ensure well-spaced, uniform distributions of particles on the surface. Drop casting, dip coating and Langmuir-Blodgett techniques have also been used. The sample is placed into the microscope and micrographs at a suitable magnification ($\sim 200,000\times$) are obtained. In order to ensure that there is no bias in the size analysis, several images representing diverse regions of the TEM grid and several hundreds to thousands of nanoparticles are taken. This helps to avoid artificial size separation or skewing as a result of drying effects or aggregation.

Analysis of the obtained micrographs can be the most difficult aspect of the size analysis. Following developing of the positive film, the images are digitized and undergo image manipulations in Adobe Photoshop software to enhance the contrast of the nanoparticles. The steps used are as follows: (i) the positive film is inverted, yielding black spots (nanoparticles) on a gray background. (ii) levels adjustment increases contrast, by lightening the background and darkening the nanoparticles. (iii) Unsharp mask is used to further enhance contrast between the nanoparticles and the background, but may also increase background noise, which is eliminated using a gaussian blur. Throughout the many steps, every effort is taken to avoid distorting the nanoparticle size distribution.

The digitally enhanced image is then opened in the software Image J and threshold adjusted to highlight the nanoparticles over the background and then automated size analysis is carried out. Because nanoparticle aggregates and background noise can influence particle size measurements, nanoparticles with a circularity less than 0.75 (1 being a perfect circle) are removed as possible aggregates. This series of steps is carried out for each of the obtained images, and the average core diameter and size-distribution is calculated in Excel.

Though every step of the process may introduce some variability in the observed core sizes, the Hutchison lab has worked very hard to ensure that size analysis is carried out in a uniform fashion over all nanoparticle samples in order to reduce this variability.

Overview of Dissertation

In previous sections, the concepts of well-defined nanomaterials in general and well-defined gold nanoparticles specifically were developed. Despite much progress in the last few decades, significant challenges remain in obtaining well-defined gold nanoparticle samples. Methods for preparing gold nanoparticles with decreased size and shape dispersity and increased purity are required to ensure that the promise of gold nanoparticles in future technologies is met. In this dissertation, two techniques, diafiltration and aptamer mediated synthesis, are proposed as methods for achieving the goals of well-defined gold nanoparticle samples.

Diafiltration is a membrane-based method wherein pore size dictates the retention and elution of material from a sample, as depicted in Figure 1.17. This approach offers the opportunity to consolidate purification and separation based upon size into a single

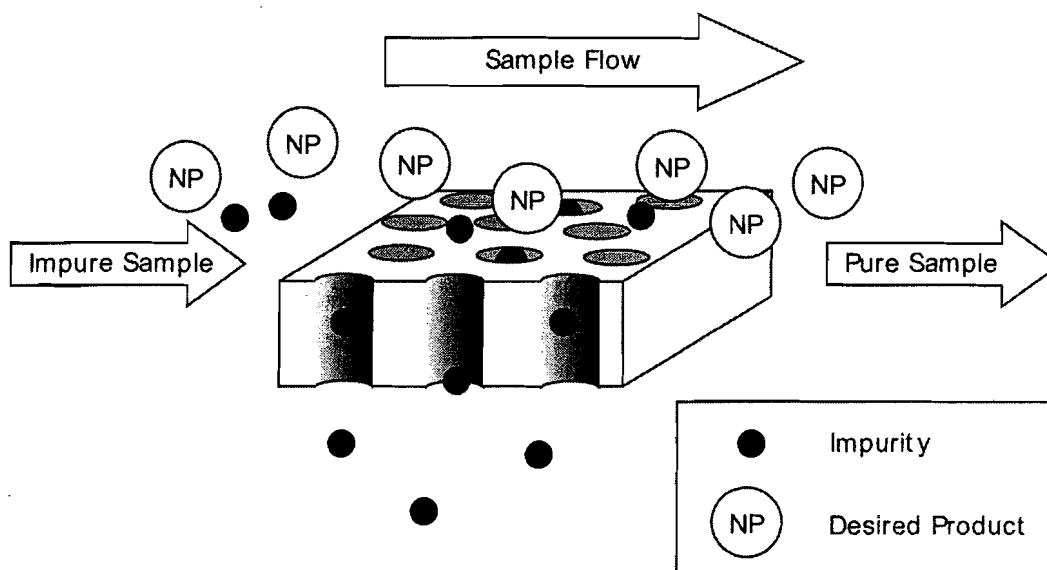


Figure 1.17. Schematic of the diafiltration process, showing small impurity elution and larger nanoparticle retention.

step, making diafiltration more efficient than any combination of previously reported techniques. Due to simple equipment requirements and the scalability of the technique, diafiltration is affordable, convenient and versatile. Furthermore, organic solvent dependence is reduced, contributing to greener nanoparticle syntheses.

In Chapter II (published and co-authored with Gerd Woehrle), the use of diafiltration for the purification and size separation of water-soluble gold nanoparticles is introduced. In the chapter, 3-nm gold nanoparticles are purified via numerous routes. The purity obtained for each method is compared to that obtained with diafiltration, showing that diafiltration offers the highest available purity for these materials. It is also shown that diafiltration is useful for the separation of bimodal distributions of gold nanoparticles and a promising technique for the fractionation of polydisperse nanoparticle samples. This early work has led to more recent preliminary work, outlined in Chapter III (co-authored with Matt O'Conner), where diafiltration is utilized as part of an overall scheme for increasing the yields of linked nanoparticle structures. Previously reported procedures lead to yields of 10-15% of linked structures. Using diafiltration, we are able to increase this yield to ~36%, with possible future improvements. Taken together, these two chapters provide ample evidence that diafiltration is well-suited for the preparation of well-defined gold nanoparticles in terms of size and purity, as well as for the isolation of linked gold nanoparticle structures.

The use of biomolecules, either peptide or nucleotide aptamers, for the synthesis of nanomaterials has garnered significant recent interest (Figure 1.18). There exist many examples from nature of biomineralization leading to control over feature size down to

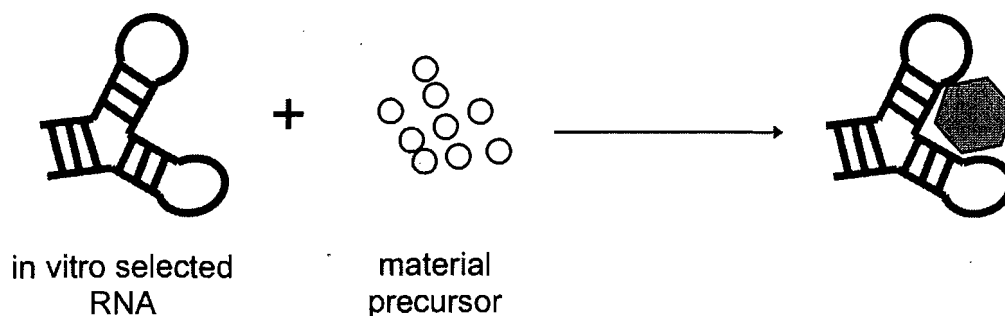


Figure 1.18. Illustration showing the synthesis of a hexagonal material using an RNA aptamer.

the nanoscale. Based upon these observations, it has been postulated that in vitro evolution of biomolecules for the express purpose of materials synthesis will allow for similar control over materials relevant for technological applications. These concepts are explored in Chapters IV through VI.

Chapter IV serves as a general introduction and review of in vitro selection for materials applications. In this chapter, the technique of in vitro selection is discussed, both for peptides and for nucleotides. Several examples from the recent literature are explored in terms of their contributions to the field. Current challenges facing in vitro selection for materials applications are discussed, culminating in several recommendations for advancing the field of in vitro selection for materials applications.

In Chapter V (co-authored with Amy Mahady), a novel technique useful for carrying out in vitro selection for materials, in vitro selection on surfaces (ISOS), is described. Using this technique, aptamers that bind to planar gold surfaces are identified and characterized using several techniques. This work is followed up in Chapter VI with the preliminary studies into the synthesis of different solution and surface-based gold nanoparticles using aptamers isolated via the in vitro selection on surfaces process.

CHAPTER II
RAPID PURIFICATION AND SIZE SEPARATION OF GOLD NANOPARTICLES
VIA DIAFILTRATION

Reproduced with permission from Sweeney, S. F.; Woehrle, G. H.; Hutchison, J. E. *J. Am. Chem. Soc.* **2006**, *128*, 3190-3197. Copyright 2006 American Chemical Society

Introduction

Development of methods that provide convenient access to ligand stabilized nanoparticles, offer greater control of structural definition and can be conducted at larger scales is becoming increasingly important for fundamental studies¹⁻⁵ and applications⁶⁻¹³ of nanoparticles. In particular, a high degree of purity and monodispersity are often crucial as these variables can complicate the assessment of structure-function relationships, confound electronic and optical measurements or impede the self-assembly processes by which nanoscaled structures are prepared.^{14,15} Although a number of syntheses of gold nanoparticles have been developed that allow for the preparation of nanoparticles of varying core dimension and surface functionality,¹⁶⁻²² a significant challenge remains in developing strategies for the preparation of nanoparticles of high purity (i.e., free of excess ligand, salt and starting material) and that exhibit low polydispersity. An additional challenge remains in the removal of nanoparticle monomers and aggregates from well-defined self-assembled nanoparticle superstructures.^{23,24}

The influence of purity on the chemistry and properties of nanoparticles is often overlooked; however, recent results indicate that the extent of purification can have a significant impact. Murray et al. have recently reported the effects of purification on the optical properties of CdSe nanoparticles, showing that PL intensity and peak location changes with differing concentration of free ligand in solution.²⁵ Ploehn has reported that the extent of purification of dendrimer encapsulated Pt nanoparticles can bias size determination via AFM.²⁶ We have recently shown that the self assembly of gold nanoparticles in 1D and 2D arrays is dependent upon the purity of the gold nanoparticles.^{14, 15} It is also known that gold nanoparticles in the presence of excess thiol ligand (as with ligand exchange) will rapidly decompose.²⁷ These results underscore the necessity of identifying convenient, efficient and more stringent purification methods for nanoparticle samples.

The purification of water-soluble gold nanoparticles is particularly difficult because the nanoparticles and the impurities have similar solubility, often making standard purification techniques (i.e. precipitation, extraction, chromatography, centrifugation or dialysis) inadequate or inefficient.^{16, 20, 21, 28} Although reasonable purity is afforded via these methods, the nanoparticles remain contaminated with precursor molecules, e.g., salts and free ligand. In addition, conventional purification methods do not address several significant challenges, namely: large volumes of organic waste, the high cost of chromatography supports, time intensiveness and the ability to reasonably prepare large quantities of nanoparticles. Finally, most purification schemes are

developed for one type of nanoparticle and are often not applicable for the purification of nanoparticles with differing core or ligand shell properties.

Similar, but often more challenging, issues are faced in approaches for decreasing the polydispersity of nanoparticle samples. Particle size and size dispersity can be controlled to a certain extent by synthetic methods, such as deliberate variation of the gold to ligand ratio¹⁹ and dendrimer encapsulation;²⁹⁻³¹ however, these methods are often sensitive to minute changes in reaction conditions. Centrifugation,³² electrophoresis,^{33, 34} fractional crystallization,³⁵ chromatography,^{32, 36-38} stirred-cell ultrafiltration³⁹ and size-dependent solubility^{35, 40} have also been reported for size-based separation.

Unfortunately, the fractionation of nanoparticle samples by these methods is often dependent upon specific core or ligand shell properties, time-consuming, difficult and expensive.

Diafiltration offers a versatile alternative to the methods described above for the purification and size separation of nanoscale materials. Though not yet reported for the preparation of water-soluble gold nanoparticles, diafiltration has been used frequently for biological^{41, 42} and colloidal applications.^{43, 44} Diafiltration is a membrane-based method wherein pore size dictates the retention and elution of material from a sample, as depicted in Figure 2.1. This approach offers the opportunity to consolidate purification and size-separation into a single step, making diafiltration more efficient than any combination of previously reported techniques. Due to simple equipment requirements and the scalability⁴⁵ of the technique, diafiltration is affordable, convenient and versatile.

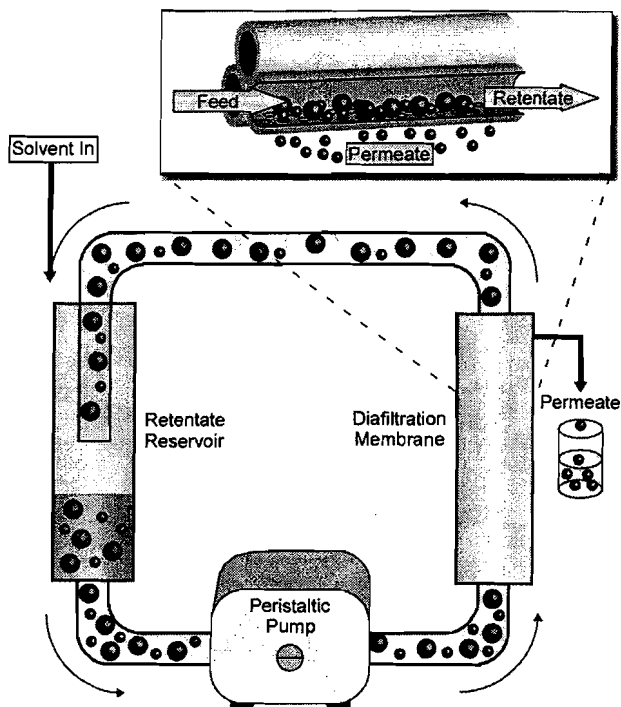


Figure 2.1. Schematic of the continuous diafiltration setup used in this study. Sample and make-up solution are introduced to the retentate reservoir. The solution is pumped by the peristaltic pump through the diafiltration membrane. Small molecule impurities or small nanoparticles (blue) are eluted in the permeate, while the large nanoparticles (purple) are retained. The expanded view is of a hollow-fiber type diafiltration membrane, and depicts the elution of small impurities and nanoparticles and the retention of larger particles.

Furthermore, the membranes can be reused and organic solvent dependence is reduced, contributing to greener nanoparticle syntheses.^{45, 46}

In this article, we report that diafiltration is a rapid and convenient approach to the preparation of higher purity water-soluble gold nanoparticles and has considerable potential as a method for the size separation of heterogeneous nanoparticle samples. We compare diafiltration to conventional purification methods, demonstrating through XPS, TGA and ¹H-NMR analyses that diafiltration yields nanoparticles of higher purity, in less time (~15 minutes vs. 3 days) and with less waste (4 L H₂O/g product vs. 15 L solvent/g product) than conventional methods such as dialysis extractions, centrifugation and

chromatography. The size separation of a mixture of 1.5 and 3-nm nanoparticles is also presented, demonstrating through TEM and UV-vis analyses the utility of diafiltration for separating nanomaterials of disparate core dimensions. Finally, we report on the fractionation of a polydisperse 3-nm sample into four fractions of differing mean core diameter. Analysis of these fractions by UV-vis and TEM demonstrates the potential of diafiltration for fractionation and suggests areas of improvement in the pore morphology of diafiltration membranes. Our experiments demonstrate that diafiltration is an efficient and versatile approach for the consistent preparation of nanoparticle samples that exhibit a high degree of purity and that this method may prove useful for the size separation of nanoparticle samples.

Experimental Section

Materials. Hydrogen tetrachloroaurate ($\text{HAuCl}_4 \cdot 3\text{H}_2\text{O}$) was obtained from Strem Chemicals, Inc. and used as received. Nanopure water (18.2 $\text{M}\Omega$ cm resistivity) was prepared using a Barnstead NANOpure filtration system and used for all aqueous samples. The thiol ligands 2-(2-mercaptoethoxy)ethanol (**1**) and 2-[2-(2-mercaptoethoxy)ethoxy]ethanol (**2**) were synthesized according to known procedures.²⁷ Sephadex LH-20 was obtained from GE Healthcare/Amersham Biosciences. 15 kDa dialysis membranes (SpectraPor) were obtained from Spectrum. 10 kDa, 30 kDa, 50 kDa and 70 kDa MWCO poly(sulfone) diafiltration membranes (MiniMate) were obtained from Pall. All other reagents and solvents were purchased from Aldrich or Mallinkrodt and used as received.

Analytical Procedures. X-Ray photoelectron spectroscopy (XPS) was performed on a Kratos HSi instrument operating at a base pressure of $\sim 10^{-8}$ mmHg using monochromatic Al K α radiation at 15 mA and 13.5 kV. Nanoparticles were drop cast from concentrated aqueous solution onto a clean⁴⁸ silicon wafer. Samples were charge compensated and binding energies were referenced to carbon 1s at 284.4 eV. UV-visible spectroscopy was performed on an Ocean Optics USB2000 spectrometer using 1 cm disposable plastic cuvettes. Thermogravimetric analysis (TGA) was performed on a Hi-Res TGA 2950 Thermogravimetric Analyzer. Lyophilized nanoparticle samples (3-5 mg) were placed into Al pans and heated at 10 °C/min to 110 °C followed by a 10 min isotherm to remove any remaining solvent. The samples were then heated at 5 °C/min to 500 °C followed by a 20 min isotherm to ensure no further mass loss. Nuclear magnetic resonance (NMR) spectra were collected at 25 °C on a Varian Unity Inova 300 MHz instrument. Transmission electron microscopy (TEM) was performed on a Phillips CM-12 microscope operating at 120 kV accelerating voltage. Aliquots of dilute nanoparticle samples (10 μ L) were aerosoled onto SiO $_x$ coated 400-mesh copper TEM grids (Ted Pella) and dried under ambient conditions prior to inspection via TEM. Images were recorded and processed as described previously.⁴⁷

General Diafiltration Procedure. The diafiltration setup used for the experiments reported herein is shown in Figure 2.1. Following preparation and dissolution in water, nanoparticle samples are transferred to the reservoir (a 20 mL syringe with the plunger removed). The sample is drawn from the reservoir and into the diafiltration membrane through a peristaltic pump. The speed of the pump is slowly

increased to the maximum rate, equilibrating the feed pressure to the membrane at ~100 kPa. The rate of water addition to the reservoir is monitored and adjusted so that it equals the rate of elution. When the volume of material eluted is equal to the hold-up volume in the reservoir, this is considered one diafiltration volume. The diafiltration is continued through a number of volumes until the purification or size separation is complete. The relationship between the percent purity (%P) and the number of diafiltration volumes (V_D) is shown in Equation 1,

$$\%P = (1 - e^{-V_D(1-\sigma)}) \times 100\% \quad (1)$$

where σ is the rejection coefficient, which is determined experimentally for different solutes and affected by pore morphology, nanoparticle properties such as core diameter and surface functionality and solution properties such as ionic strength. In the case of purification, $\sigma = 0$, meaning that five diafiltration volumes are necessary to see complete purification. In the case of size separation, 15 volumes ($\sigma = 0.33$) are often necessary.

Sample Descriptions. Samples for the purification experiment were prepared and stabilized using ligand **2** and samples for the size separation experiments were prepared using ligand **1**. All diafiltered nanoparticle samples are named using the following scheme: Au_x -*Descriptor*, where x is the mean core size of the particle and *Descriptor* defines the membrane pore size and whether the sample is the permeate or retentate. For example, $Au_{3.0}$ -70R describes a 3.0-nm gold nanoparticle sample that is the retentate of a 70 kDa diafiltration. Exceptions to this scheme are crude nanoparticle samples which are named Au_x -Crude, samples purified via extraction, chromatography and centrifugation, which are named Au_x -ECC, dialyzed samples which are named Au_x -D,

triphenylphosphine stabilized particles which are named Au_x-TPP and the mixed 1.5 and 3-nm sample which is named Au_x-Mix.

Preparation of Water-Soluble ~3-nm Gold Nanoparticles (Au₃-Crude).

Water-soluble 3-nm gold nanoparticles were synthesized using a procedure developed by Brust et al. with minor modifications.²⁰ Briefly, in a 100 mL round bottom flask were dissolved **1** (0.0131 g, 0.107 mmol) or **2** (0.0178, 0.107 mmol) and HAuCl₄ (0.1094 g, 0.322 mmol) in 50 mL of 2-propanol, yielding a yellow solution. To this solution, 5 mL of a 3.5 M NaBH₄ solution in methanol was added rapidly with stirring, resulting in an immediate color change from yellow to dark purple. The solution was allowed to stir under ambient conditions for 2 h and then filtered through a 150 mL 60F fritted funnel. The resulting purple solid was collected from the frit and dissolved in 20 mL of water.

Water-Soluble ~3-nm Gold Nanoparticles Purified via Extraction, Chromatography and Ultracentrifugation (Au₃-ECC). The water soluble nanoparticles Au₃-Crude (100 mg) were extracted with 5 × 20 mL of dichloromethane to remove excess ligand and disulfide. The aqueous layer was isolated and dried overnight under a stream of nitrogen. The resultant solid was dissolved in a minimum amount of water and purified via gel permeation chromatography (Sephadex LH-20, eluent H₂O) to further remove salts and organic impurities. Following chromatography, the nanoparticles were centrifuged (and the supernatant removed) twice at 200,000 × g for 10 h at 4 °C to remove any remaining impurities. The resultant nanoparticles were lyophilized and analyzed by XPS, NMR, TEM and TGA.

Water-Soluble ~3-nm Gold Nanoparticles Purified via Dialysis (Au₃-D). The water soluble nanoparticles Au₃-Crude (50 mg) in 20 mL of water were transferred to a 15 kDa dialysis membrane and dialyzed with 3 × 3 L of water for 6 h each. Following dialysis, water was removed via rotary evaporation and the particles were resuspended in 10 mL of water. The resultant nanoparticles were lyophilized and analyzed via XPS, NMR, TEM and TGA.

Water-Soluble ~3-nm Gold Nanoparticles Purified via Diafiltration (Au₃-70R). The water soluble nanoparticles Au₃-Crude (100 mg) were diafiltered with 5 × 20 mL of water using a 70 kDa diafiltration membrane. The solution was concentrated to 10 mL by ceasing make-up flow and the nanoparticles were collected by pumping the solution into a 20 mL scintillation vial. The membrane was flushed with an additional 3-5 mL of water which was combined with the original 10 mL. The resultant nanoparticles were lyophilized and analyzed by XPS, NMR, TEM and TGA.

Synthesis of Triphenylphosphine-stabilized 1.5-nm Nanoparticles (Au_{1.5}-TPP). Triphenyl-phosphine-stabilized nanoparticles, Au₁₀₁(PPh₃)₂₁Cl₅, were synthesized according to a previously described procedure.²¹

Water-Soluble 1.5-nm Gold Nanoparticles via Ligand Exchange (Au_{1.5}-10R).²⁷ Au_{1.5}-TPP (20 mg in 5 mL of CH₂Cl₂) and **1** (20 mg in 5 mL water) were stirred rapidly at room temperature for 6 h until the transfer of the darkly colored nanoparticles to the aqueous layer was complete. Upon completion of the exchange, the layers were separated and the residual CH₂Cl₂ was removed from the aqueous layer *in vacuo*. The

aqueous layer was diafiltered with 5×10 mL of water using a 10 kDa diafiltration membrane.

Separation of 1.5 and 3.1-nm Water-Soluble Nanoparticles via Diafiltration.

A mixture of Au_{1.5}-10R (3.9 mg) and Au_{3.1}-70R (39.1 mg) nanoparticles in 10 mL of water was diafiltered with 15×10 mL of water using a 50 kDa diafiltration membrane. At this point, the retentate (Au_{2.9}-50R) was collected as previously described and the combined permeate fractions were concentrated using a 10 kDa diafiltration membrane yielding Au_{1.5}-50P. TEM images and UV-vis spectra were obtained for the initial nanoparticles, the nanoparticle mixture, as well as for the permeate and retentate.

Fractional Separation of Water-Soluble 3-nm Gold Nanoparticles via Diafiltration. We prepared four nanoparticle fractions by performing a series of diafiltration steps using membranes of decreasing pore size. Following the preparation of Au_{2.9}-70R, the permeate Au_x-70P was concentrated and diafiltered with 15×20 mL of water using a 50 kDa diafiltration membrane. The retentate Au_{2.6}-50R was collected and the permeate Au_x-50P was concentrated and diafiltered with 15×20 mL of water using a 30 kDa diafiltration membrane. The retentate Au_{2.5}-30R was collected and the permeate Au_x-30P was concentrated on a 10 kDa diafiltration membrane yielding Au_{2.0}-10R. TEM images and UV-vis spectra were collected for samples Au_x-10R to 70R.

Results and Discussion

Sufficient purification of nanoparticle samples can often be more challenging than the preparation itself, involving tedious, time consuming and wasteful procedures such as extensive solvent washes and fractional crystallization. Yet, obtaining gold nanoparticle

samples that are free of impurities such as free ligand, precursor molecules, salts and undesired nanoparticles is necessary for many applications. In this section, we describe the results of studies aimed at evaluating the efficacy of diafiltration for (i) removal of small molecule impurities from gold nanoparticles, (ii) separation of a bimodal population of nanoparticles into the corresponding small and large fractions and (iii) the fractionation of a polydisperse nanoparticle sample.

Traditional Methods of Purification

Purification of the 2-[2-(2-mercaptoethoxy) ethoxy]ethanol 3-nm particles is typically achieved by precipitation in hexane followed by diethyl ether and ethyl acetate washes and finally ultracentrifugation twice at 60,000 rpm.²⁰ However, some impurities often remain after such treatments. Due to our interest in the properties and self-assembly of ligand-stabilized nanoparticles, we sought purification schemes that would yield higher purity nanoparticles in a more efficient fashion. As a first approach, we carried out a rigorous combination of extraction with CH_2Cl_2 , Sephadex chromatography and ultracentrifugation, each of which is considered a standard purification technique. A second approach, dialysis, has also been employed for purification. Dialysis is advantageous due to the fact that purification can be carried out using only water. Despite an improvement in purity over the literature method²⁰, these two approaches had some drawbacks that needed to be addressed: (1) Extractions are not generally applicable for the removal of free ligand, especially when the solubility of the ligand and ligand stabilized particle are similar. Additionally, while we've reduced the volume of organic solvent used, a more toxic halogenated solvent has been employed; (2) 3-nm

nanoparticles tend to irreversibly bind to the Sephadex chromatography support, decreasing the yield and limiting reuse of the chromatographic material; (3)

Ultracentrifugation can be difficult or impractical on larger scales and requires a significant time investment, increasing the time required for preparation of nanoparticle samples to 3 days; (4) Dialysis produces a large amount of aqueous waste and requires a significant time investment.

Diafiltration as an Approach to Nanoparticle Purification

To address the drawbacks of the standard purification techniques described above, we investigated a third approach, diafiltration, as a means of preparing pure nanoparticles while reducing solvent dependence, increasing yields and increasing the efficiency of the purification process. Diafiltration has been commonly used in the biological sciences for a number of applications.^{41, 42, 48, 49} Like dialysis, diafiltration membranes are rated by their nominal molecular weight cutoff (MWCO), wherein a 10 kDa membrane will retain 90% of a globular protein with a molecular weight >10 kDa.⁵⁰ In the case of nanoparticles, the MWCO can be correlated to such nanoparticle properties as core size, ligand shell thickness and hydrodynamic radius, and to solution properties such as pH and ionic strength. In our studies, we have found that membranes with a MWCO of 10-100 kDa are appropriate for neutral, water-soluble nanoparticles with a core diameter of 1 to 5-nm. Unlike other membrane filtration techniques, such as dialysis or stirred-cell ultrafiltration, diafiltration (Figure 2.1) is considered a continuous flow process, wherein the sample to be purified or separated is continually passed over the membrane surface. While traditional ultrafiltration can be hindered by the buildup of material on the

membrane surface, the continuous flow and constant volume of diafiltration aid in the decreased incidence of membrane fouling. As compared to dialysis, wherein filtration occurs via passive means, hydrostatic pressure as a result of continuous flow is the driving force behind diafiltration. Additionally, each diafilter contains a number of membrane surfaces, greatly enhancing the surface area available for filtration. Due to the continuous flow and high surface area of this technique, diafiltration allows for very efficient and rapid purification and size separation.^{50, 51}

Diafiltration vs. Conventional Methods for Nanoparticle Purification

In order to compare the effectiveness of diafiltration to a conventional purification scheme involving extraction, chromatography and centrifugation and to dialysis, 3-nm gold nanoparticles passivated with ethylene glycol ligand **2** were purified by one of the three methods and analyzed via NMR, TGA and XPS.

The amount of organic impurities (thiol and disulfide) in the crude nanoparticles, as well as the conventionally purified, dialyzed and diafiltered samples, was assessed via ¹H-NMR spectroscopy (Figure 2.2.). The spectrum of free ligand **2** shows a triplet at 2.60 ppm, corresponding to the methylene protons α to the thiol and peaks between 3.46 and 3.62 that correspond to the remaining methylene protons. The spectrum of Au_{2,9}-Crude exhibits a characteristic broadening of the baseline as is expected for the presence of nanoparticle bound ligand; however, the sharp signals between 3.20 and 3.92 ppm correspond to a significant amount of free ligand and disulfide in the sample. The NMR of Au_{2,7}-D and Au_{2,8}-ECC show significantly reduced fine structure indicating near-complete removal of free ligand; however, some disulfide remains as indicated by the

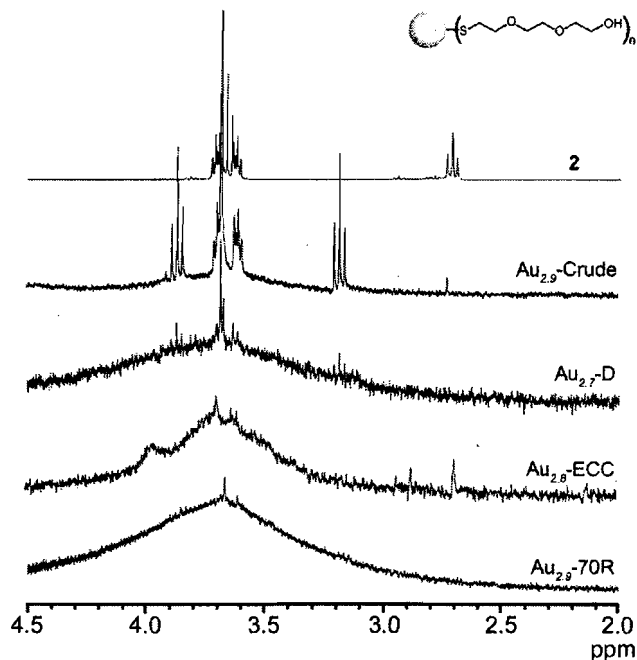


Figure 2.2. ^1H -NMR spectra of ligand **2**, crude nanoparticles ($\text{Au}_{2.9}$ -Crude), dialyzed nanoparticles ($\text{Au}_{2.7}$ -D), nanoparticles purified via extraction, chromatography and centrifugation ($\text{Au}_{2.8}$ -ECC) and nanoparticles purified via diafiltration $\text{Au}_{2.9}$ -70R. Fine structure in the conventionally purified samples indicates free thiol or disulfide. The absence of fine structure in the diafiltered sample indicates a concentration of free ligand and disulfide below the detection limit of the instrument.

peak at 3.92 ppm. In contrast, The NMR spectrum of $\text{Au}_{2.9}$ -70R lacks any significant peaks, indicating a free ligand concentration under the detection limit of the NMR.

The extent of purification by each method was further assessed by XPS and TGA (Table 2.1). TGA can be used to quantify the percent volatile component in a sample and to distinguish between bound and unbound ligand in a sample based upon differences in the onset time of sample decomposition. A comparison of the total volatile component in $\text{Au}_{2.7}$ -D (9.9%), $\text{Au}_{2.8}$ -ECC (13.1%) and $\text{Au}_{2.9}$ -70R (7.8%) provides strong evidence for greater nanoparticle purity of the diafiltered sample. Calculation of the volatile component based upon a core diameter of 2.9-nm as determined by TEM gives $\sim 7.14\%$,

consistent with the TGA data for the diafiltered sample.¹⁹ The TGA traces for both the Au_{2.9}-Crude and Au_{2.8}-ECC samples show initial sharp decreases in mass between 120 and 200 °C, followed by a gradual mass loss up to 500 °C. The initial mass loss is likely due to free ligand in the sample, which is easily volatilized at lower temperatures. As the temperature increases beyond 200 °C, nanoparticle bound ligands desorb and are volatilized. In contrast, the diafiltered sample Au_{2.9}-70R shows a continuous decrease in sample mass over the entire TGA trace with the greatest change in mass occurring once the temperature reaches 200 °C. These results strongly indicate that the diafiltered sample contains no free ligand.

Table 2.1. TGA, XPS and TEM Results for Different Purification Methods

sample	TGA (%vol) ^a	XPS (atomic %)				TEM (d _{CORE} nm)
		Au 4f	S 2p	Na 1s	Cl 2p	
Au _{2.9} -Crude	10.5 ^a	4.1	0.9	38.7	8.4	2.9 ± 1.0
Au _{2.8} -ECC	13.1	48.3	6.9	20.6	24.2	2.8 ± 1.0
Au _{2.7} -D	9.9	85.82	14.18	— ^b	— ^b	2.7 ± 0.9
Au _{2.9} -70R	7.8	79.8	10.8	4.0	3.3	2.9 ± 0.7

^a Organic content in Au_{2.9}-Crude appears low due to the high concentration of salt in sample, as evidenced in XPS. ^b Concentration below the detection limits.

We further employed quantitative XPS analysis as a method for determining the relative atomic percentage of Au, S, Na and Cl in each sample, allowing for the measurement of both free and bound ligand as well as salts in the sample. The Au_{2.9}-Crude, Au_{2.8}-ECC, Au_{2.7}-D and Au_{2.9}-70R samples exhibit Au:S ratios of 4.6:1, 7.0:1, 6.1:1 and 7.4:1 respectively, further demonstrating that Au_{2.9}-70R has the lowest

concentration of free thiol. The atomic percentage of both Na and Cl is also reduced in Au_{2.9}-70R compared to Au_{2.8}-ECC and within experimental error of Au_{2.7}-D, demonstrating the ability of diafiltration to remove not only free ligand, but also excess salt in the samples.

Analysis of the NMR, TGA and XPS data clearly demonstrates that diafiltration allows for the preparation of nanoparticle samples with a higher degree of purity than is available by conventional means, showing in all cases impurity concentrations below that of conventionally prepared samples. This high degree of purity made possible by diafiltration has recently been exploited in the preparation of 1D and 2D self-assembled structures.^{14, 15} Our comparison further shows that diafiltration is more convenient, efficient and green than conventional purification, allowing for the removal of both free ligand and excess salts in a single purification step using only water. In addition, diafiltration is more rapid allowing for complete purification in as little as 15 minutes compared with up to three days for conventional approaches to purification. Thus, diafiltration offers a much more attractive route to the preparation of high purity nanoparticles than is available by any previously reported method.

Size Separation of 1.5 and 3-nm Nanoparticles

In addition to its utility for purifications, we found that diafiltration also reduces the polydispersity of as-synthesized nanoparticle samples. While using a 70 kDa diafiltration membrane for the purification of 3-nm nanoparticles, a fraction (as much as 50%) of the nanoparticles passed through the membrane. TEM analysis of the resultant nanoparticles showed a decreased polydispersity over nanoparticles purified by

conventional methods (Table 1). Based upon these results, we explored the possibility of using diafiltration for the deliberate separation of nanoparticle samples.

As an initial experiment, we investigated the separation of a bimodal mixture of nanoparticles (Au_x -Mix) prepared from purified 1.5 and 3.1-nm nanoparticles. A 1:1 molar mixture of $Au_{1.5}$ -10R and $Au_{3.1}$ -70R was prepared and diafiltered with 15×10 mL of water using a 50 kDa diafiltration membrane. Following diafiltration, the permeate and retentate fractions were analyzed via TEM and UV-vis and the data compared to those for $Au_{3.1}$ -70R, $Au_{1.5}$ -10R and Au_x -Mix.

We used the intensity, peak width and peak location (λ_{MAX}) of the plasmon peak in the UV-vis spectra as an indicator of the core size of each sample (Figures 2.3A and 2.3B). The initial 3.1-nm sample ($Au_{3.1}$ -70R) exhibits the characteristic plasmon resonance expected for a nanoparticle with a large core diameter.⁵² In contrast, $Au_{1.5}$ -10R lacks a plasmon peak, indicative of sub-2-nm gold particles (Figure 2.3A). The spectrum of Au_x -Mix is similar to the initial 3.1-nm sample but with a slightly broadened plasmon peak due to the presence of an equivalent of 1.5-nm particles, as expected for a more polydisperse sample.⁵² Following separation of the mixture using diafiltration, the UV-vis spectrum of the retentate $Au_{2.9}$ -50R exhibits the plasmon absorption expected for large nanoparticles (Figure 2.3B). The permeate shows no plasmon peak in the UV-vis spectrum, consistent with the smaller core size of the particles that have been eluted during diafiltration.

The successful separation of the bimodal nanoparticle mixture suggested by UV-vis spectroscopy was confirmed by TEM analysis of the core sizes (Figures 2.3C-F).

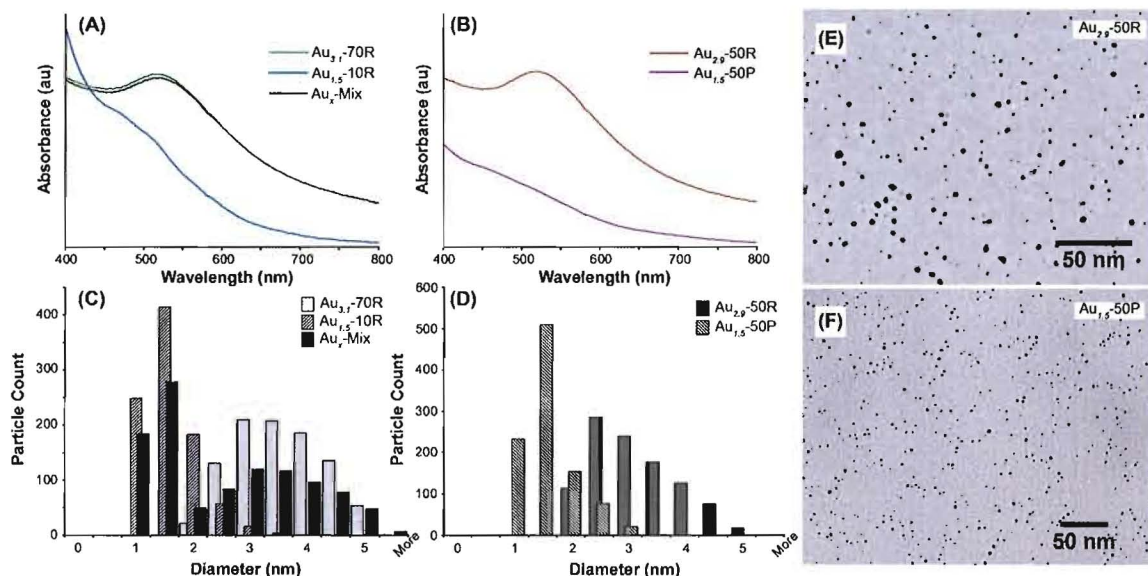


Figure 2.3. (A) UV-vis spectra for the initial samples Au_{3.1}-70R, Au_{1.5}-10R and the mixture Au_x-Mix. (B) UV-vis spectra of the separated fractions Au_{2.9}-50R and Au_{1.5}-50P. (C) Stacked TEM histograms for the initial samples Au_{3.1}-70R, Au_{1.5}-10R and mixture Au_x-Mix. (D) Stacked TEM histograms for the separated fractions Au_{2.9}-50R and Au_{1.5}-50P. (E and F) Representative TEM images of the separated fractions Au_{2.9}-50R and Au_{1.5}-50P.

Figure 2.3C shows the size distributions for the initial 1.5 and 3.1-nm samples and the mixed sample, which has the expected bimodal distribution. Following diafiltration, the histograms of Au_{2.9}-50R and Au_{1.5}-50P are unimodal (Figure 2.3D) with core diameters of 2.9 ± 1.0 and 1.5 ± 0.5 nm, showing successful separation into fractions similar to the initial nanoparticle samples. The slight decrease in core size of the retentate in comparison to the initial 3.1-nm sample is due to some fraction of larger particles from the 1.5-nm sample being retained. Given the initial overlap of the particle distributions, minor changes in the mean core size and distribution are expected.

The performance of the diafiltration approach for this type of size separation is remarkable due to the high resolution of the separation and because it can be carried out on the bench top using simple equipment and water. The ease of this separation as well as

the versatility afforded in the separation of water-soluble materials with as little as 1.5-nm size difference will make diafiltration an invaluable tool in a number of applications, from synthesis and catalysis to assessing the biological impacts of nanoparticles.

Fractionation of Nanoparticles

Based upon the performance observed in our original separation experiment, we attempted to use diafiltration for the fractionation of a polydisperse gold nanoparticle sample. Because standard nanoparticle preparations yield nanoparticles with a polydispersity of up to 30 percent, the ability to fractionate samples into several monodisperse fractions would be very valuable. For example, by removing the upper and lower edges of a size distribution, samples approaching monodispersity could be envisaged.

Figure 2.4 outlines the fractionation of a polydisperse nanoparticle sample using multiple diafiltration steps. In the first step, the crude nanoparticles are diafiltered for 15 volumes using a 70 kDa diafiltration membrane to remove the largest fraction of nanoparticles and aggregates yielding Au_{2.9}-70R. The process is repeated, each time concentrating and diafiltering the permeate of the previous step using a smaller MWCO membrane (i.e. 50 kDa, 30 kDa). The final diafiltration step using a 10 kDa diafiltration membrane serves as a purification of the smallest core size fraction.

Size separation can be observed visually through a change in color for each fraction, with the 70 kDa fraction having a distinct purple hue characteristic of large gold nanoparticles and the 10 kDa fraction having the brown color of smaller gold nanoparticles. Normalized UV-vis spectra for each of the diafiltered fractions are shown

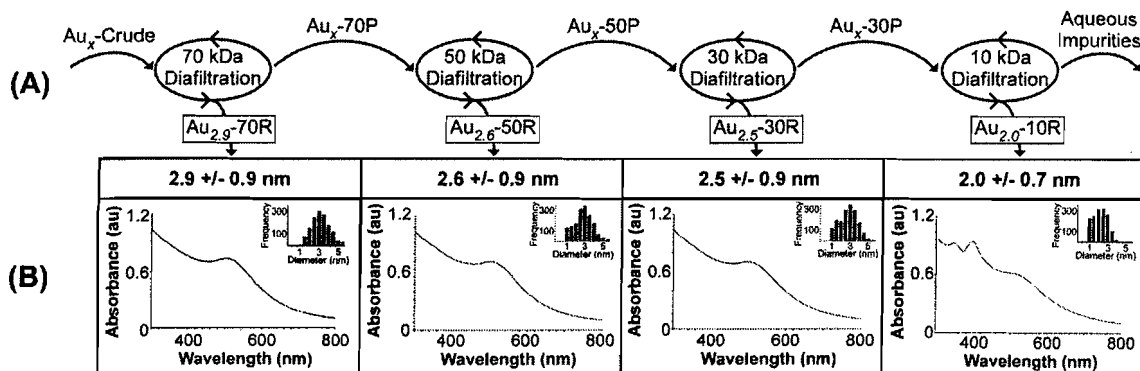


Figure 2.4. (A) Diafiltration scheme used for obtaining nanoparticle fractions.⁵⁸ Following each diafiltration step, the retentate is analyzed via UV/vis and TEM and the permeate is further diafiltered on a smaller MWCO membrane. (B) Summary UV/vis and TEM data for each fraction. With each decrease in pore size, the average core size decreases, with corresponding blue shifts and broadening of the plasmon resonance peak in the UV/vis.

in Figure 2.4B and Figure A.5. The spectrum of the 70 kDa fraction exhibits the most pronounced plasmon peak with a λ_{MAX} of 527 nm. The 50 kDa spectrum has a λ_{MAX} of 522 nm, whereas λ_{MAX} has shifted to 521 nm for the 30 kDa fraction, and both have broadened, indicating that the average core size decreases from the 70 kDa fraction to the 30 kDa fraction. The largest change in the plasmon peak can be seen for the 10 kDa fraction which is significantly broadened indicating a smaller mean core size; additional peaks at 350 nm and 410 nm suggest the presence of nanoparticles of ~1-nm diameter.⁵³

We further evaluated the core diameter and size distribution for each fraction via TEM analysis (Figure 2.4, Figure A.6). In agreement with the UV-vis data, the 70 kDa retentate fraction exhibits the largest core size with an average core diameter of 2.9 ± 0.9 nm. As the MWCO of the membranes decrease the average core diameters also decrease to 2.6 ± 0.9 nm and 2.5 ± 0.9 for the 50 kDa and 30 kDa retentate samples respectively. The 10 kDa retentate fraction displays the greatest decrease in core size and polydispersity with an average diameter of 2.0 ± 0.7 nm.

While we have shown that the separation of 1.5 and 3-nm nanoparticles is possible using diafiltration, the results of the fractionation reveal the lower limits of diafiltration's ability. Though a decrease in average core diameter is observed, the size dispersity of the fractions is higher than desired when using commercial diafiltration membranes. Two main factors contribute to the polydispersity of the samples. First, irregularities in the membrane pores lead to an increase in the passage of nanoparticles into the permeate that are larger than expected for a given MWCO. Second, the similar size of the nanoparticles and the membrane pores leads to a lower rate of small particle removal per volume (increased σ). A further consequence of the similar size is membrane fouling due to the occlusion of nanoparticles within the membrane pores, decreasing separation efficiency. Electrostatic repulsion or attraction between charged particles and the membrane surface can similarly affect σ or lead to membrane fouling. Though diafiltration remains a promising approach for convenient nanoparticle fractionation, there is a clear need for the development of membranes with appropriate material and pore characteristics for preparing monodisperse nanoparticle fractions.

Conclusion

In this article we have demonstrated that diafiltration is capable of efficient and convenient purification and size separation. Our experiments have shown that diafiltration is particularly well suited for the purification of aqueous nanoparticle samples, removing all detectable organic impurities and salts, and surpassing the purity achievable via conventional means. Diafiltration is an efficient, rapid and versatile purification method, allowing for the complete purification of any small, water soluble

nanoparticle in as little as 15 minutes. In addition to using a more benign solvent (water) and reducing the volume of organic solvents used in the nanoparticle preparation, the diafiltration membranes are fairly inexpensive for routine use and can be reused with proper care, making diafiltration a greener purification scheme than the other methods discussed. The higher purity afforded by diafiltration will allow for more precise determination of electronic and optical properties, easier assessment of structure-function relationships in toxicology studies and greater reproducibility in the self-assembly of nanoparticles. Additionally, the ability to separate small molecules from nanoparticles should allow for the assessment of catalytic activity and allow for the isolation of catalysis products from nanoparticles.

Our results have also demonstrated that diafiltration is capable of separating 1.5 and 3-nm nanoparticles. Though the σ values for this separation are larger than for purification, leading to some polydispersity, diafiltration remains more efficient and convenient than other reported techniques for the separation of similar samples. The ability to quickly size separate samples is a powerful tool and can be exploited to separate a wide number of nanoscaled materials, allowing for access to and the characterization of materials never before isolated. For example, heterogeneous 3D structures formed from the self-assembly of semi-conducting and metal nanoparticles could be separated from individual nanoparticle monomers. Other possible applications include the separation of excess nanoparticles from biological substrates or the separation of seed particles from nanorods, cubes or wires.

We expect that these results will establish diafiltration as a convenient and powerful tool for the preparation of pure nanoparticle samples in a simple, efficient, scalable⁴⁵ and green fashion and will allow for convenient access to a wide variety of nanoscaled materials.

TGA and UV-vis data as well as additional TEM images/analysis are available in Appendix A.

Bridge

Our success in the use of diafiltration for the purification and size separation of gold nanoparticles has led to a number of advancements not otherwise possible. We have seen an increased ability to self-assemble gold nanoparticles into arrays for electronic characterization, an enhanced ability to screen the interactions between gold nanoparticles and biological substrates (nanotoxicology) and diafiltration has been used to gain access to functionalized citrate nanoparticles. We have recently begun work on isolating linked nanoparticles structures using diafiltration. Chapter III outlines our efforts thus far.

CHAPTER III

ISOLATION OF LINKED GOLD NANOPARTICLES VIA DIAFILTRATION

Co-authored material with M. J. O'Conner, M. M. Haley and J. E. Hutchison. M. J. O'Conner was responsible for carrying out organic linker synthesis. I carried out all other experimental work and writing. Remaining co-authors provided editorial assistance.

Introduction

Nanoparticle homo- and hetero- structures, such as dimers and trimers, represent an emerging class of composite materials that are expected to have technologically useful electronic and optical characteristics.¹ Specifically, plasmon-plasmon² coupling between metal nanoparticles and plasmon-exciton coupling³ between metal and semiconducting nanoparticles are being actively investigated. Although a number of methods have been demonstrated for the preparation of linked nanoparticle structures, such as dimers and trimers, they are often low yielding and lead to mixed populations of monomers, aggregates and the desired structure.⁴ The presence of these impurities impedes the measurement of the electronic and optical properties of the assembled structures. Although a number of methods have been proposed for assembly, some deficiencies remain: (i) synthesis of the required linker can be difficult for routine preparations, (ii) linked nanoparticle preparations often result in mixed populations of monomers, linked structures and aggregates and (iii) the linked structures are often prepared using citrate nanoparticles and are not functionalized, limiting their utility. Methods that provide

convenient access to the desired nanostructures with useful functionality would greatly enhance our ability to measure their unique properties and allow for the further development of linked structures for a number of applications.

The assembly of nanoparticles into dimeric and trimeric structures is usually achieved by using multi-functional linkers. Feldheim et al. have shown that citrate stabilized gold nanoparticles can be linked using rigid phenylethynyl di-, tri- and tetrathiols, yielding the resultant dimers, trimers and tetramers in ~10% yield.⁴ Recent work has shown that nanoparticles can be monofunctionalized with carboxylic acid peripheral groups using Wang resins and subsequently linked using diamines to form well-defined dimer structures.⁵ Alivisatos et al. have developed methods for the assembly of nanoparticles into linked structures through the use of complimentary base-pairing between DNA molecules.⁶ Still others have formed nanocomposite agglomerates and aggregates through the assembly of nanoparticles without regard for what type of structures are formed.⁷ Despite multiple preparation methods, yields of the desired linked structure are often very low.

This deficiency was quickly realized and methods for isolating or harvesting the desired nanostructures from monomers and aggregates were developed. These methods typically rely upon the use of size-exclusion chromatography or centrifugation. In the case of size-exclusion chromatography, yields of up to 55% of dimeric, 20% monomer and 25% undefined have been obtained.⁸ Although these methods are useful, they rely upon costly chromatography supports, can require significant time, may not be applicable for the preparation of large quantities of materials and may not be applicable for the wide

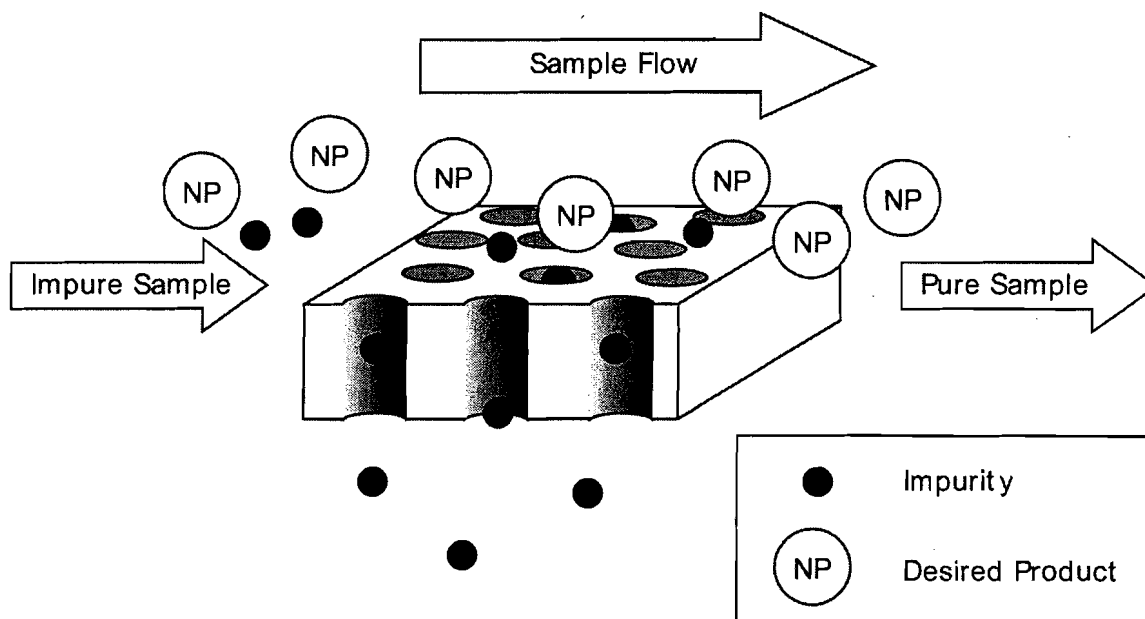


Figure 3.1. Illustration of diafiltration, showing the elution of small impurities (organics, salts, nanoparticles) from the desired products.

variety of nanostructures that are prepared. Furthermore, it has been shown that nanoparticles will often irreversibly aggregate onto chromatography supports. To avoid some of these roadblocks, we sought to leverage our existing diafiltration methods for the isolation of such nanoparticle structures.

Diafiltration is a membrane-based method wherein pore size dictates the retention and elution of material from a sample (Figure 3.1). In the previous chapter, we showed that diafiltration was useful for both the removal of small molecule impurities as well as separating nanomaterials of disparate size. Based upon those results, we expected that diafiltration would allow for the isolation of gold nanoparticle trimers. In contrast to previously reported methods, diafiltration offers the opportunity to separate both monomers and aggregates from the desired structure using a single approach with the

additional benefits of fairly simple equipment requirements, scalability and convenience for rapid and routine separations.

Herein, we report (1) an improved, modular synthesis of rigid phenylethynyl trithiol ligands, first reported by Feldheim, for linking gold nanoparticles, (2) an improved two-step linking protocol for preparing functionalized trimeric nanoparticle structures using both 1.5 and 5-nm nanoparticles, and (3) the utilization of diafiltration to isolate linked nanoparticle structures. TEM analysis of the resultant nanoparticle structures indicates that the methods developed here may be a promising, general approach for the isolation of functionalized, linked nanoparticle structures.

Experimental Section

1-(4-(2-(trimethylsilyl)ethynyl)phenyl)-2-(piperidin-1-yl)diazene (4): A solution containing 11.58 g (36.7 mmol) of 1-(4-iodophenyl)-2-(piperidin-1-yl)diazene (**3**), 58 mg (0.073 mmol) of $\text{PdCl}_2(\text{PPh}_3)_2$, 27 mg (0.15 mmol) of CuI in 500 mL of a 1:1 THF/ DIPA mixture was degassed under for 30 minutes. TMSA (5.68 mL, 40.3 mmol) was then added and allowed to stir overnight at room temperature. The solvent was then removed under reduced pressure and vacuum. The crude reaction mixture was run through a silica plug with 3:1 MeCl_2 /Hexanes mixture to yield 11.52 g of product in 90% yield: mp 86-88 °C; ^1H NMR (300 MHz, CDCl_3) δ 0.25 (s, 9H), 1.71 (bs, 6H), 3.79 (bs, 4H), 7.35 (d, $J = 8.7\text{Hz}$, 2H), 7.44 (d, $J = 8.7\text{Hz}$, 2H).

Three fold Symmetrical base (6): Compound **1** (5.0 g, 17.5 mmol) was stirred with 8.06 g (58.5 mmol) of K_2CO_3 for 30 minutes until terminal alkyne was deprotected. The reaction mixture was then filtered, extracted into 100mL of ether and washed

successively with water, dried (MgSO_4), and filtered. After removing the ether under reduced pressure, the material was redissolved in toluene and degassed under argon for thirty minutes. Another vessel containing $\text{Pd}(\text{PPh}_3)_4$ (289 mg, 0.25 mmol), CuI (95 mg, 0.50 mmol), and 1,3,5-tribromobenzene (1.57 g, 5.0 mmol) in a 1:1 PhMe/DIPA mixture was also purged thoroughly with argon and set at reflux. The solution containing the free alkyne was slowly injected into the catalyst aryl halide mixture over 3 days. After completion, the solvent was then removed under reduced pressure and material crudely purified using a silica plug with 3:1 MeCl_2 /hexanes to remove the catalyst and ammonium salts to yield 2.72 g of three fold cross coupled product (**5**) and excess alkyne. Due to instabilities of triazenes on silica, the product was taken directly to the next step and dissolved in 50mL of iodomethane freshly distilled over molecular sieves. Reaction mixture was sealed in pressurized flask and allowed to react overnight at 120 °C. Solvent was removed under reduced pressure and crude product run through a silica plug (1:1 MeCl_2 /hexanes). The product was then purified by recrystallization in hexanes to yield 2.45g (3.3mmol) triiodinated product **6** in 64% overall yield. mp 265-280 °C; ^1H NMR (300 MHz, CDCl_3) δ 7.24 (d, $J = 8.3\text{Hz}$, 6H), 7.63 (s, 3H), 7.70 (d, $J = 8.3\text{Hz}$, 6H); ^{13}C NMR (75 MHz, CDCl_3) δ 88.99, 89.75, 94.71, 122.14, 123.80, 133.10, 134.14, 137.60; MS (APCI) m/z (%) 827 (100, M^+ +THF); IR (NaCl) ν 2151, 2208, 2845, 2953, 3042 cm^{-1} .

Three fold Symmetrical TMS ethynylated arene(7): Triiodotriyne **6** (200 mg, 0.27 mmol), $\text{PdCl}_2(\text{PPh}_3)_2$ (2.1 mg, 0.0026 mmol), and CuI (1.0 mg, 0.0059 mmol) was dissolved in 5mL of 1:1 THF/DIPA solution and purged for 30 minutes under argon.

TMSA (0.15 mL, 1.056 mmol) was then added via syringe and the solution stirred overnight. The solvent was then removed under reduced pressure and material ran through a plug of silica with 1:1 MeCl₂/Hexanes. Hexayne **7** was isolated in 97% yield (172 mg, 0.26 mmol). mp 159-166 °C; ¹H NMR (300 MHz, CDCl₃) δ 0.271 (s, 27H), 7.46 (s, 12H), 7.63 (s, 3H); ¹³C NMR (75 MHz, CDCl₃) δ -0.11, 89.50, 90.26, 96.54, 104.48, 122.70, 123.34, 123.86, 131.46, 131.94, 134.13; MS (APCI) *m/z* (%) 737 (100, MH⁺+THF); IR (NaCl) ν cm⁻¹.

Three Fold Ligand (1): Hexayne **7** (100 mg, 0.149 mmol) was reacted with 1.0mL 1.0M TBAF solution (1.0 mmol) in 5mL of THF. The reaction was stirred for 20 minutes and then extracted into ether. The ethereal solution was then washed with water, dried over MgSO₄, and solvent removed under reduced pressure. The fully deprotected hexayne was then added to the arene **8** (145 mg, 0.521 mmol) and CuI (3 mg, 0.0149 mmol) and dissolved in 2.5mL of 2:1 DMF/THF solution and 0.75mL Hunnig's base. The solution was then freeze pump thawed for 3 cycles before adding the Pd(PPh₃)₄ (9 mg, 0.00745 mmol) and freeze pump thawed one additional cycle. The reaction was allowed to react at room temperature overnight. The solvent was then reduced under reduced pressure and material extracted into MeCl₂ (15 mL) before being washed with water (5 mL, 4×), dried (MgSO₄), and solvent removed under reduced pressure. The three fold symmetrical ligand **1** was isolated in 34% yield (50 mg) as a white solid. mp 169-171 °C; ¹H NMR (300 MHz, CDCl₃) δ 2.45 (s, 9H), 7.4 (d, *J* = 8.4Hz, 6H), 7.53 (s, 12H), 7.56 (d, *J* = 8.4Hz, 6H), 7.67 (s, 3H); ¹³C NMR (75 MHz, CDCl₃) δ 30.29, 89.64,

90.32, 90.61, 90.67, 122.77, 123.14, 123.88, 125.17, 128.32, 131.66, 132.17, 134.23, 193.39.

Extended iodide (9): A solution of **4** (603 g, 2.12 mmol) was first stirred with 10mL of 1.0M TBAF solution in 30mL of THF for 20 minutes and ether added. The resulting solution was then washed several times with 10% NaCl and then water; dried over MgSO₄, and solvent removed under reduced pressure. The free alkyne was then added to the triyne **6** (603 mg, 2.1 mmol) in 40 mL 1:1 THF/DIPA mixture and purged with argon for 30 min. Pd(PPh₃)₄ (31 mg, 0.026 mmol) and CuI (10mg, 0.0529mmol) were then added and reaction sealed and reacted overnight at room temperature. The solvent was then removed under reduced pressure and material ran through a silica plug with 3:1 MeCl₂:hexanes. The material was immediately taken to the next step due to instabilities of triazenes in chromatography and dissolved in MeI (freshly distilled over dry molecular sieves) and reacted overnight in a pressurized vessel at 120 °C. The solvent was then removed under reduced pressure and material flash chromatographed with 10% MeCl₂: Hexanes. Material can be recrystallized with hexanes to yield **9** 365 mg in 65% yield. mp 169-171 °C; ¹H NMR (300 MHz, CDCl₃) δ 7.25 (d, *J* = 8.3Hz, 6H), 7.52 (s, 12H), 7.66 (s, 3H), 7.70 (d, *J* = 8.4Hz, 6H).

Extended Three fold Symmetrical TMS ethynylated arene(10): Triidotriyne **9** (100 mg, 0.095 mmol), PdCl₂(PPh₃)₂ (5 mg, 0.0057 mmol), and CuI (3.0 mg, 0.0114 mmol) was dissolved in 5mL of 1:1 THF/DIPA solution and purged for 30 minutes under argon. TMSA (0.053 mL, 0.38 mmol) was then added via syringe and the solution stirred overnight. The solvent was then removed under reduced pressure and material ran

through a plug of silica with 1:1 MeCl₂/Hexanes. **10** can be further purified by recrystallizing in hexanes. Nonayne **10** was isolated in 92% yield (91 mg). mp 159-166 °C; ¹H NMR (300 MHz, CDCl₃) δ 0.271 (s, 27H), 7.46 (bs, 12H), 7.52 (bs, 12H), 7.66 (s, 3H).

Three Fold Extended Ligand (2): Nonayne **10** (54 mg, 0.056 mmol) was reacted with 1.0 mL 1.0 M TBAF solution (1.0 mmol) in 5mL of THF. The reaction was stirred for 20 minutes and then extracted into ether. The ethereal solution was then washed with water, dried over MgSO₄, and solvent removed under reduced pressure. The fully deprotected hexayne was then added to the arene **8** (93 mg, 0.335 mmol) and CuI (1 mg, 0.0056 mmol) and dissolved in 1.5 mL of 2:1 DMF/THF solution and 0.25mL Hunnig's base. The solution was then freeze pump thawed for 3 cycles before adding the Pd(PPh₃)₄ (3 mg, 0.0028 mmol) and freeze pump thawed one additional cycle. The reaction was allowed to react at room temperature overnight. The solvent was then reduced under reduced pressure and material extracted into MeCl₂ (15 mL) before being washed with water (5 mL, 4×), dried (MgSO₄), and solvent removed under reduced pressure. The three fold symmetrical ligand **7** was isolated in 75% yield (50 mg) as a white solid. mp 169-171 °C; ¹H NMR (300 MHz, CDCl₃) δ 2.45 (s, 9H), 7.40 (d, *J* = 8.3Hz, 6H), 7.53 (m, 24H), 7.56 (d, *J* = 8.3Hz, 6H), 7.68 (s, 3H).

TOAB Nanoparticle Synthesis. In a 200 mL round-bottom flask, dissolved tetraoctylammonium bromide (1.11 g, 2.0 mmol) in 80 mL toluene. To this, added HAuCl₄ (0.34 g, 1.0 mmol) in 20 mL Nanopure water. This was stirred until all of the gold was transferred to the toluene layer. NaBH₄ (0.4665 g, 12 mmol) was dissolved in

30 mL of water. 25 mL of this NaBH_4 solution was added to the biphasic reaction mixture. Within 30 s, the solution had become a rich, ruby red color. This solution was allowed to stir for thirty minutes, then the aqueous layer was separated from the toluene dispersed nanoparticles. The nanoparticles in toluene were stored at 4°C until use.

Trimer Synthesis. To a 20 mL scintillation vial, added 938 μL of as prepared gold nanoparticles was diluted in 8.5 mL of toluene. In a 1 mL Eppendorf tube, 24 μL of a 10 mg/mL (100:1 linker:nanoparticle ratio) solution of linker **2** in ethanol:THF (70:30) was diluted to 500 μL in the same ethanol:THF mixture. The linker mixture was added dropwise to the gold nanoparticle solution with vigorous stirring. Following addition, the linking was allowed to continue for 4 hrs or overnight. In the case of deprotection, a couple of drops of ammonium hydroxide were added to the trithiol linker prior to addition to the nanoparticle sample. Similar conditions were used for other linker:nanoparticle ratios. Please see synthetic scheme in Appendix B.

Ligand Exchange. Water soluble, linked gold nanoparticles were prepared by adding an excess of sodium 2-mercaptoethanesulfonate (MES), 2-(2-mercaptoethoxy) ethanol (MEE) or 4-dimethylaminopyridine (DMAP) to the nanoparticle solutions. In general, the mass of nanoparticles in solution was estimated and an equivalent mass of ligand was added to the solution. Following addition, the ligand exchange was allowed to proceed until full exchange was noted (almost immediately for DMAP, ~4 hrs for MEE). Following exchange, the aqueous layer was separated from the toluene and washed with methylene chloride. A stream of N_2 gas was bubbled through the solution to remove any residual methylene chloride.

Diafiltration. To isolate the linked structures from monomers in solution, ligand exchanged products were diafiltered on a 300 kDa diafiltration membrane until no remaining color could be seen in the retentate, indicating that all nanoparticles or structures smaller than the pores had been eluted.

TEM Inspection. Samples for TEM inspection were aerosoled onto SiO TEM grids and imaged. Collected images were inspected manually for the presence of dimeric and trimeric species. Generally, more than 500 individual particles and linked structures were counted to determine the percentage of linked structures in a sample.

Results and Discussion

The work described here is based upon previous work by Feldheim et al. using rigid arylethynyl-thiolate ligands.⁴ In their work, large citrate stabilized gold nanoparticles of 8 to 10-nm obtained commercially were linked using di-, tri- and tetrathiols. To carry out the procedure, the linker dissolved in EtOH:THF was added dropwise to an aqueous dispersion of the nanoparticles. As prepared, the yield of linked structures is ~5-15%. Follow-up work by their group showed that size-exclusion chromatography could be used to enrich the population of linked structures to ~55%.⁸ Despite some improvement, we sought to improve this existing method by: (1) Developing an improved, modular synthesis of the trithiol ligand used to link the nanoparticles, allowing for more convenient access and allowing for easy tailoring of the terminal functional group allowing for the linking of diverse classes of nanomaterials. (2) Developing a novel linking approach that allows for homogeneous linker-nanoparticle mixing and also allows for convenient functionalization following linking. (3) Leveraging our existing

diafiltration platform to isolate the linked nanoparticle structures from monomers and aggregates. Our previous results suggest that diafiltration is well suited to the separation of linked structures from impurities such as excess linker, monomers and aggregates. It was anticipated that the approach developed here would allow for more convenient access to the desired linked nanoparticle structures at higher yields than previously reported.

Linker Synthesis

The previous reports of the three fold symmetrical ligands **1** and **2** do not detail the synthesis nor full characterization of the molecules.⁴ In this report we provide a detailed and improved synthetic report of both ligands as shown in Figure B.1 and B.2 (Appendix B). Due to additional stability, the diethylamine derived triazene was replaced with the piperidine derived triazene **3**. Trimethylsilyl acetylene was cross coupled to **3** under Sonogashira cross coupling conditions to produce monoyne **4** in 87% yield. Monoyne **4** was deprotected using mild base in 1:1 THF/ MeOH affording the free alkyne and taken to the next step. Slow injecting the free alkyne into a solution containing the cocatalysts Pd(PPh₃)₄ and CuI, 1,3,5-tribromobenzene in refluxing 1:1 PhMe/DIPA (diisopropylamine) mixture afforded the three fold cross coupled product **5** and excess free alkyne with little formation of dimer. Taking the reaction mixture to the next step was found to minimize degradation of **5** in chromatography. Triazene **5** was then dissolved in freshly distilled MeI and heating to 120 °C overnight to produce the triiodo-triyne **6** which could be easily isolated chromatographically in overall 64% yield (3

steps). TMSA cross coupling of **6** under Sonogashira cross coupling conditions easily afforded the hexayene **7** in 94% yield.

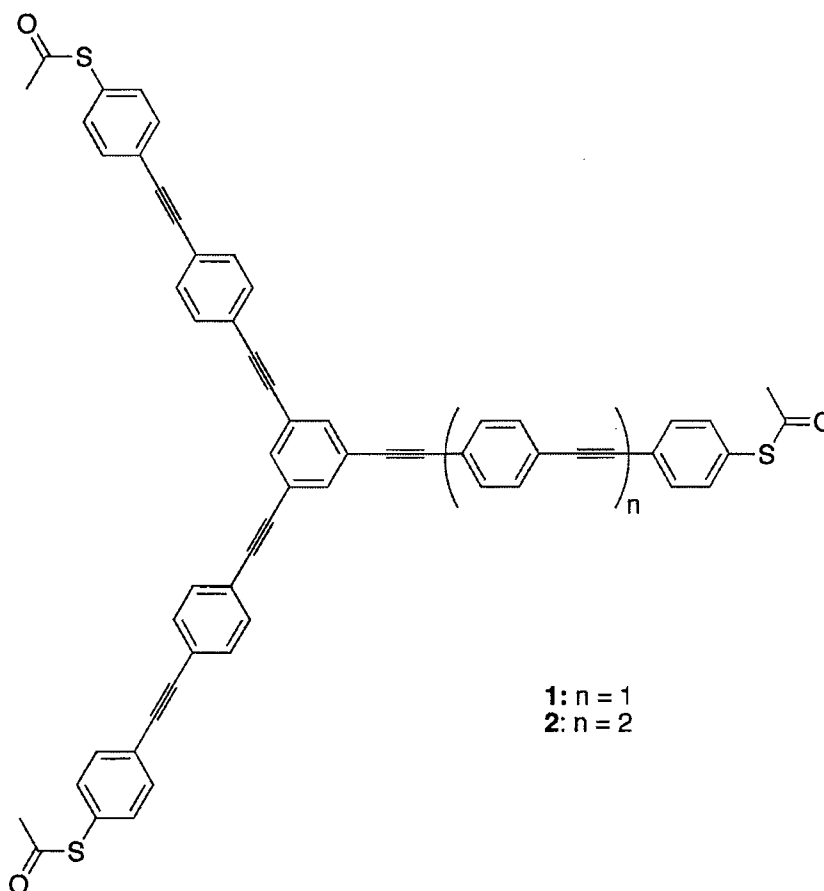


Figure 3.2. Structure of the three-fold linkers **1** and **2** used in this study.

Figure B.2 shows the synthesis of the final protected thiol capped ligands **1** and **2**. In order to increase yield, 4-Bromophenylthioacetate was replaced with 4-iodophenylthioacetate⁹ (**8**). Hexayene **7** was first deprotected with TBAF and then cross coupled to **8** under ambient conditions with a modified preparation reported by Hortholary and Coudret⁹ using Hunnig's base, DMF, and THF forming ligand **1** in 50% yield.

The extended ligand **2** was synthesized from triyne **6** which was cross coupled to deprotected **4** then iodinated in MeI to form **9** in 65% overall yield. Cross coupling TMSA to the terminal iodides produces **10** in 94% yield (Figure B.1). Final cross coupling of **10** was done under identical conditions as **7** to generate **2** in 45% yield (Figure B.2).

Linked Nanoparticle Preparation

In Feldheim's original report,⁴ citrate stabilized gold nanoparticles were linked with rigid linkers in water. The linkers were dissolved in THF:ethanol and added dropwise to the aqueous nanoparticle solutions, yielding a low population of the desired structures. A couple of factors may have led to the low yields of the desired material. First, citrate nanoparticles are notoriously difficult to functionalize with thiols and only very recently have efficient functionalization methods been developed. Second, the linkers are not soluble in water and the volume of co-solvent added is quite small with respect to the overall volume. This heterogeneity could lead to difficulties in the linking procedure. Taken together, these factors would lead to low yields overall.

To overcome these issues, we attempted a number of alternative preparative strategies, including (i) amide coupling of carboxylic and amine stabilized nanoparticles, (ii) coupling of carboxylic acid stabilized nanoparticles with diamines, (iii) coupling of thiol stabilized and citrate stabilized nanoparticles with water soluble dithiols. In all cases, very little of the desired dimeric species were attained either because of poor sterics (i.e. the linker was too short) or because of poor coupling efficiency. As a result, methods for taking advantage of the rigid linkers used by Feldheim were sought.

As a first improvement, the citrate nanoparticles were substituted with 5-nm tetraoctylammonium bromide (TOAB) stabilized nanoparticles.¹⁰ These particles are very easy to functionalize with thiols,¹¹ and should provide for easy linking. Furthermore, these nanoparticles are organic soluble, which would allow for the linker to be in the homogenous environment with the nanoparticles and hopefully increasing linking efficiency with a resultant increase in linked nanoparticle yield. As a final improvement, it was envisioned that the existing, labile ligand shell could be exchanged for thiols bearing another functionality, yielding linked, thiol functionalized nanoparticle structures (Figure 3.3).

As a first step, TOAB stabilized nanoparticles in toluene were mixed at ratios of 6:1, 3:1, 1:1, 1:3 and 1:6 (nanoparticle:linker) with the rigid linker. After mixing for four hours or overnight, the nanoparticles were inspected via TEM. Although it was expected

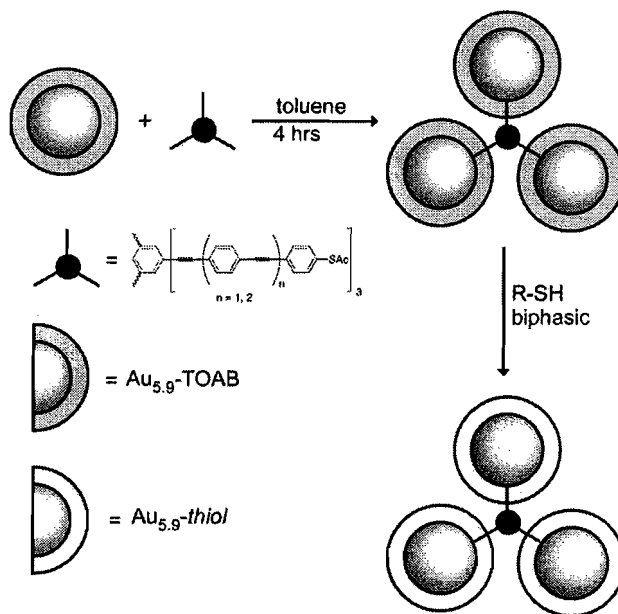


Figure 3.3. Trimer formation scheme. Initial TOAB stabilized nanoparticles are linked with either **1** or **2**, followed by ligand exchange to form the functional linked structure.

that changes in the ligand to gold ratio would impact the yield of linked structures, TEM inspection showed no discernible difference amongst the samples. Further studies at more extreme nanoparticle:linker ratios (up to 1:1000) showed similar results. In all cases, trimer yields were ~2-3% of the total species present, and all linked structures (dimers and trimers) ranged from ~10 to 15%. Because linker concentration did not affect linked structure formation, it was hypothesized that the acetyl protecting group on the linker was interfering with the linking procedure. Deprotection¹² under mild, basic conditions prior to the linking reaction yielded no further improvements in linking. Although it had been envisioned that the use of labile ligands, such as TOAB, under homogenous reaction conditions would improve linked nanoparticle structure yield, in fact, no appreciable improvement was realized.

Ligand Exchange and Diafiltration

Diafiltration was attempted to increase the population of linked structures. Since the linking was carried out in toluene, the linked structures were transferred to the aqueous phase via a ligand exchange reaction. This was done by (i) adding an excess of a water soluble ligand to the linked nanoparticles in a biphasic water/toluene system, (ii) separation and (iii) solvent washes to remove excess toluene. Ligand exchange was attempted with 2-mercaptoethanesulfonate (MES), 2-(2-mercaptoethoxy) ethanol (MEE) or 4-dimethylaminopyridine (DMAP). MES exchange was unsuccessful, likely due to interactions between the MES and TOAB. However, both DMAP and MEE exchanges were successful. TEM inspection following the exchange showed similar 10-15% yields of linked structures.

A 300 kDa diafiltration membrane, chosen based upon anticipated trimer diameter, was used to isolate the linked structures from monomers in solution. Diafiltration was carried out until no color was seen in the permeate, indicating that all species smaller than the pore size had been eluted. Following the diafiltration step, the diafiltered sample was inspected via TEM. Manual counting of the linked species indicated an enrichment of total linked structures to ~36%, with ~6% of those being trimeric species (Figure 3.4). Although this was an improvement, the overall yield of trimers was far short of what is possible using diafiltration. Based upon this, it was theorized that perhaps there were some inherent limitations to this approach.

Ligand Exchange / Linking Dynamics

In order to gain a greater understanding of the linking chemistry, the dynamics of ligand exchange were studied. Ligand exchange is the most common method for introducing peripheral functionality to gold nanoparticles, and allows for control over both solubility and over the reactivity of the nanoparticles. Generally, the gold

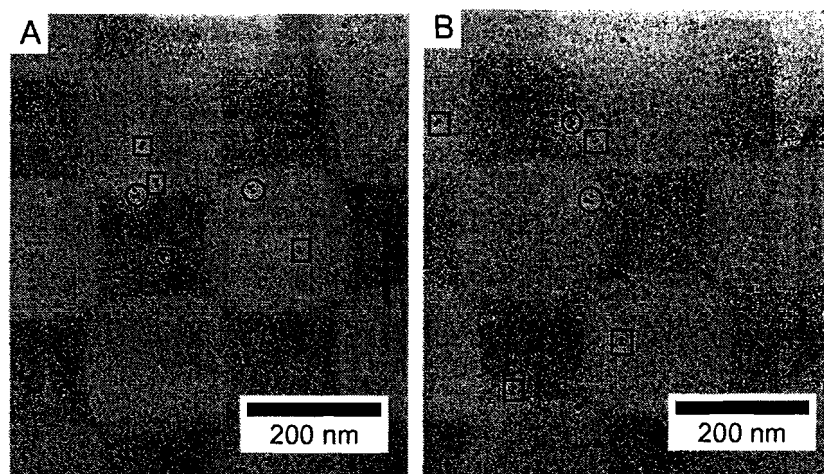


Figure 3.4. TEM images of ligand exchanged (A) and diafiltered (B) linked structure samples. Dimers are in squares, trimers are circled.

nanoparticles are dispersed in a suitable solvent, and then an incoming ligand either under monophasic or biphasic conditions is added. This is allowed to stir for several hours or days either under ambient conditions or at elevated temperatures. Following the exchange, excess and exchanged ligand are removed via suitable purification methods.

The exact mechanistic details are not understood, however in thiol-stabilized nanoparticles, it has been suggested that ligand dissociation occurs via a concerted mechanism whereby an incoming ligand transfers a proton to the sulfur of an outgoing ligand.¹³ It has been further hypothesized that certain locations on a nanoparticle are more reactive during ligand exchange (Figure 3.6). Vertex sites (areas where gold atoms have few nearest neighbors) are expected to have the highest reactivity, followed by edge sites, near edge face sites and then interior face sites. It is likely that the vertex sites are the most reactive because (1) the gold atoms at the vertex have the highest potential, and therefore show the highest reactivity (i.e. for redox chemistry) and (2) ligands at these sites are not stabilized by Van der Waals interactions. By the same arguments, interior surface sites show the greatest stability because the gold surface is more uniform and there is much higher ligand packing density, which increases the stability of the monolayer.¹³

Several other factors have been shown to be important during the ligand exchange process. First, it has been shown that ligand exchange occurs most readily when the precursor particle has a ligand shell that is labile and has a short alkyl chain. Longer alkyl chain lengths lead to greater monolayer stability and lower exchange rates. It has also been shown that for the same reasons, incoming ligands that have favorable Van der

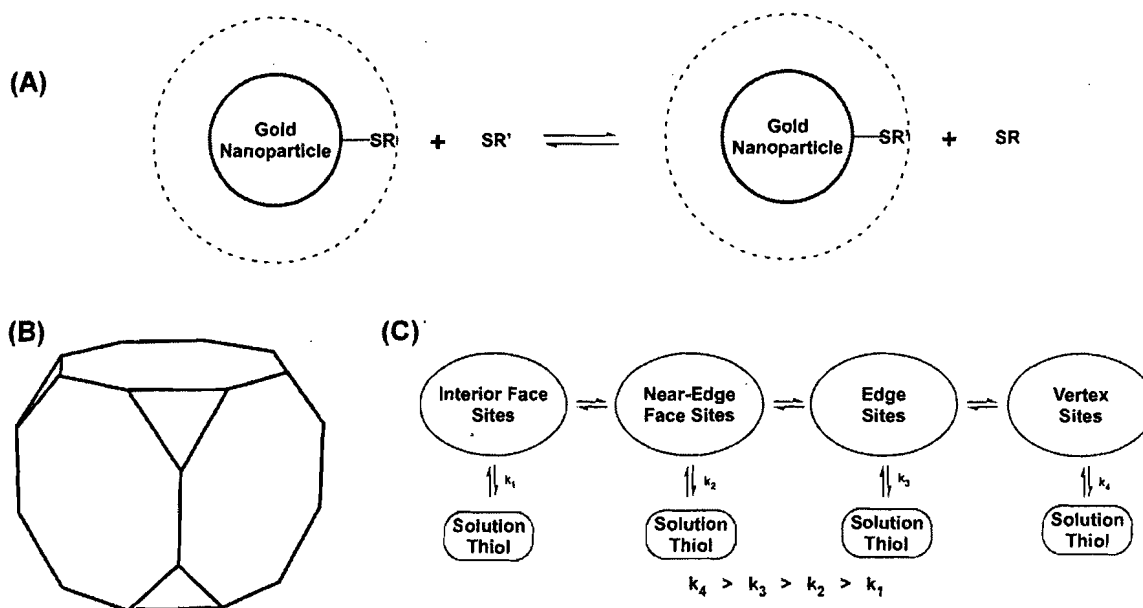


Figure 3.5. (A) General scheme for ligand exchange on a thiol stabilized gold nanoparticle. (B) Hypothesized truncated-cube structure of a gold nanoparticle. (C) Exchange rates for different sites on a gold nanoparticle with a truncated-cube like structure.

Waal or hydrogen bonding interactions will show higher exchange rates.¹³ The concentration of incoming ligand also plays a large role. Although there is a 1:1 ligand exchange ratio, a high concentration of incoming linker is required to force the ligand exchange reaction to completion. The reason for this is that there is significant interchange of thiols both on the surface and in solution. As with any equilibrium situation, pushing the reaction towards completion requires a significant excess of the incoming thiol. Additionally, time and temperature play a role in forcing the reaction.

The linking reaction used to form a gold nanoparticle trimer is similar to a ligand exchange reaction. Based upon this, some reasons for the low yield of linked structures include: (i) instability of the linker on the surface of the nanoparticle. Because the linker likely associates at a vertex or edge site, it can be very quickly exchanged. Furthermore, there are no favorable interactions between it and other molecules on the surface to

stabilize it, thus linkers more than likely exchange very quickly on the surface of the particle. (ii) While association of a linker on a particle is probable, the association of this species with a second nanoparticle is expected to be limited due to size and sterics. The probability of this dimeric species interacting favorably with a third nanoparticle is even less likely, thus the trend of monomers > dimers > trimers observed in the work here. These results suggest that other approaches, based upon external linking mechanisms, may be more useful in the synthesis of linked nanoparticle structures.

Conclusion

Herein were described attempts at increasing the yield of linked gold nanoparticle structures through the use of rigid arylolethynyl-thiolate linkers. Specifically, we described an improved synthesis of the linkers, allowing for a modular approach to their synthesis and a likely ability to tailor the peripheral functionality to diverse classes of materials. We described attempts at the linking of TOAB stabilized nanoparticles that could have led to greater yields of linked nanoparticle species, but remained limited to ~15% as previously reported. Diafiltration of these linked structures allowed for an enrichment of up to 36% for both dimers and trimers in solution. Unfortunately, the low yields were likely due to the dynamics of ligand exchange on gold nanoparticles, which can place limits on the introduction of molecules on the surface of nanoparticles. Although not proven here, diafiltration remains a promising choice for the isolation of linked nanoparticle structures. Future work should focus upon increasing the yields of linked nanoparticle structures through alternative linking schemes. For example the use of base-pairing in DNA, as described by Alivisatos et al., the use of chelating moieties as

described for plasmon resonance based sensors or the use of coupling chemistry are all promising alternatives to the methods for nanoparticle linking described here.

Bridge

In the previous two chapters, we have discussed our work with diafiltration for the purification and size separation of nanomaterials. In the next three chapters, the use of biological aptamers, derived via in vitro selection experiments, for the preparation of gold nanomaterials will be discussed.

CHAPTER IV

ADVANCING IN VITRO SELECTION FOR MATERIALS APPLICATIONS

Introduction

Bioinspired approaches to materials synthesis have become areas of considerable promise and interest. Recently, Nam et al. described an engineered mosaic M13 bacteriophage for the preparation of hybrid gold / cobalt oxide wires for use in Li ion battery applications.¹ Tetraglutamates, identified using predictive design, were used to precipitate cobalt oxide nanostructures on the surface of the phage particle and a gold binding peptide, identified using in vitro selection, was used to assemble gold nanoparticles on the surface, and both were bound to the N-terminus of the major pVIII coat protein. In addition to the enhanced battery performance, they were able to show that these virus-templated wires would self-assemble into liquid-crytalline arrays on a polymeric substrate, making them useful for a wide-variety of applications where flexible batteries are of benefit. In another example, published by Pender et al., a bifunctional peptide was used dissolve carbon nanotubes and assist in the precipitation and growth of either silica or titania on the surface of the nanotubes.²

These examples are two of many where the interface between biomolecules and materials plays an important role in the preparation of high-performance, next generation

materials and nanomaterials and it draws upon traditional materials science, biomimetic / bioinspired materials, synthetic biology,³ green chemistry⁴ and the ever-present challenge of preparing well-defined materials. Central to this approach is the ability to identify useful biomolecules or *aptamers* for the specific materials application at hand. In the examples above, *in vitro* selection, a powerful technique for identifying useful biomolecules from large, combinatorially derived libraries, was used to identify the aptamers. In fact, *in vitro* selection is playing an increasingly important role in the development of novel methods for the synthesis and self-assembly of technologically useful materials.

Why base the preparation of materials on *in vitro* derived molecules via bioinspired approaches when other, more traditional approaches are available? One answer is that an important aspect of materials synthesis is routine access to well-defined materials. As the dimensions of materials decrease to that of the nanoscale, control over the size, shape and crystallinity becomes not only more important but also more difficult. The development of methods for the control over these aspects in a routine, convenient and efficient fashion will be important for the advancement of materials technologies. A close inspection of hard materials produced in nature reveals intricate structures with precise feature size, shape and crystallinity. For example, many unicellular organisms, such as coccoliths and radiolarians, utilize biomineralization to produce intricate microskeletons of silica or calcium carbonate.⁵⁻⁷ Other examples of biomineralization or synthesis of hard tissues include bones and teeth, shells, exoskeletons, magnetobacteria⁵ and mechanisms for sequestering metals *in vivo*.⁸ Recently, biomimesis and bioinspiration⁹

have arisen as approaches for problem solving based upon the ingenuity of nature, e.g., a solar cell inspired by a leaf or epoxy suitable for dentistry inspired by mollusks. Though bioinspired materials synthesis using biomolecules promises to address many of the issues related to well-defined materials, one difficulty is that nature has not evolved all of the necessary biomolecules for the production of materials useful for technology applications. For this reason, methods for the directed evolution of biomolecules specific for materials applications are required. In vitro selection is one such method for the identification of biomolecules that are useful for the synthesis of materials.

One area of research where the application of in vitro selected, materials specific aptamers is particularly pertinent is the growing field of green nanoscience.¹⁰ Green nanoscience seeks to develop methods for the preparation of useful nanomaterials using the twelve principles of green chemistry, with the specific aims of minimizing chemical hazards to health and the environment, reducing waste and preventing pollution. The in vitro selection of materials specific aptamers offers the opportunity to replace traditional methods of synthesis, utilizing potentially hazardous precursors and reaction conditions with new, bioinspired syntheses that take advantage of the properties of biomolecules, allowing for the preparation of similar materials under ambient conditions using benign reagents. Specifically, the use of aptamers for materials applications may assist in reducing the use of hazardous solvents and reagents and improve material and energy efficiency, while yielding well-defined, technologically relevant materials.¹⁰

The goal of this review is to draw from three disciplines - peptide display,¹¹ Systematic Evolution of Ligands via EXponential Enrichment (SELEX)^{12,13} and

bioinspired materials - and to encourage the advancement of in vitro selection for materials applications. Specifically, this review will focus on the special requirements of identifying biomolecules useful for materials applications and draw from recent advances in the field of in vitro selection in order to suggest possible paths forward. Because of the limited scope, yet broad base, not all advancements and sub-disciplines can be covered. Furthermore, the limited scope has forced the generalization of some terms. For example, aptamer (from aptus, “to fit”) is used to describe both useful RNA and peptide sequences. In vitro selection is used generally to describe both peptide display and SELEX. Though there are many variations of peptide display (phage, yeast, bacterial) and SELEX, phage display and RNA SELEX will be the focus of the discussion, as the same principles that apply to these techniques can be broadly applied to other in vitro selections. These considerations aside, in vitro selection is a powerful technique that holds significant potential for the synthesis and self-assembly of technologically useful materials. The ideas discussed here draw upon materials chemistry, organic and inorganic chemistry, molecular biology and biochemistry, offering the opportunity for broad, interdisciplinary research. The challenge, and exciting opportunity, is to carefully consider all aspects and special considerations of these fields in order to discover a one-in-a-trillion aptamer.

Introduction to In Vitro Selection

The discovery of molecules with a high affinity or specificity for a target or process has been a major driver of chemical research for many years. Such molecules are invaluable as potential pharmaceuticals and drug delivery agents, as well as in sensing and separation applications. Similar efforts have focused on identifying molecules and

ligands useful for materials applications, such as synthesis and assembly. The discovery of these molecules often requires brute-force methods such as rational design or combinatorial methods. In either case, candidate molecules are designed, synthesized and screened for a given purpose on a “one-at-a-time” basis. Although combinatorial methods offer considerable improvements in throughput, screening thousands or tens of thousands of candidates still requires significant time and resources, not to mention some degree of luck. Methods that allow for the simultaneous screening of billions to trillions of candidates would surely benefit efforts aimed at identifying useful molecules. In vitro selection is one such method.¹⁴

In vitro selection, also known as directed evolution or “bio-panning,” is a method for screening a large, randomized combinatorial library of candidate biomolecules for useful molecules, or aptamers, that have a high affinity or propensity for a given target or process. In vitro selection has found wide spread use in biotechnology, biochemistry and molecular biology both as a research tool and as a method for targeting biomolecules for drug delivery and other applications. The power of in vitro selection hasn’t gone unnoticed by chemists, and there have been many reports of the use of in vitro selection for identifying aptamers useful for separations,¹⁵ sensing¹⁶ and for affecting organic transformations.¹⁷ More recently, a number of researchers have been investigating aptamers for materials applications, such as synthesis and self-assembly.¹⁸⁻²²

The two most common methods of in vitro selection are phage display²³ for identifying peptide aptamers and Systematic Evolution of Ligands via EXponential Enrichment (SELEX) for identifying oligonucleotide aptamers.^{12,13} Though the specifics

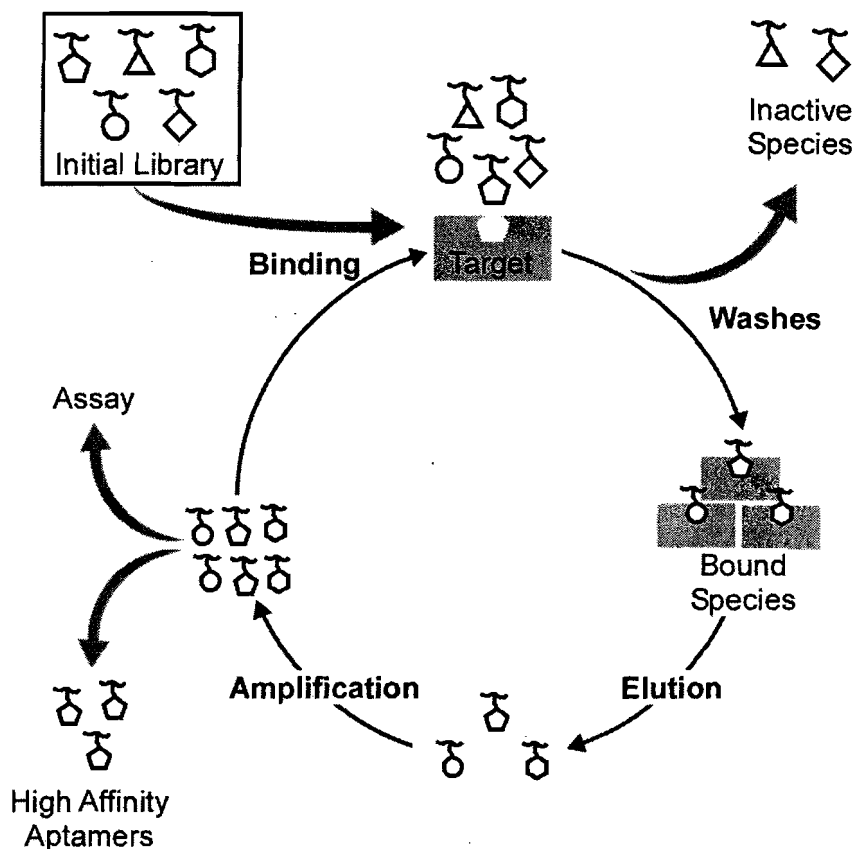


Figure 4.1. Schematic of the in vitro selection cycle. The library is incubated with the target. Following incubation, inactive species are washed from the target. Bound species are eluted, amplified and then incubated with the target again. Following a number of rounds, high affinity aptamers are isolated.

of phage display and SELEX are different, the same general principles of in vitro selection apply. Shown in Figure 4.1 is a typical in vitro selection cycle. In the first step, an initial library (typically containing 10^9 - 10^{14} individual candidates) is mixed with the intended target. The candidate pool is given a chance to interact with the target under specific conditions as determined by the experimenter. In the second step, non-binders and poorly bound species are washed away from the bound species, which are subsequently eluted away from the target. The eluted target binders are amplified via suitable biochemical methods generating a new library that is enriched with target

binders. The cycle of incubation, washes/elution and amplification are repeated several times until appropriate assays indicate that the desired aptamers have been isolated. The

Table 4.1. Selection criteria and considerations

Selection Criterion	Considerations
Library Creation	<ul style="list-style-type: none"> • in vitro selection system <ul style="list-style-type: none"> • SELEX (RNA, DNA) • Peptide Display • degree of randomization • randomized region size • predetermined structure • no. of copies of individual candidates • artificial nucleotide or peptide building blocks
Target Selection	<ul style="list-style-type: none"> • choice of material • material properties <ul style="list-style-type: none"> • crystallinity • chirality • functional groups • purity • defect sites • counter-selection target
Incubation	<ul style="list-style-type: none"> • selection solution <ul style="list-style-type: none"> • buffer, pH • salts, ionic strength • surfactants • additives • biomolecule and target concentration / ratio • incubation time • temperature
Washes / Elution	<ul style="list-style-type: none"> • wash stringency <ul style="list-style-type: none"> • solution • time • temperature • elution method <ul style="list-style-type: none"> • denature • competitor • in situ amplification
Amplification	<ul style="list-style-type: none"> • library effects • mutation introduction

art of the in vitro selection process is to design a suitable starting library, identify a suitable target and to define the set of fitness criteria by which a subset of aptamers can

be identified from the large initial library. In order for the selection to be successful, these criteria must be very carefully considered and chosen. Outlined in Table 4.1 are the elements of the in vitro selection process and some of the considerations that must be taken into account.

In Vitro Selection for Materials

The use of in vitro derived aptamers for materials applications is potentially wide in scope, ranging from sensors, batteries and dental applications to nanoelectronics and optical applications. The utility of aptamers is derived from the ability to select them to recognize and act upon specific targets under specific conditions. For example, aptamers selected to recognize the atactic versus syndiotactic phase of a polymer could be used to produce only syndiotactic materials. Aptamers could also be selected to identify defect sites in the dentin in teeth, and assist in the biomineralization of hydroxyapatite for tooth repair. While there are many possible applications for aptamers in materials science, the two most common challenges for which aptamers are being targeted are the self-assembly and synthesis of nanomaterials. As the applications of nanomaterials have expanded, it has become clear that our ability to assemble well-defined nanomaterials in a manner by which they can be addressed from the macro scale is lacking. For example, Figure 4.2 is a generic schematic outlining the formation of a regular 1D array of material assembled onto a substrate using a bifunctional aptamer. In this case, the aptamer has been selected to identify a specific binding site on the surface of the substrate. Once assembled, a set of material precursors, or growth solution, is introduced to the system and the desired material is synthesized in situ.

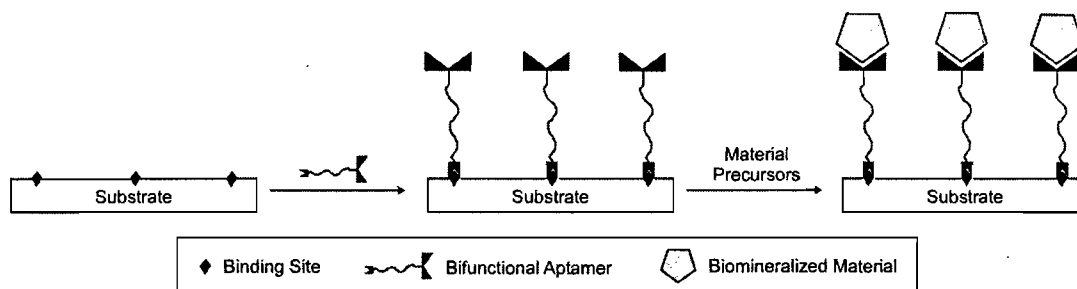


Figure 4.2. The synthesis and self-assembly of a material using a bifunctional aptamer. A similar approach was used by Pender et al.² to synthesize and self-assemble materials on carbon nanotubes.

While the identification of aptamers that bind specific targets is a fairly straightforward application of *in vitro* selection, the identification of aptamers that can nucleate and grow novel materials of defined size, shape and crystallinity is far more difficult. Often times, aptamers that have been identified for the synthesis of materials have been arrived at empirically and not necessarily predicted. Yet, the reason for pursuing bioinspired or biomimetic syntheses using aptamers is that it holds the promise for obtaining desired, well-defined materials in a predictable fashion. The difficulty lies in identifying aptamers that allow for predictable syntheses, which involves choosing the proper initial library, identifying suitable targets for selection and mixing these two components together under the right conditions.

Some cues for designing the selection criteria come from the systems we seek to mimic, specifically those of biomineralization.⁶ Biomineralization is a process by which organic molecules regulate the nucleation, growth, morphology and assembly of materials using one of two methods. The first method is interfacial growth, wherein lipid vesicles or other soft templates compartmentalize precursors and mediate nucleation and growth. The second is epitaxial crystal growth, wherein a template protein initiates and

controls growth, but does not directly template the growth. In general, the role of the biomolecule is to lower the barrier to nucleation of the material and to assist in the growth of the material through favorable overlaps in lattice geometry or charge distribution with the material.⁶ With these criteria in mind, one can begin to formulate an approach for identifying aptamers that will form the desired material.

Take, for example, the aptamer mediated synthesis of gold nanorods, a research effort in our labs. It is known from traditional nanorod syntheses that a surfactant binds to a specific crystal face (Au (100)) acting as a directing agent and templating the growth of the rod.²⁴ In this case, the surfactant acts much like an interfacial growth agent. Thus designing the selection experiment to mimic this may be beneficial. To this end there are two approaches. The first approach would be to select aptamers that bind specifically to and assemble on Au (100) during crystal growth. In this case, the target material would be single-crystal Au (100), in other words the selected aptamers would have favorable overlaps in lattice geometry with a growing crystal. In the second approach, aptamers are identified that either individually or in concert assemble to form a template within which the nanocrystal forms. In this case that target would be the actual nanorod that the aptamer would be templating the synthesis of.

Because the use of in vitro derived aptamers for materials is still in a nascent stage, considerable efforts will be needed to fully understand what approaches will be most appropriate for identifying the best aptamers for a particular application. In the following sections, the various methods by which one can design selection experiments, using the

elements from Table 4.1, will be discussed generally. In the final sections, phage display and SELEX will be considered separately.

Elements of In Vitro Selection

The Library

In vitro selection is a process for identifying useful biomolecules from a large, randomized library of initial biomolecules. The two key features of each member of the library are (i) a known component that allows for easy replication and amplification and (ii) a randomized region whose permutations provide access to a structurally and functionally diverse pool of molecules. In vitro selection for RNAs (SELEX) utilizes a randomized region linking two known regions that contain primer sequences and polymerase promoter sites. Peptide display utilizes a randomized peptide sequence expressed on the exterior coat proteins of either a cell or a phage particle, allowing for straightforward replication.

Though in vitro selection is often carried out using standardized libraries, either from the literature or from commercial sources, advanced libraries can be designed in order to provide access to aptamers with enhanced structure or function. The factors that can be manipulated in the initial library include (a) the length of the randomized region, which affects the probability of a given function or structure being present in the pool; (b) a predetermined structure or sequence within the randomized region, allowing, for example, the search for aptamers containing dual functionality; (c) the use of artificial amino acid or nucleotide building blocks, giving access to functionalities not normally present; (d) post-synthetic modification of the library, giving access to functionalities not

normally present and decreasing the likelihood of problems during replication and amplification; and (e) the number of copies of individual members of the library, important for selections where the binding affinity is low. The extent to which these manipulations may be utilized is limited to some extent by the use of natural propagation mechanisms, however recent progress has broadened the scope of library design.

In addition to the aforementioned factors, library design should also take into account the eventual use of the aptamer. If the aptamer is expected to play a functional role, for example in synthesis, then some de novo library design based upon the principles of biomineralization may be used. As an example, Slocik et al. showed that a peptide discovered via in vitro selection could be used to synthesize gold nanoparticles.²¹ It was postulated that tyrosine residues in the selected peptides were able to reduce gold ions to Au(0) and initiate nucleation and that the remaining amino acids in the sequence were responsible for controlling the size, shape and morphology of the resultant particles, though there was very little control over these factors. Using this information, one could design an initial library that contained tyrosine as a constant and then randomize over the remainder of the sequence in order to identify peptides that could not only nucleate the material, but also provide access to nanoparticles with predictable geometry through favorable interactions between the peptide and the growing crystal.

The Target

While proper library design can ensure the presence of aptamers with the desired binding specificity or functionality, identification of these aptamers requires choice of the proper target. In general there are two types of targets, the positive target, for which the

aptamer is expected to have an affinity for and the counter- or negative selection target, for which the aptamer is expected to have no affinity for. The role of the counter or negative selection target is to ensure that the selected aptamers are not binding preferentially to the target support (for example the bead to which a small molecule is bound) or binding to a material that is very similar to the positive target. In some cases, proper choice of the counter or negative selection target can be just as important, and require just as much forethought, as selection of the positive target.

As mentioned above, the role of aptamers for materials applications falls roughly into two categories. The first category is aptamers that play a role in recognition, organization or self-assembly. Aptamers in this category are identified using a target that is simply the molecule, material or structure that the aptamer must recognize and stick to. In these cases, the *in vitro* selection process can be carried out using similar techniques as those that are used for biological applications, with similar consideration of counter or negative selection.

The second category of aptamers are those that have a functional role in the synthesis of materials, in which case target selection can be more complex. As mentioned previously, this type of aptamer typically plays two roles: to assist in nucleation and to template growth. In some cases the desired, well-defined material can be selected for directly. For example, Gugglioti et al. selected RNA aptamers that bound to Pd crystals grown in solution with the RNA.¹⁸ Our group has more recently begun selecting RNA molecules that bind to gold nanorods. In other cases the target to be selected for may not be well-defined. Many examples in the literature cite the use of metallic powders,

amorphous solids or single crystalline semiconductor materials. In very few cases, however, is the target adequately described in terms of size, shape, morphology, crystallinity, etc. Even when some details are included, they are often not sufficient. For example, the use of single crystal planes (i.e. GaAs (111)²⁵) is often claimed, yet there is no mention of how this particular face is isolated from defects, edges or other planes. Yet, in order to template the synthesis of materials, aptamers that target specific crystal planes or specific shapes, morphologies or defects will be required. In addition, careful note of the effects of the selection conditions on the target also need to be made.

In order to advance the field, and to identify aptamers that are truly useful for materials applications, well-defined or well-characterized targets will need to be employed. Such targets will allow for better assessment of biomolecule-material interactions, allow for predictive design of libraries, and allow for the preparation of better targets. One such approach that our lab has pioneered is *in vitro* selection on surfaces (ISOS), which allows for the isolation of specific targets on a planar surface, for example specific crystallographic orientations. It is anticipated that this approach will allow for a greater understanding of biomolecule-materials interactions and assist in the isolation of aptamers useful for materials synthesis. Similar, parallel approaches will also need to be developed if the true potential of aptamers for materials synthesis is to be met.

Incubation

The first step of the selection process is to bring the library of biomolecules into contact with the chosen target. The library is suspended in a suitable selection medium that serves several roles. First, the selection medium serves to stabilize the library

components, and in the case of structured libraries, facilitates secondary and tertiary structure formation. Second, the reaction medium carries agents which prevent non-specific binding of non-aptamers to the target, typically surfactants or weak-competitors. In the case of affinity selections, this is typically sufficient. During the selection, the concentration of some components of the reaction medium is usually varied in order to increase the stringency of reaction. Typically, the surfactant, salt or competitor concentration will be increased in order to favor aptamers that have a high avidity for the target. In general, the reaction medium should mimic the conditions under which the aptamer will be utilized, as the structure and function of aptamers is known to be conditions specific.²⁶ Another important aspect of the reaction medium is that it should not modify (unless fortuitously) the material for which the particular biomolecule is being selected. Proper choice of the components of the reaction medium is an important aspect of the selection process, yet the majority of selections for materials applications have not taken this into account.

Aside from the reaction medium, other incubation conditions that affect selection stringency include the library:target concentration ratio, selection time and selection temperature. Changes in the library:target ratio over several rounds of selection allow for control over the competition amongst members of the library for the target and allows for the isolation of the most competitive binders. The ratio is typically manipulated by changing the concentration of the target, as changes in the library concentration can lead to an adverse misrepresentation of members of the library. Temperature may be used to decrease non-specific binding, as well as to help isolate aptamers that have robust

structures. The temperature used must be carefully chosen, as it may also have an effect on the activity of the aptamers. Changes in selection time can be used to distinguish between aptamers that bind rapidly versus those that have the highest degree of specificity. In general, longer reaction times can allow for the selection of aptamers with higher specificity. Control experiments can be used before the formal selection experiment to determine optimum ratios, temperature and time of selection as well as the components of the selection medium.

Washes / Elution

While the first three steps are crucial for ensuring that all elements of the library have equal access to the desired target, allowing for selection of the best aptamers, the washing and elution steps are crucial for ensuring that the best aptamers are separated from non-aptamers. Following incubation, the target will typically be washed several times with the selection medium to ensure all non-target specific species have been removed. Much like with the incubation step, the stringency of the washing step can be increased during successive rounds of washing.

Following sufficient washes to ensure that all non-specific species are removed, the aptamers must be isolated from the target. This is typically achieved by adding a chaotropic agent or competitor, increasing temperature, varying pH or some combination of these methods. For example, in phage display, the bound phage are often eluted using low pH. Chaotropic agents are used to disrupt any supermolecular interactions (H-bonding, van der Waals interactions, etc.) between the aptamers and the target, either through competition or denaturing. Other agents may bind the substrate covalently,

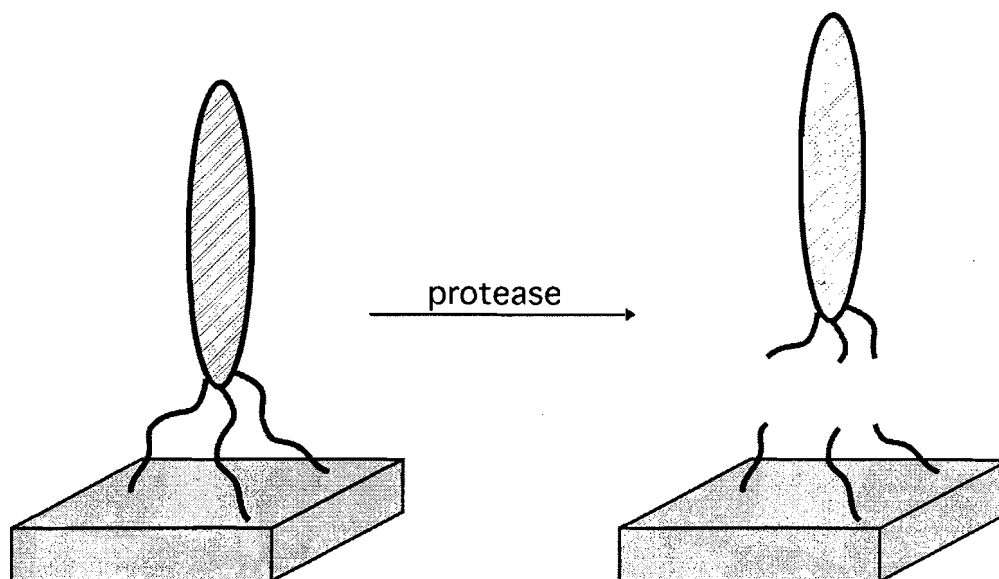


Figure 4.3. Schematic showing the release of phage from the target surface using a protease.

displacing bound aptamers. Many times, a chaotropic agent will be used in conjunction with increased temperature to ensure efficient elution. It has been shown that, in some cases, the selected aptamers bind to the target irreversibly, which would lead to their non-representation in the final aptamers.²⁷ In these cases, in situ reverse transcription or infection may allow for the capture of these species. Another approach, useful in phage display, is the use of proteases to cleave the bound sequence (Figure 4.3), allowing for retrieval of the active phage for infection.²⁸ Since the random sequence is coded within the genome, all progeny will continue to have the same sequence. An opposite technique, wherein photo-active agents have been introduced to the RNA sequence, have been used in SELEX.²⁹

Amplification

Once eluted, the selected aptamers need to be amplified for further rounds of selection or for characterization. RNA is reverse transcribed to DNA, amplified via PCR

and then transcribed back into RNA, yielding the new selected library. Phage is incubated with its host to generate new copies of the selected phages. While amplification is typically a straightforward procedure, complications can often arise as a result of complexities within the library. For example, elements of the library may be particularly structures can interfere with the transcription process in RNA. It is known that some sequences of amino acids displayed on the surface of phage can interfere with the transport of the virus into and out of the cell.^{11,28} Similarly, the use of artificial amino acid^{30,31} or nucleotide³² building blocks may also limit amplification efficiency. Many times, the region responsible for amplification (constant regions or coat proteins) is also involved in binding, which can also impede amplification. Unfortunately, it is impossible to control or predict all possibilities and as a result, some aptamers may be lost due to insufficient amplification. That said, the use of highly efficient reverse-transcription enzymes in SELEX, the use of phage wherein the randomized region is not associated with coat proteins responsible for infectivity and other library design techniques can help. Furthermore, in situ RT or infection may also benefit situations where species are bound strongly to the target.

One technique for improving selection that can be carried out during the amplification process is the introduction of mutations within the randomized region. During the selection process, it is anticipated that the population of aptamers is being enhanced with aptamers of greater suitability or fitness. However, this enhancement is limited by the number of elements in the initial library. For example, the most commonly used phage display library has a randomized region of 12 amino acids, allowing for, in

principle, $\sim 10^{13}$ possible unique sequences. However, due to the inherent difficulties of synthesizing such large libraries, typically only 10^9 unique sequences are available in the initial library. One method for circumventing this limitation is to introduce mutations that allow for exploration of sequences close to those that show an enhanced selectivity for the target. The initial selection can be considered a low resolution overview of possible sequences, while the mutated selection can allow for a higher resolution inspection of sequences of interest (Figure 4.4.). Using this technique, it is possible to explore a larger

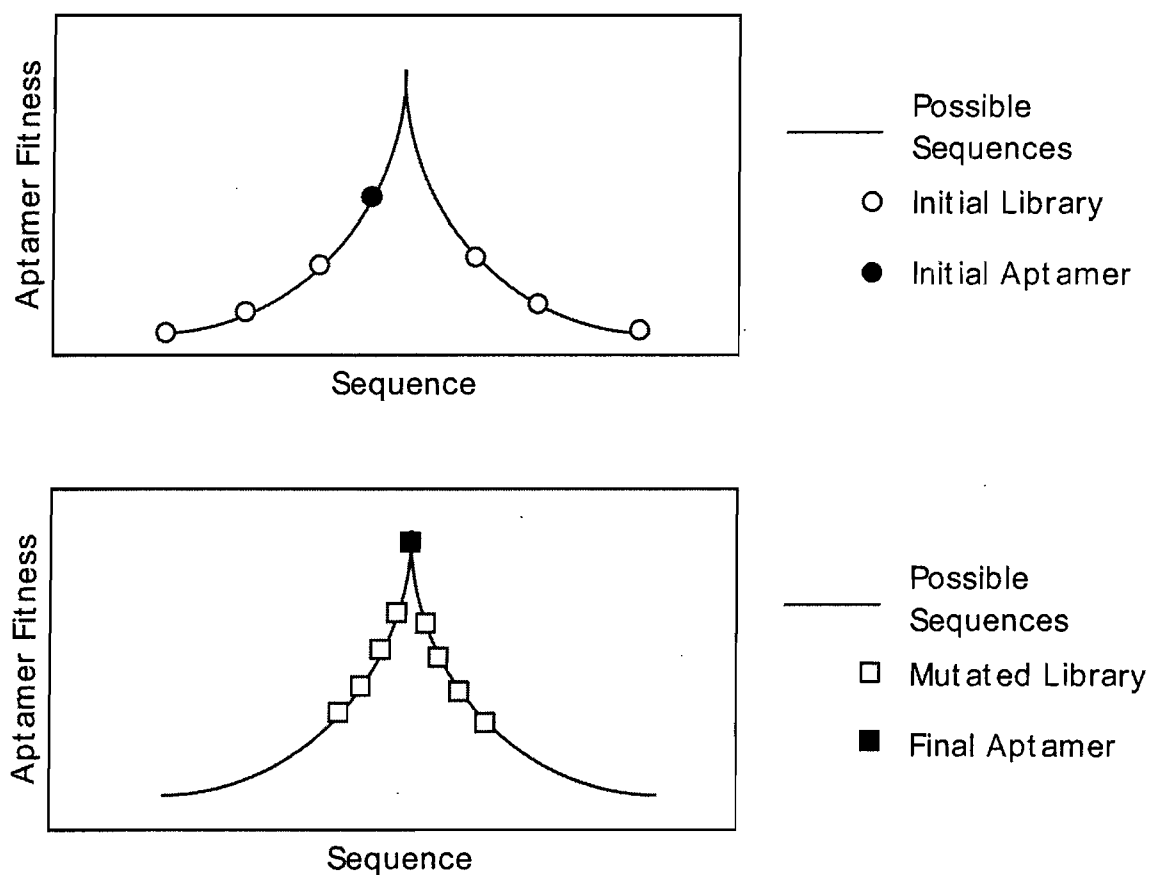


Figure 4.4. Probing of sequence space using mutations. In the top graph, sequences that are relatively far apart in sequence space are screened for fitness, yielding an initial aptamer. The initial aptamer is mutated, yielding sequences close to the initial aptamer from which the final aptamer is isolated.

region of sequence space, allowing for the identification of aptamers with a greater utility than may otherwise be available in the starting library.¹¹

Characterization

Following the selection process, and often during, the aptamers that have been discovered will typically be assayed and characterized. Characterization typically involves determining the amino acid or nucleotide sequence of a subset (~20-50 sequences) of the isolated aptamers. Within the subset of aptamers sequenced, conserved regions or motifs are often found that contain either the necessary structure, function or both that make the aptamer useful. Analysis of the conserved region with regards to the properties of the building blocks can often lead to the development of sequence-function relationships. While it is often desirable to have very similar or exact overlap between sequences, often the sequences will only be related by some intrinsic property such as isoelectric point, hydrophobicity or structure. Often times, specific residues will be replaced within the randomized region of identified aptamers in order to probe the function of specific building blocks on the functionality of the aptamer. For larger sequences, and where structure may play a role in the activity of the aptamer, predictive structural modeling may be used to better understand the structure.³³ Crystallography, melting points and circular dichroism may also be used to understand the structure of the isolated aptamers, however these techniques have not been explored significantly for materials applications. More recently, computational methods have been utilized to probe the relationship between structure, sequence and target binding.³⁴

Along with structural characterization, binding studies are often carried out to determine the specificity and affinity of the selected aptamers for the target, often taking the form of binding assays. For materials, this is often done by defining a known area of the material to be assayed onto a substrate and quantifying by appropriate means the concentration of aptamer that will bind to the material. Shown in Figure 4.5 is a gold dot assay that we used to understand the binding of RNA aptamers to a gold surface. In this case, the RNA was incubated with the gold surface under varying RNA concentration. This varying concentration is shown as a gradient in the resultant dots. In another assay, Belcher et al. expressed short peptide sequences on the surface of yeast cells, and used routine cell-counting techniques to determine binding affinities.³⁵ Other assays, using quartz-crystal microbalances or surface plasmon resonance have also been explored for

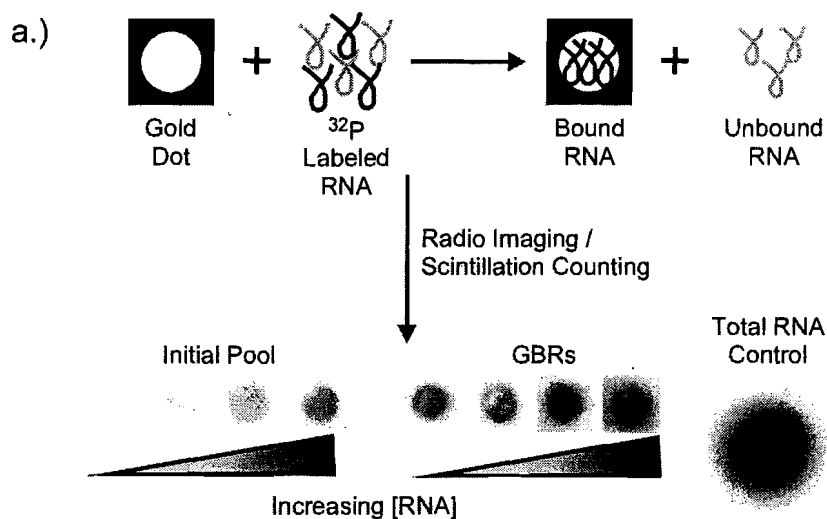


Figure 4.5. Gold dot assay used to quantify RNA binding to gold. ^{32}P labeled RNA was incubated with gold dots on an SiO_2 substrate. Following imaging or scintillation counting, the quantity of bound RNA could be determined. At the bottom are the results of a concentration gradient assay.

quantifying binding between noble metals and aptamers.^{22,36} Because the nature of materials and the properties selected for can be so diverse, assays often have to be designed on a per-experiment basis, often making assays time consuming and difficult.

As an alternative, materials aptamers are frequently tested directly for their intended application, side-stepping any need for complete characterization. Since complete characterization can be costly and time consuming, assaying for usefulness can often be more efficient. Once aptamers have been identified that are useful for the intended application, then complete characterization can be carried out to determine how and why the aptamer is useful for the intended application.

Peptide/Phage Display

Introduction to Phage Display

The in vitro selection technique most often used for materials applications is peptide display, and more specifically phage display. In peptide display, the genome of a cell or virus is engineered so as to “display” a randomized peptide sequence as a fusion to a coat protein located on the surface of the carrier.^{11,28} Thus displayed, the randomized peptide is free to interact with the environment and the target materials of interest. Phage display is an attractive option for materials applications because commercially available phage display kits make it easy to carry out, the phage are fairly robust and the displayed peptides confer a wide array of functionality. Conversely, the short length of the peptides displayed (generally 12 or less amino acids) limits the usefulness of commercial phage display libraries where structure is expected to play an important role. Additionally, the relatively small size of the displayed sequence in comparison to the phage as a whole

may also factor into the selection process. Nevertheless, peptides have been identified that bind to metals, e.g. Au,³⁷ Ag,³⁸ oxides,^{39,40} semiconductor,²⁵ zeolites,⁴⁰ polymers,⁴¹ and carbonaceous nanomaterials.^{2,42}

Introduction to Bacteriophages

A bacteriophage is a virus that infects bacterial cells and uses the hosts replicative mechanisms to propagate itself.⁴³ The phage used for phage display all target *E. Coli* as their host, and the phage most commonly utilized is the M13 filamentous phage (Figure 4.6). The M13 phage is non-lytic, and contains a circular, single-stranded DNA genome packaged within the major coat proteins. The coat protein pVIII is the major coat protein,

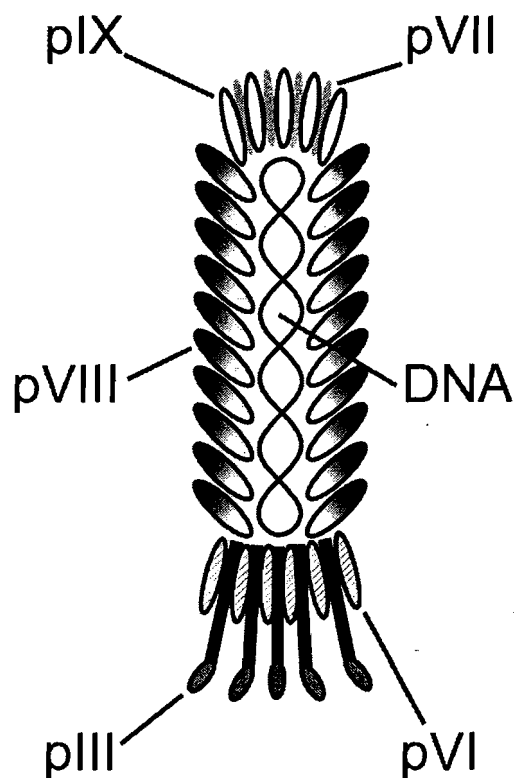


Figure 4.6. Diagram of the M13 filamentous bacteriophage, with all labeled coat proteins. Coat proteins pIII and pVIII are the most commonly modified for phage display, though all have been used. pIII is also responsible for infectivity.

and makes up the majority of the surface of the phage. Coat proteins pVII and pIX are responsible for transporting the phage through the cell membrane and pIII and pV assist in terminating the self-assembly of the phage particle. pIII is also for the infectivity of the phage and contains recognition sites for receptors on the surface of the bacteria.⁴³

When designing a phage display library, the goal is to modify one of these coat proteins with a combinatorially derived, randomized peptide without affecting the stability or infectivity of the phage. Although all five coat proteins have been modified for phage display, pIII and pVIII remain the most commonly utilized.¹¹ In fact, the phage display system almost exclusively used for materials applications, the Ph.D. 12 kit from New England Biolabs, relies upon fusions to the N-terminus of the pIII coat protein. Despite the fact the pIII is most commonly utilized, there may be advantages to using pVIII instead. Because pVIII is the major coat protein, the number of copies of the randomized peptide (display density) can be as high as ~2700, important when binding affinities are low. For example, two rounds of selection using pIII expressed peptides yielded 40% positive identification of the desired aptamer, whereas pVIII yielded >75% positive identification.²⁸ In addition, because pIII is important for infectivity, tight binding of an aptamer fused to pIII could reduce infectivity and potentially lead to the loss of the best aptamers. Though pVIII is an attractive alternative, it has been shown that pVIII is far less stable to modification than pIII, potentially limiting its utility in phage display.^{11,28} To modify the coat proteins, the DNA sequence containing the peptide sequence to be displayed is inserted within the genome of the phage between the sequence coding for the

signal peptide and the amino terminal region of the intended coat protein. This insertion leads to the expression of the desired peptide sequence on the surface of the phage.

Because phage display is often carried out using commercial libraries, modification of the library for materials applications is relatively rare. Nevertheless, using custom made libraries it is possible to manipulate such factors as randomized peptide length, structure, and degree of randomization. Additionally, recent progress has allowed for the use of non-natural peptides in phage display. Sandman et al. in 2000 reported the use of

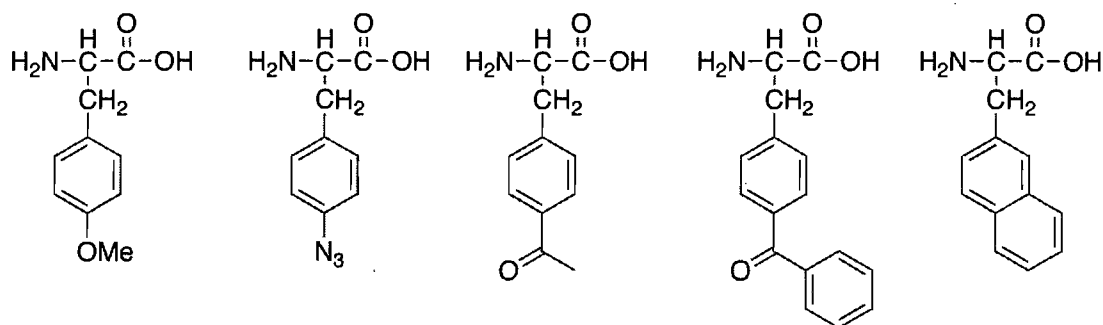


Figure 4.7. Chemical structures of the modified alanine derivatives used for phage display.

peptide sequences containing selenopeptides for phage display.³⁰ In 2004, Tian et al. reported the use of a number of alanine derivatives for phage display³¹ (Figure 4.7). Of course, extensive modification of the displayed peptides is limited to those that do not have a deleterious effect on the life-cycle of the phage. For example, extensive modifications of the pVIII coat protein in M13 phage can render the virus inactive. As well, the inclusion of cystein residues on the PIII coat protein can lead to difficulties in the secretion of the phage through the periplasm of the infected bacterium.²⁸ Because in vitro peptide display has become such an attractive tool, however, many of these

limitations are being overcome, either through clever experimentation or via the use of alternative peptide display methodologies.

Peptide / Phage Display For Materials

Perhaps the earliest, and most thorough, example of in vitro selection being carried out for materials applications was the pioneering work by Stanley Brown.⁴⁴ In 1992, he described the construction of an *E. Coli* peptide library containing a nine peptide randomized sequence displayed on the exterior lambda receptor of the bacterium. This library was used to identify peptides that bound specifically to iron oxide. To carry out the selection, the *E. Coli* and iron oxide were cosuspended in a buffer solution. After a 10 minute incubation at room temperature, the iron oxide particles with *E. Coli* bound were magnetically separated from the solution. After suitable amplification of the binding species, additional rounds of selection, five total, were carried out. To test the fidelity of the selection, binding to mixed iron oxide was compared to other metal oxides (Fe_2O_3 , Fe_3O_4 , Cr_2O_3) and it was shown that binding was conferred only to the target species and not the Fe(II), Fe(III) or the Cr species individually. This early work demonstrated some key components of successful in vitro selection for materials: (i) the use of an intrinsic property of the target to isolate the desired peptides and (ii) thorough characterization of the selected peptides to ensure the selection was successful. Brown followed up this work with a report in 1997, identifying peptides that bound to gold using a similar *E. Coli* peptide display library.³⁷ One important point made in this report is the need for substrates free of contaminants that could complicate selection.

In 2000, Brown co-authored a report detailing the selection of gold-binding peptides or GBPs using similar cell-display techniques.⁴⁵ At first, five rounds of selection were carried out for binding to the gold powder. Following this selection, fifty of the isolated gold binders were assayed to determine their effect on the kinetics of gold crystal growth. From this pool, five peptides were isolated and further characterized. They surmised that the isolated peptides could either act through perturbation of local environment (through changes in pH) or through preferential absorption to Au (111) faces to direct gold crystal growth. Furthermore, it was expected that these isolated gold binders were physisorbed via polar side groups onto the surface rather than chemisorbed. As a follow up to this work, Braun et al. carried out structure prediction and molecular dynamics simulations to better understand how structure may play a role in the binding of the GBPs to the gold surface.³⁴ A predicted structure of GBP was calculated and “placed” onto Au (111) and Au (211) surfaces so that the largest number of hydroxyl groups (those thought to bind the surface) would contact. It was hypothesized that interactions between Au (111) and the GBP were favored over (211) due to the ability of water molecules to diffuse between the GBP and the gold surface on the less atom-dense surface of (211). Further followup work by Tamerler et al. utilized quartz crystal microbalance and surface plasmon resonance experiments to probe both the specificity of the the GBP to gold versus other noble metals and to better understand the kinetics of binding.^{22,36} This series of experiments has been important to the development of the field of in vitro selection for materials as it moves from discovery to understanding how the peptides bind to the surface. This level of understanding may eventually allow for (i) the design of better,

more well defined targets for selection, (ii) the design of libraries to further probe the sequence space near to the isolated GBPs or (iii) the design of organic ligands that closely mimic the activity of the isolated GBPs. In any case, this work provides a good foundation by which others can carry out similar experiments.

In 2000, Whaley et al. reported the use of phage display to identify peptides that bound to GaAs with a higher affinity than GaAs(111A) or (111B).²⁵ In this work, “single crystal” GaAs (100) (most likely chips) was incubated with a commercial phage display library using standard kit procedures. Sequencing of the isolated phage revealed that no consensus sequences. Identified phage were tagged either with fluorescent molecules or gold nanoparticles and the binding specificity to GaAs (100) was confirmed through the use of fluorescence and scanning electron microscopy. Interestingly, they did not carry out controls in order to determine whether the displayed peptide or the phage particle itself was responsible for binding. Follow up work by another group showed that, in fact,

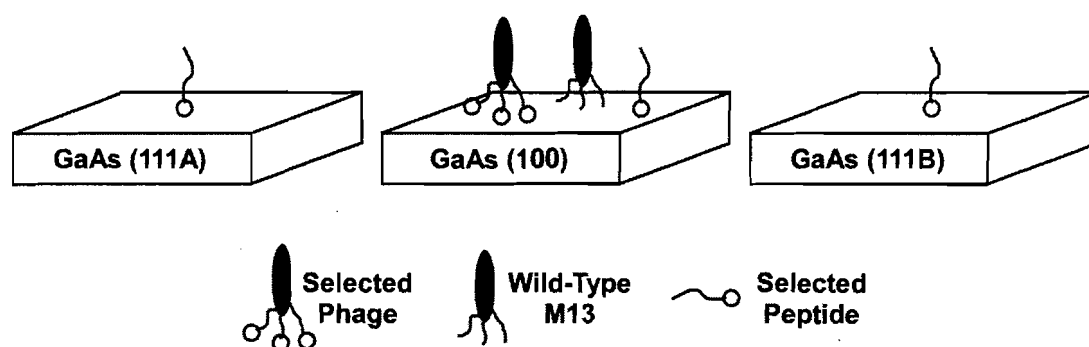


Figure 4.8. Whaley reported the binding of phage to GaAs with a high degree of specificity for (100). Follow up studies showed that the selected peptide has no specificity and that in fact the pVIII major coat proteins were responsible for the specificity, not the selected peptides. Thus, the selected phage and the wild-type phage have identical specificity for GaAs (100).

the displayed peptides were not responsible for binding, but instead the pVIII coat proteins bound to the substrate⁴⁶ (Figure 4.8). Despite being a very influential paper in the field, this report offers lessons not necessarily from what they did, but from what they did not do: (i) choose a target that was well-defined, (ii) carry out negative selections and (iii) carry out sufficient controls in order to ensure that their conclusions were founded. Nevertheless, the ideas and concepts presented in this paper have helped to foster further interest in the area of aptamers for materials.

The Naik group has published extensively on the identification of peptides via phage display that will both assist in the synthesis and self assembly of a range of materials from silica and titania to silver and gold.^{2,21,38,47} In 2002, the identification by phage display of peptides that would mediate the formation of silver nanocrystals was reported.³⁸ Standard kit phage display techniques were used on acid-etched silver powders. Following selection, the ability for these isolated peptides to catalyze the growth of anisotropic silver crystals was observed via both TEM and UV/vis spectroscopy. Interestingly, in 2005 Slocik reported the use of one of these silver binding peptides, A3 (AG3 previously), for the preparation of spherical gold nanoparticles of 12-15 nm diameter.²¹ It was postulated that tyrosine residues in the A3 peptide were responsible for reducing Au (III) to Au (0) and leading to nucleation, while the remainder of the peptide was responsible for surface passivation. A3 modified with the Flg peptide sequence could be assembled onto an anti-Flg coated surface. Here, two of the hallmarks of a bioninspired approach, synthesis and assembly, are combined and show the ease by which simple biological building blocks can be combined to yield multifunctional

molecules. In comparison, a similar approach using organic synthesis to design a molecule that could reduce, nucleate, mediate the synthesis of and assemble gold nanoparticles would be exceedingly difficult.

One approach that the Naik group has developed that has contributed significantly to the advancement of the field is polymerase chain reaction-driven phage display²⁷ (Figure 4.9). In their earlier work with silver binding phage, three silver binding peptides were identified. Of these, only one was proficient in the synthesis of silver nanoparticles. This prompted them confirm whether or not all of the phage was being eluted during the standard reduced pH phage elution step. Phage display was carried out on commercially obtained silver or cobalt nanoparticles using standard selection conditions. Following acid elution, the nanoparticles were heated to 95°C in a lysis buffer to denature any

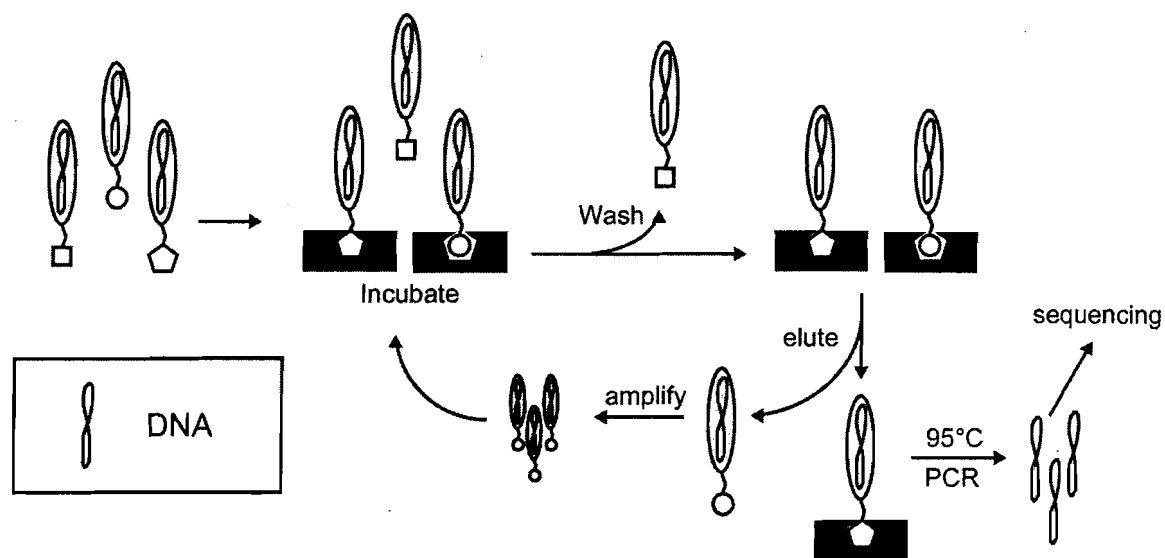


Figure 4.9. PCR driven phage display as described by Naik et al. Selection is carried out as normal, however following elution, any remaining phage is denatured and released DNA is amplified and sequenced. It is expected that these remaining bound phage contain aptamers of greater binding strength.

remaining phage and release the phage DNA. Following PCR amplification it was noted that in fact some phage remained on the surface of the silver nanoparticles after acid elution. Comparison of the eluted sequences and the sequences obtained following PCR showed no sequence overlap. In the case of cobalt nanoparticles, sequences were obtained for PCR, eluted-PCR and standard phage display samples. In this case, the PCR and eluted PCR samples did have some sequence overlap. These experiments show that in some cases, the aptamers may become irreversibly bound to the target and may require some ingenuity to isolate and analyze. Because of such irreversible binding, there remain some questions regarding other phage display experiments that have utilized very basic methods for isolating the bound phage. Methods such as PCR driven phage display, or protease driven phage display may provide some utility in improving the accuracy of such selections. Another option is to utilize phage display libraries (i.e. T7 phage display) wherein the displayed peptide does not interfere with infectivity. Using such libraries, in situ infection of the host bacteria should be possible.

In 2005, Zuo et al. reported the identification of peptides that bound to both steel and aluminum using a standard M13 phage display library, with the expectation that these peptides could be expressed on the surface of bacteria in order to form biofilms that could protect against corrosion.²⁶ For this reason, the choice of target was simply either of the metals cut from sheet stock, with no emphasis on the details of the surface. The aspect of this work that is interesting is the incubation conditions, and the methods by which the isolated the strongest binders. For the first three rounds of selection, the phage were incubated with either the steel or aluminum in a solution known as the Vaatanen nine

salts solution, which mimics a corrosive marine environment. Because aptamers can be very sensitive to the conditions under which they are selected, it is important that the selection medium closely mimic the intended application. Following three rounds of selection in the Vaatanen nine salts solution, the phage were exposed to a more stringent treatment, sonication. Those phage that remained bound following sonication were considered to be the strongest binders. With this work, Zuo et al. were able to step outside of that standard procedures typically used and isolate peptide aptamers that function under extreme conditions.

Peptide / Phage Display Wrap-Up

Peptide display has played an important role in the development of in vitro selection for materials applications. Although some early work by Brown and some follow up by Sarikaya has employed the use *E. Coli* surface display, the majority of the work carried out has been done with the commercially available Ph.D. 12 phage display library. Despite the ease of selection and the utility of the peptides derived from this library, the continued use of the Ph.D. 12 library for materials applications may not be warranted beyond proof-of-principle work. Some reasons include:

(1) Infectivity and display rely on same coat protein. This limits the degree to which the library can be modified and also limits the degree to which alternative elution / capture of the selected phage may be carried out. Ideally, the displayed peptide should be separate from the functionality of the phage.

(2) As the peptides are displayed on the pIII coat protein, display density is limited to ~5 copies / phage. Because knowledge with regards the binding of peptides to

materials is still in a nascent stage, the ability to tune the display density, at least initially, would be useful. This is especially true where binding affinity may be very low.

(3) Displayed peptides are limited to either 7 or 12 amino acids in length in the commercial libraries. The ability to use larger libraries can allow for greater diversity and greater access to peptides with potentially useful structures.

(4) In comparison to other bacteriophage, the M13 phage that is most commonly used may denature under the conditions of selection most useful for materials, for example high ionic strength or extremes in pH.

A number of alternative peptide display systems exist that may be better suited to materials applications. The aforementioned E. Coli display techniques (available commercially as FliTrx from Invitrogen), yeast display and a variety of other phage including T4 and Lambda phage. One particularly promising candidate for an alternative peptide display system is T7 phage display, of which Novagen's T7Select system may be the most readily available. T7 has the ability to display peptides of up to 50 amino acids in length at a moderate display density of up to 415 / phage. At the other extreme, peptides of up to 1200 amino acids have been displayed at 1 / phage. This flexibility arises from the fact that T7 is a lytic phage, so the limits placed upon M13 phage display are not so severe, though practically, 50 amino acids is standard. This longer randomized region length allows for greater access to structured peptides, as well as peptides containing predefined structural or functional regions. In terms of elution, the most convenient method is direct infection, as the displayed amino acids do not interfere with infectivity. T7 can also be modified with protease sites that cleave T7 from the target, allowing for

elution of phage from the target. T7 is stable under a wider variety of conditions, including high ionic strength and a wide range of pH. These factors make T7 a promising alternative to M13 phage display for materials applications.²⁸

SELEX

Introduction to SELEX

The use of SELEX for the identification of RNA aptamers suitable for materials applications is a recent development, and in comparison to various peptide display techniques, remains relatively unexplored. Yet, the larger randomized regions available and larger number of individual sequences, as well as access to secondary and tertiary structures make SELEX attractive for applications where structure and diversity are important. In addition, RNA is being shown to have much greater functional diversity than previously thought. Whereas phage display can be limiting in design of the initial library in terms of size and structure, SELEX offers much more flexibility and, in principle, is more convenient to modify.

The first step of the SELEX process is to design and synthesize the initial randomized pool of ssDNA sequences using standard synthesis techniques. The individual elements of the library contain a known region, followed by a combinatorially synthesized randomized region and a final known region. The initial pool is PCR amplified to generate several copies of each individual ssDNA in its double stranded form. And finally, transcription of the dsDNAs yields the ssRNAs that are used for the SELEX experiment.

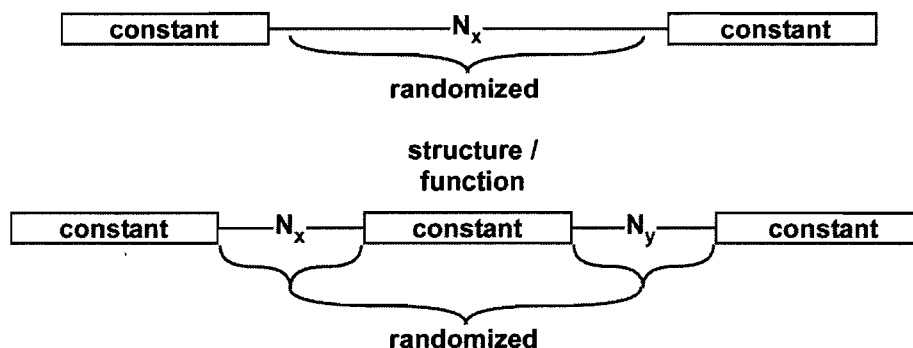


Figure 4.10. Example SELEX templates. At the top is a generic template containing two known regions for propagation and a randomized region. At the bottom is a more complex template containing a region of known structure or function between two randomized regions.

In Figure 4.10 are two example SELEX templates. The top figure shows the most basic template, with two constant regions that contain primers sites and polymerase promoters. Because it is expected that the constant sequences also will be found within the randomized region, highly efficient and specific promoters should be used. Typically, promoters for bacteriophage T7 polymerase enzymes are employed. Between the known regions is the randomized region of length x as defined by the designer of the template. This type of template is useful for general SELEX experiments where the primary goal is to identify RNAs that bind to a specific target.¹³

One common method of modifying the SELEX template is to insert within the randomized region a known region that contains some structural or functional component that is useful for the intended purpose of the selected aptamer. Typically, this constant sequence will have been discovered during previous selection experiments. The point of carrying out such an experiment is to gain access to the sequence space near the known region in order to identify aptamers with enhanced functionality. Similar permutations of

known and randomized regions may be used to identify bifunctional aptamers. Another common method for modifying the SELEX template is to vary the ratio of nucleotides during the combinatorial synthesis. For example, one could use more pyrimidines than purines, leading to a greater proportion of Cs and Us in the final SELEX library.¹³

The length of the randomized region is another variable of the initial template that can require special attention. The length of the randomized region plays a role in both the frequency and complexity of aptamers isolated from a given pool. Legiewicz et al. carried out studies that screened different length randomized regions for RNAs that contained a known aptamer for isoleucine. They found that while the shortest randomized region (25 nt) contained the correct binding site, mid-sized randomized regions of 30-70 nt had not only the correct binding site, but also an optimal secondary structure. Interestingly, the longest sequences showed very little activity. It was surmised that in the case of mid-sized randomized regions, there was enough sequence space to gain access to binding and structure as well as replicative ease. Longer RNAs can be more difficult to replicate and shorter RNAs are not sufficiently structured.⁴⁸

A final method for modifying the SELEX library is through the introduction of artificial nucleotides. Despite the fact that modified nucleotides can interfere with the functioning of polymerases, some recent work has shown that the pyrimidines, most notably uracil, can be modified without adversely affecting reverse transcription. Recent work by Bugaut et al. has shown that 2'-amino uracil can be easily substituted in the randomized region of the RNA (Figure 4.11).³² Post-synthetic coupling of the primary amine with aldehydes was used to introduce functionality to the backbone of the RNA

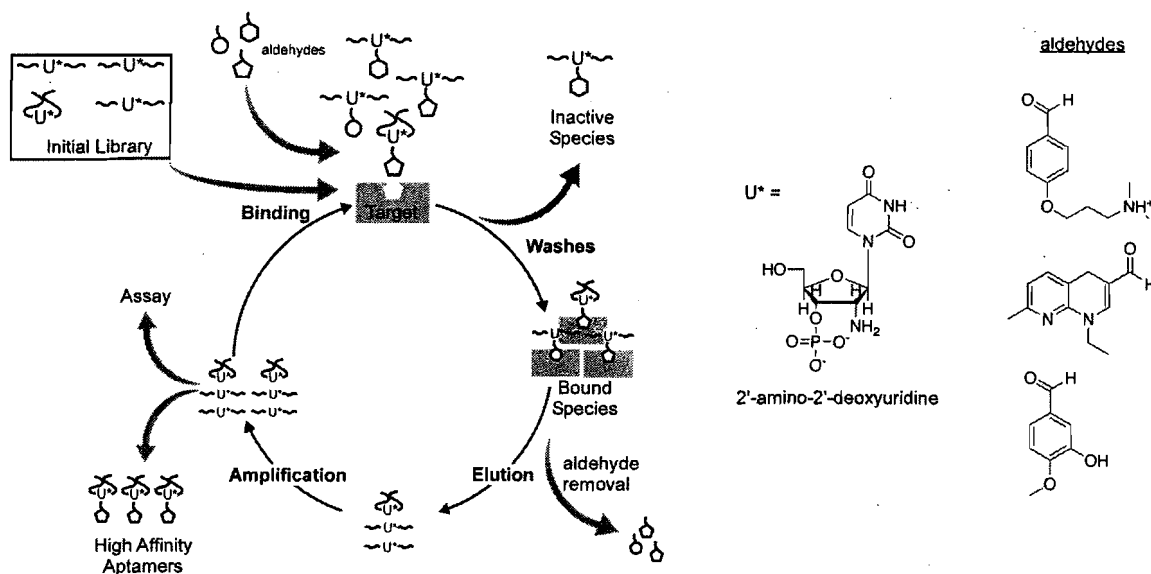


Figure 4.11. Schematic of the SELEX process utilizing a post-synthetic modification scheme to introduce functionality to the SELEX library.

that would otherwise be unavailable. These RNAs are carried through the selection and upon elution, the added functionality can be hydrolyzed from the RNA leaving the native library which can then be amplified. Similar approaches can be used to introduce chelating groups, reducing groups, or other functionalities useful for materials synthesis. In addition, post-synthetic modifications can be used to enhance the stability of the RNAs to degradation by RNAses.

SELEX For Materials

In 2004, Gugliotti et al. reported the use of SELEX for the identifications of RNA aptamers that mediate the synthesis of Pd crystals.¹⁸ Motivated by earlier work with phage displayed peptides, and by the fact that RNA had been shown to catalyze a number of catalytic processes, they sought to identify RNAs that would be useful for materials applications. They designed a SELEX template containing a 40 nt randomized region and used a modified nucleotide, 5-(4-pyridylmethyl)-uridine-5'-triphosphate to confer

additional metal coordination sites. To carry out the in vitro selection, their RNA library (10^{14} constituents) was incubated with a zero-valent palladium precursor (dibenzylidene-acetone palladium(0)), yielding a crystalline precipitate. To separate functional RNAs

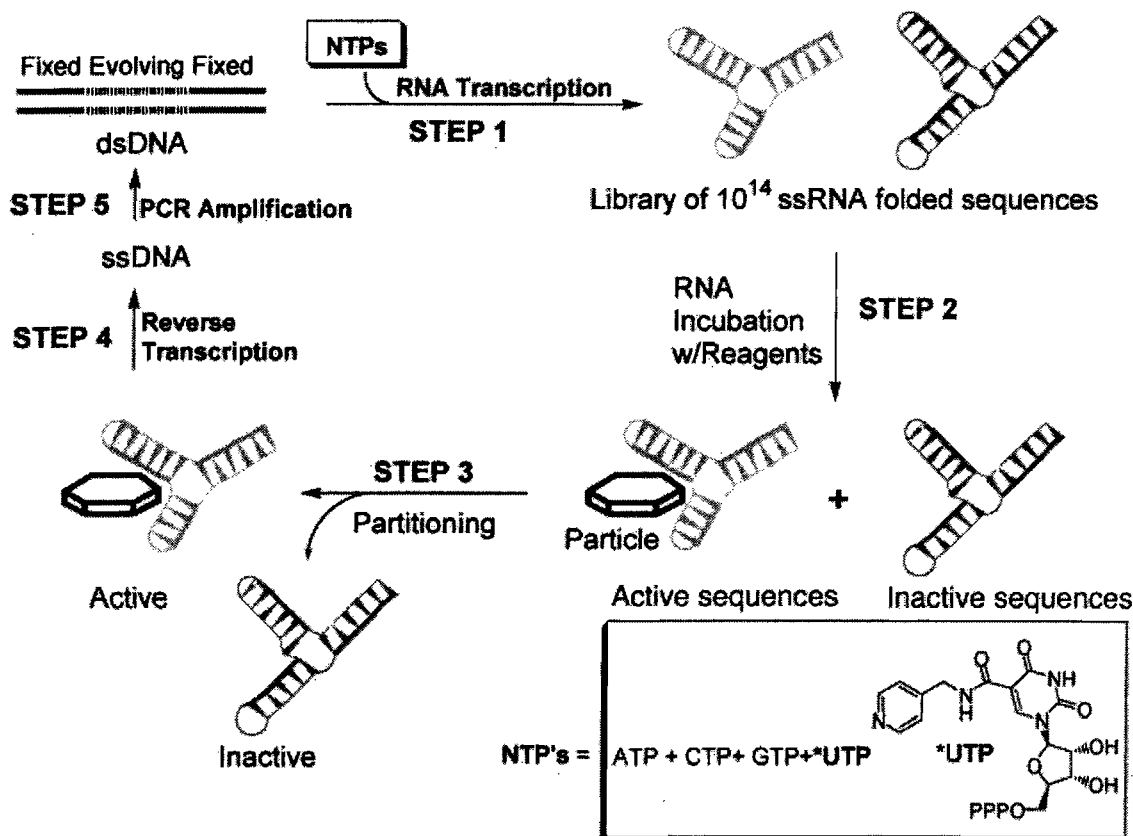


Figure 4.12. SELEX scheme used by Gugglioti et al. to identify RNA aptamers that catalyzed the formation of Pd crystals. Note the use of modified UTPs. From Guggliotti, L. A.; Feldheim, D. L.; Eaton, B. E. *Science* **2004**, *304*, 850. Reprinted with permission from AAAS.

from non-functional RNAs, the product was filtered on a size-exclusion membrane and washed. Those bound to the crystals were appropriately amplified and the cycle was repeated several times to isolate RNA aptamers that catalyzed the formation of small Pd crystals of micron to sub-micron dimensions (Figure 4.12). Aside from being the first report of SELEX being used for materials synthesis applications, this report was

significant in that (i) the initial library was designed specifically for the intended application, (ii) the spontaneous formation of particles in the presence of the RNA provided an ideal target substrate and (iii) the selection was sufficiently successful to yield strong a strong consensus sequence amongst the selected RNAs.

Follow-up work has shown that the RNAs selected in this experiment could be useful for the formation of both Pd, Pt and Ni crystals with different morphologies that were dependant upon the metallic precursor and the RNA sequence.⁴⁹ For example, Pt₂(DBA)₃ yielded spherical, cubic and hexagonal particles with majority spherical particles using one RNA aptamer and majority hexagonal particles using another RNA aptamer. Pt(PPh₃)₄ yielded all spherical particles independent of the RNA aptamer used. More recently, they have tethered these aptamers to gold surfaces through a 5' phosphorothioate modification. The tethered RNAs were then used to synthesize tethered Pd crystals. Lithography was used to form patterns on the surface, yielding circular regions of crystals on the surface. In this case, two hallmarks of a bioinspired approach are being demonstrated: self-assembly and biological synthesis.¹⁹

Recently, we have reported the use of SELEX for the identification of RNA aptamers that bind to gold surfaces (see Chapter V). To carry out the selection, we developed a novel approach known as in vitro selection on surfaces (ISOS) for the identification of aptamers useful for materials applications. ISOS is distinguished from previously described approaches in that a microreactor is used to define a specific area on a surface of interest upon which the selection will occur (Figure 4.13). This approach allows for the selection of aptamers that can identify specific crystallographic

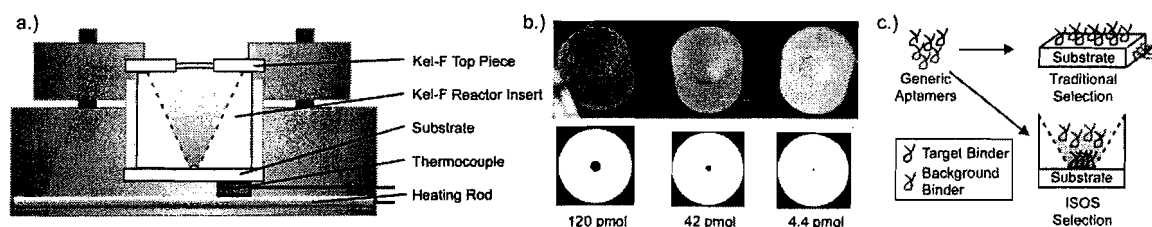


Figure 4.13. (a.) The ISOS microreactor, with important elements labeled. (b.) ISOS inserts that provide access to the surface of interest. (c.) Comparison of ISOS selection to traditional to selection using 3D substrates.

orientations, defect sites, monolayers and other surface targets. In addition, the design of the approach allows for easy control over the concentration of the target surface, allowing for more competitive selections.

To carry out the selection, an RNA library containing a 40 nucleotide randomized region was exposed to an evaporated gold surface using ISOS. Following incubation, unbound RNAs were washed away using the selection medium and the bound species were eluted using formamide at high temperature. After suitable amplification, additional rounds of selection were carried out. After six rounds of selection, binding assays and structural probing indicated that the gold binding aptamers were highly structured and were enriched with single-stranded adenine binding sites.

In comparison to previously reported selections for materials, and gold in particular, this work contained several important advances, namely (i) a well-defined target with controlled concentration, (ii) a selection medium that reflected the eventual intended use of the aptamer, (iii) selection conditions that induced competition amongst the RNAs for the surface, (iv) use of temperature, salt and added competitor to assist in isolating the fittest aptamers and (v) full characterization of the isolated aptamers. The full report of this work can be found in Chapter V.

Comparison of SELEX to Peptide Display

Phage and cell surface display of peptides have seen wide-spread for in vitro selection on materials. In comparison to SELEX, phage display is rapid and relatively easy to carry out. In addition, the wide variety of functional groups represented in the 20 amino acids can be beneficial for numerous applications. On the other hand, SELEX has some advantages over peptide display. First, it is far more convenient to design custom SELEX libraries given robust and efficient primer / polymerase promoter sites. Control over the randomized region length, the inclusion of known structures or functions, and the use of modified nucleotides are possible. As mentioned previously, a number of catalytic RNAs have been recently identified, and it has been conjectured (via the RNA world hypothesis) that RNA aptamers could be discovered with as much functional diversity as peptide aptamers. That said, because much longer RNA libraries are typically used than for peptide display, RNAs are expected to contain a much greater structural component in their aptamer functionality. So, for example, RNAs may make superior templates for the synthesis of materials. While both in vitro selection techniques have their drawbacks and benefits, together they offer a considerable opportunity to improve upon our ability to synthesize and self-assemble a wide variety of materials.

Summary and Paths for Advancement

In vitro selection is rapidly developing into a promising tool for the discovery of both polypeptide and polynucleotide aptamers for materials. Aptamers have been discovered that bind to almost every class of technologically useful materials, and which

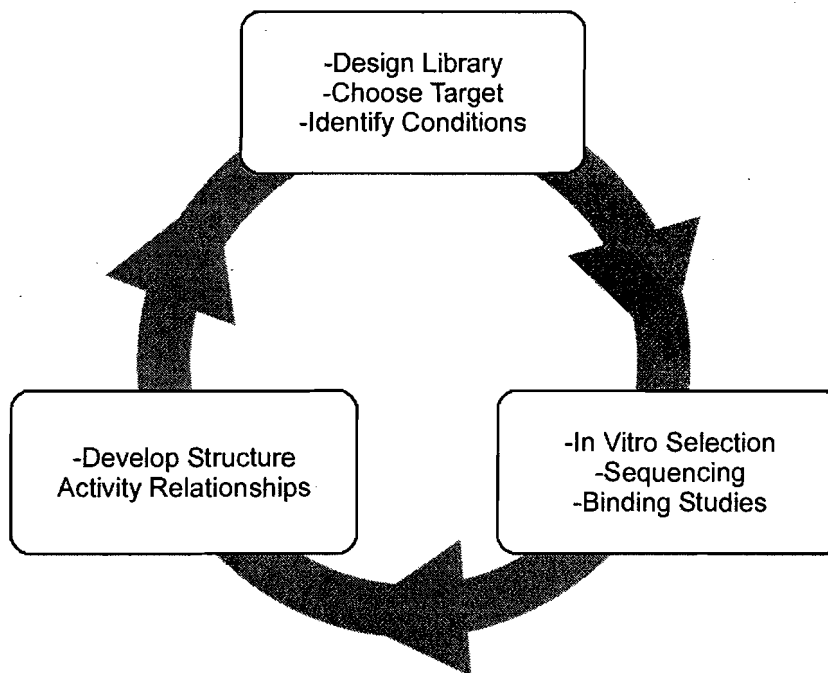


Figure 4.14. Scheme showing the development of structure-activity relationships to guide the development of increasingly advanced in vitro selections for materials.

also assist in the growth and self-assembly of materials. Continued progress in the field faces considerable research challenges in terms of optimizing selection, understanding materials-aptamer interactions and developing aptamer-mediated approaches to materials problems, requiring a multi-disciplinary approach. It may be several years before the cycle of selecting materials aptamers, understanding their interactions and designing new selection experiments yields aptamers that truly meet the promise of this approach (Figure 4.15). Nevertheless, over-coming these challenges will be of significant benefit to materials science. The aim of this review has been to (i) introduce the concepts behind in vitro selection, (ii) describe the key features of in vitro selection and how they may be tuned to meet the needs of materials science, (iii) discuss some key examples of in vitro selection for materials and (iv) discuss some possible methods for advancing in vitro

selection for materials applications. Consideration of the examples presented in this review and elsewhere in the literature underscore the need to continue fundamental research in the field in order to address some key challenges such as the screening of relevant libraries, identification of suitable targets under the right conditions, development of strategies for isolation of the best aptamers and finally, the development of methods for fully characterizing and understanding the relationship between the selected aptamers and their materials properties.

Specific areas where advancements can be made, and where continued fundamental research should be focused include:

(1) Development of advanced libraries. As we gain increased knowledge with regards to the functioning of aptamers for materials applications, new libraries enhanced by this knowledge need to be used. The use of known structure or function within the library can greatly increase the probability of finding the right aptamer when balanced with proper choice of target. As of now, the use of advanced libraries has been extremely limited for materials applications, yet for biological applications significant improvements in library design have been made. Specific suggestions include:

-Use of T7 phage display to increase the utility of phage display for materials. T7 offers significant improvements over the current M13 selection paradigm including longer randomized regions, tunable display density and increased stability.

-Investigation of artificial building blocks and/or post-synthetic modification in order to enhance functionality and/or stability for materials applications. Although both amino acids and nucleotides offer functionality, artificial building blocks may be useful

for stabilizing intermediates, assisting in nucleation or growth, or allowing for covalent attachment of the library to substrates.

-Use of structure-activity relationships (SARs) to imbue in vitro selection libraries with useful structures or functions, allowing for the screening of sequence space nearby, leading to aptamers with enhanced functionality. Although initial libraries are extremely diverse, the number of possibilities is far greater than what is feasible. Designing libraries that already contain some portion of the desired aptamer can greatly narrow the search, improving the probability of identifying truly useful aptamers.

(2) Careful choice of target. The majority of targets reported for materials in vitro selection have been commercially obtained samples. Very little information with regards to the composition of the targets, the crystal faces targeted, surface defects or contaminants amongst other factors is given. However, there is a clear relationship between the identity of the aptamer and the target for which it was selected. In order for there to be progress with regards to understanding the interactions between aptamers and target materials, careful description of the target materials will be required. Assuming that the target is well-defined or compositionally uniform is not sufficient. Specific recommendations include:

-Accurate descriptions of targets, including composition, crystallinity, possible defects or contaminants, porosity, chirality, etc. Such information will greatly aid in the understanding of aptamer-target interactions. As part of this, description of the material under the incubation conditions should be given.

-Development of methods for better targeting materials, specifically surfaces of interest. Our recent work with in vitro selection on surfaces is one example of a materials centric approach to in vitro selection.

-Use of targets that better represent the eventual purpose. Many aptamers discovered thus far target a material, and coincidentally will also generate some material, but thus far there has been very little control over the resultant materials. Targets that are similar to the desired structure (i.e. targeting specific crystal morphologies) may assist in the identification of aptamers that template growth.

-Proper choice of negative or counter selection targets to ensure that the selected aptamers are highly specific. This is common practice for biological applications of in vitro selection, yet has not been widespread for materials applications.

(3) Careful choice of incubation conditions. Because commercially available M13 phage display kits have been the standard for materials in vitro selection, the incubation conditions used for materials in vitro selection has not strayed from the kit instructions. For this reason, the aptamers that have been isolated may not be optimal for their intended applications, as it has been shown that aptamers are very sensitive to environmental factors such as ionic strength, pH, target concentration, and temperature. Specifically:

-Control over the library:target concentration ratio to ensure adequate competition for the surface.

-Proper choice of reaction medium (buffer) in order to balance the stability of the library with the conditions required for the aptamer to function.

-Use of time, temperature and appropriate competitors to identify the most suitable aptamers for the intended application.

(4) Adequate washes and elution. Ensuring proper elution of the desired aptamers from the surface may be one of the biggest challenges, as shown by Naik and coworkers. The use of chaotropic agents, covalent-binding competitors and reduced pH are all standard methods for eluting materials. Other methods have been proposed here, which include:

-In situ reverse-transcription or infections to avoid elution altogether. Use of T7 phage display will make this possible in the realm of peptide display. With regards to SELEX, in situ reverse transcription could be limited unless very efficient promoters are used. Similar to this are the PCR-driven selections described herein.

-Use of protease sites on displayed peptides in order to cleave the phage or cell from the surface for infectivity.

-The use of techniques for “releasing” RNA from targets under some given condition, for example light, pH, or electrical potential.

Consideration of the ideas presented here, as well as the continuous advances in the field of in vitro selection, will ideally lead to aptamers useful for the synthesis and self-assembly of a wide range of materials.

Bridge

This chapter has reviewed in vitro selection techniques and their application to materials. In Chapter V, a specific example of the identification of gold binding RNA aptamers will be discussed.

CHAPTER V

IDENTIFICATION OF GOLD BINDING RNA APTAMERS VIA IN VITRO

SELECTION ON SURFACES (ISOS)

Co-authored material with A. E. Mahady, J. A. Berglund and J. E. Hutchison. A. E. Mahady collaborated extensively on this project as an expert of in vitro selection. I carried out all other experimental work and writing. Remaining co-authors provided editorial assistance.

Introduction

The development of methods for the discovery of useful biological macromolecules or *aptamers* relevant to materials science has received considerable recent attention. In particular, aptamers with surface identification and binding ability have been targeted for a number of applications ranging from drug delivery,¹ implant materials² and sensors³ to nanomaterials synthesis^{4,5} and self-assembly.⁶ Biological reagents are attractive because they are likely biocompatible and may lead to syntheses with greater control of materials properties under greener reaction conditions.⁷ Although methods have been reported for identifying surface-binding aptamers,^{8,9} significant challenges remain in the development of methods for identifying aptamers with a high degree of accuracy for surface targets (e.g., crystallographic orientation or defect sites) and providing straightforward control over target concentration (surface area) during the selection process. In this communication, we report a novel approach, in vitro selection on surfaces (ISOS), for the selection of surface specific aptamers under stringent

conditions. Specifically, we (i) describe the ISOS technique, including a prototype ISOS microreactor for carrying out ISOS; (ii) use ISOS to identify gold binding RNA aptamers (GBRs) from a pool of 10^{14} candidate RNAs; (iii) carry out detailed sequence and structural analysis to identify conserved features in our GBRs; and (iv) develop a novel “gold dot” assay to understand the binding behavior of the GBRs. Our results indicate that ISOS is a straightforward and versatile approach that is useful for identifying surface specific aptamers under rigorous and stringent selection conditions.

Study of biomineralization mechanisms has sparked great interest in the use of aptamers for the bioinspired synthesis of materials, particularly nanomaterials, due to the great deal of control over size, shape and morphology afforded under ambient conditions.¹⁰ Peptides have been identified that will bind to metals,¹¹ semiconductors,⁹ polymers¹² and carbon nanomaterials¹³ as well as catalyze the formation of micro- and nanoscale materials.^{5,14} Peptides remain a common choice for materials applications because of their relative stability, the range of functionality afforded by the 20 amino acids and because the peptide display techniques used to identify them are straightforward to carry out. Recently, RNA has been recognized as more than just an intracellular messenger and catalytic RNA or *ribozymes* have been shown to catalyze a number of interesting reactions.¹⁵ Structural studies of RNA have shown that it possesses intricate secondary and tertiary structures that modulate its chemistry and interactions with other molecules.¹⁶ Due to their interesting chemistry and because RNA libraries are often larger and more diverse than peptide display libraries, RNA is expected to play an increasing role in materials applications. In 2004, Gugglioti et al. reported the use of

RNA aptamers containing modified nucleotides for the preparation of novel microscale and sub-microscale palladium crystals.¹⁷ Follow-up work has demonstrated that these aptamers can be tethered to surfaces, allowing for both self-assembly and synthesis.¹⁸ Kelley et al. as well as Kumar et al. have reported the formation of semiconducting materials using RNA templates.¹⁹ In addition, RNA aptamers bound to surfaces through small molecule linkages have been used as proof-of-concept sensors.³

RNA aptamers are identified using an *in vitro* selection technique known as Systematic Evolution of Ligands by EXponential Enrichment (SELEX).²⁰ In this technique, a diverse and randomized pool of RNA is screened based upon affinity for a particular target. Those molecules that bind the target are isolated, amplified and subsequently screened against the target again. Each cycle of selection, isolation and amplification is considered one “round” and 4-16 rounds are typically carried out to identify aptamers with a high degree of selectivity for a given target. In order to successfully carry out SELEX and identify the fittest aptamers, the stringency of the selection must be carefully considered. Stringency is the set of fitness criteria by which the best binders are selected from non-specific and poorly bound species. Factors such as target concentration, RNA concentration and selection temperature as well as solution variables such as salt concentration and pH, play a role in the stringency of a reaction. An additional criterion is proper choice of target. A well-defined, homogeneous target that reflects the intended use of the aptamer will ideally allow for a successful selection experiment.

Although a number of approaches have been demonstrated for the identification of aptamers that bind to the surfaces of materials, we sought to improve stringency and target specificity during the SELEX process. In particular we wanted an approach that (i) was general, allowing for selection of aptamers for any planar substrate or surface bound target with a high degree of accuracy, e.g. crystallographic orientation or defect sites; (ii) allowed for convenient control over the surface area and thus concentration of the surface of interest; and (iii) was amenable to selection of both peptide and RNA aptamers. It was anticipated that such an approach would provide a versatile framework for carrying out materials specific selection experiments.

In Vitro Selection on Surfaces.

To address the criteria outlined above, we developed a novel approach known as in vitro selection on surfaces or ISOS. Central to this approach is a prototype microreactor (Figure 5.1a) that allows for control over the location and area of the surface being selected for through the use of a series of Kel-F inserts (Figure 5.1b). Each insert contains a carefully machined conical reaction chamber (500 mm^3 volume), at the bottom of which is a small aperture that defines access to the surface of interest. The base of each insert is planar and highly polished, allowing the insert to seal against the substrate without the need for external sealants that can complicate selection. The insert design allows for control over surface area (target concentration) as well as specificity for a given surface in a straightforward manner. Additionally, the microreactor has a built in heating mechanism that allows for control over the temperature during selection as well as in situ reverse transcription. These features, along with easily controlled solution

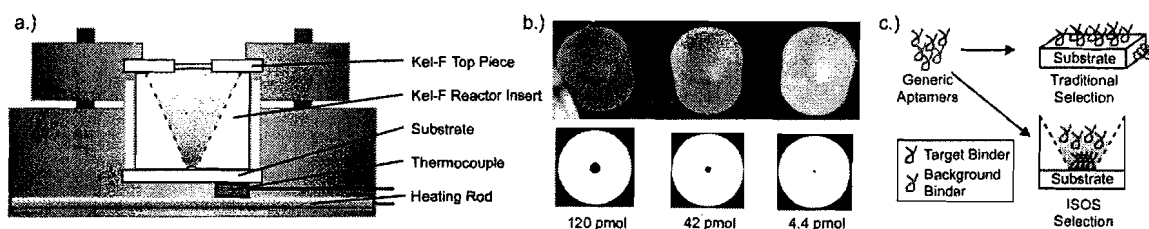


Figure 5.1. a.) Schematic of the prototype ISOS microreactor, with key components labeled. b.) Kel-F inserts. Each cylindrical insert is a conical reaction vessel with a small aperture that controls access to the surface. The base of each insert is highly polished, creating a seal between the insert and the substrate. Noted gold concentrations are for an ideal Au (111) surface. c.) Illustration of selection for both traditional “3D” and ISOS “2D” target substrates.

parameters, allow for highly stringent in vitro selection on surfaces. In contrast to traditional methods, in which the target substrate has three-dimensional character (e.g. metal powders or semiconductor wafers), the design of the ISOS microreactor allows for two-dimensional selections, permitting far more accurate aptamer selections for the surface of interest (Figure 5.1c).

The ISOS microreactor is designed to accept circular substrates of 20 mm × 3.3 mm (D × H) dimensions. For evaporated metals, self-assembled monolayers or thin-films, commercially available glass windows can be used and the appropriate target material deposited on the surface. Semiconductor substrates can also be mounted on the glass windows. For smaller or oddly shaped substrates, sample holders fitting these dimensions can be fabricated. For the experiments carried out here, a 50-Å adhesion layer of Cr followed by 1000 Å of Au was evaporated onto commercially available glass windows, yielding a polycrystalline surface with majority Au (111) faces.

To carry out the selection of GBRs, an initial library of $\sim 10^{14}$ ssRNAs with a 40 nucleotide randomized region was exposed to the gold substrate under the controlled

conditions of ISOS. Prior to beginning a selection, the ISOS microreactor was assembled with a proper Kel-F insert. Insert choice was based upon the desired gold concentration. Careful control over the RNA and gold concentration, and thus the RNA: Au ratio (Table 1), induces competition amongst the RNAs for binding sites on the gold and allows for the selection of highly competitive binders. Once assembled, the RNA (in a salt/buffer solution, the ISOS buffer) was heated, snap cooled and then pipetted into the ISOS microreactor. The salts, NaCl and MgCl₂, are required to ensure proper secondary-structure formation, and our choice of buffer (KOH/HEPES) was based upon minimizing buffer:substrate interactions. The RNA was incubated with the gold for 15 minutes, and the unbound RNA was washed from the surface. The bound RNA was eluted using

Table 5.1. Summary of ISOS Conditions

ISOS rd	[RNA] (pmol)	[Au] ^a (pmol)	RNA: Au Ratio	temp (°C)	tRNA ^b	RT enzyme ^c
1	610	122	5:1	22	no	AMV
2	610	122	5:1	22	no	AMV
3	122	42.1	10:1	22	yes	AMV
4	122	42.1	10:1	30	yes	SS
5	42.1	4.44	10:1	38	yes	SS
6	4.40	4.44	1:1	46	yes	SS

^a[Au] = concentration of gold surface atoms; ^b 0.1 mg/mL final concentration; ^c RT enzyme changed due to difficulty in getting reverse-transcription to work.

formamide at 100°C and amplified via reverse transcription and PCR. Transcription of the PCR product generated a new pool which was subsequently screened against the gold substrate. To increase the stringency of the selection, tRNA was added in rounds 3 through 6 to decrease non-specific binding and increased temperature was used to select for RNAs with robust secondary structure (Table 1). In addition to the formal selection of

GBRs, selections to remove RNAs that bound to the materials of the reactor (negative selection) were carried out at rounds 1, 5 and 6. In all, six rounds of ISOS were completed on the gold substrate, yielding our final gold binding RNA aptamers.

Sequence and Structural Analysis.

Following the six rounds of ISOS selection, we carried out sequence and structural analysis to determine the extent to which our GBRs were enriched with the known polyA gold-binding motif.²¹ MEME,²² a computer program designed to identify conserved features amongst RNA and peptide sequences, was used to analyze 41 of the isolated GBRs. Shown in Figure 5.2a is a potential grouping as predicted by MEME that is representative of the GBRs as a whole. As shown within the shaded region, our isolated aptamers are purine rich. It is significant that our GBRs are purine rich because both A and G have been shown to have an affinity for metal surfaces.²⁰ Although there is no apparent consensus motif, Khvorova et al. have shown that aptamers with a high affinity for a phospholipid membrane could be identified without a shared consensus between sequences.²³

Following the analysis of sequence, we used mfold²⁴ software to carry out predictive secondary structure modeling of our GBRs. Shown in Figure 5.2b is the predicted structure of GB1G01 with the same conserved region shown in Figure 5.2a shaded in gray. From the secondary structure of the randomized region, it can be seen that the guanine residues are prevalent primarily in the double stranded regions, whereas the adenine residues are prevalent primarily in the single stranded regions. In Figure 5.2c, we have graphed the nucleotide content of all sequenced RNAs, as well as the nucleotide

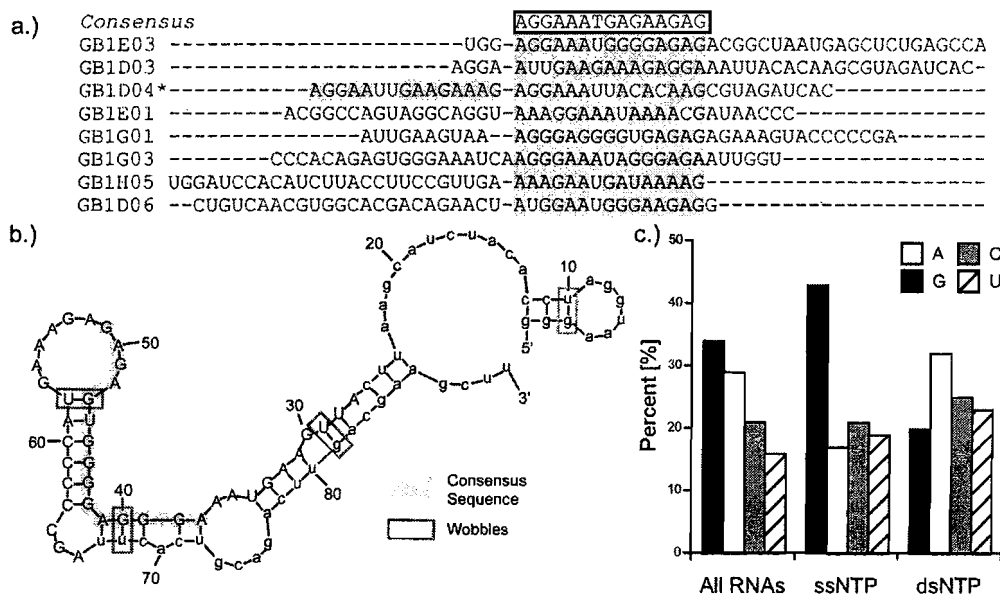


Figure 5.2. a.) Representative sequences obtained after six rounds of ISOS on evaporated gold, with the conserved purine rich region shaded in gray. GB1D04 contains two conserved regions. b.) Predicted model (mfold) of the secondary structure of RNA GB1G01 with the randomized region capitalized. In this structure, dsG regions contribute structurally, while ssA tracts are “displayed” for binding to the gold surface. c.) Analysis of the randomized region nucleotide content shows an overall preference for purines over pyrimidines. Adenine is favored in the single stranded regions and guanine is favored in double stranded regions.

content in both single- and double-stranded regions as predicted by mfold. As indicated earlier, analysis of the nucleotide content of all the RNAs shows that the isolated GBRs have an enriched purine content. In the single-stranded regions, there is a significant enrichment of adenine residues and in the double-stranded regions there is an enrichment of guanine residues.

This structural analysis based upon the mfold data suggests that the Gs may aid in the formation of stem-loops through bonding to Cs (Watson-Crick pairing) and Us (non-Watson-Crick pairing, wobbles), allowing for the display of single-stranded As. Highly structured RNAs that display single-stranded A moieties would allow for gold specific

binding while conferring stability of the secondary structure. Single-stranded A binding sites also would be consistent with earlier work that suggests that single-stranded polyA motifs are gold binding aptamers.²¹ Aside from contributing structurally, it is unknown to what extent U and C residues may affect binding.

Gold Dot Assay

In order to gain a greater understanding of our gold binding RNA aptamers, we developed a novel “gold dot” assay that allows for quantification and comparison of the binding of the GBRs and the initial pool to a gold surface. In the assay, a circular 2 mm gold dot, lithographically patterned onto an SiO₂ substrate, is incubated with ³²P-labeled high specific activity RNA. Following incubation, the gold dots are washed with the same ISOS buffer used for selection. To quantify the binding, the gold dots are either imaged using phosphor autoradiography and analyzed using ImageQuant or quantified using scintillation counting. Our assay also served as a method for determining binding specificity. In our assays, the RNA binds specifically to the gold and not to the SiO₂ substrate. As a simple test of the assay, we looked at the effect of RNA concentration on binding. As expected, an increase in RNA concentration led to an increase in binding (Figure 5.3a).

Initially we focused upon identifying conditions under which we could easily compare the binding of the initial pool zero RNA and the GBRs. In an assay of binding as a function of RNA concentration, we found that between 0.055 pmol and 0.11 pmol there was a consistent difference in binding between the pool zero RNAs and the GBRs. Using temperature as the variable, a second assay showed increased binding with increasing

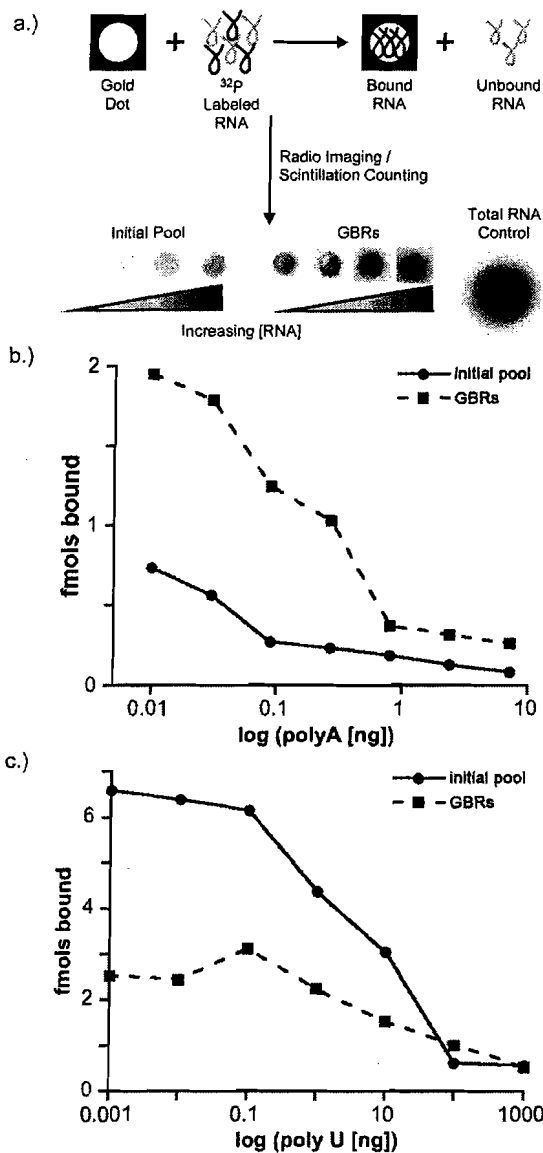


Figure 5.3. a.) Schematic of the gold dot assay. Gold dots are incubated with ^{32}P -labelled RNA, and binding quantified via radio imaging or scintillation counting. b.) Assay showing the effect of polyA on the binding of the initial pool and the GBRs. GBRs bind with a higher affinity than the original pool and are able to compete better against the known polyA binding motif. c.) Assay showing the effect of polyU on binding. polyU disrupts binding in the GBRs at low concentrations, indicating that the polyU fragments may be base pairing with the ssA binding sites.

temperature. Because we used increased temperature to increase the stringency in our selection, it should be expected that increasing temperature would lead to increased binding. Based upon these assays of RNA concentration and temperature, further assays were performed at an RNA concentration of 0.11 pmol and a temperature of 50°C.

Because our sequencing results indicate that our isolated aptamers are adenine rich (Figure 5.2), we carried out assays to determine the significance of this finding. In these assays, increasing concentrations of individual poly-NTPs (A, G, C and U) were

assayed against a constant concentration of the initial pool zero RNA and selected GBRs. It was expected that polyA would be an effective competitor, and in fact, polyA is effective at disrupting binding in both the initial pool zero RNA and the selected GBRs (Figure 5.3b). Notably, polyA is a much better competitor against the initial pool than the GBRs, indicating a higher affinity for the gold surface of the GBRs over the initial pool zero RNA. In Figure 5.3c, it is shown that polyU will disrupt binding of the GBRs at much lower concentrations than polyA. Interestingly, the Round 0 aptamers compete much better against the polyU than the GBRs. As evidenced via sequence analysis, the selected GBRs are enriched with ssA regions that are available to base pair with the polyU competitor. Such base pairing will lead to a greater decrease in binding ability for the GBRs than for the original pool. Though polyG and polyC were also able to disrupt binding at high concentrations, there was no apparent difference in their ability to disrupt the initial pool or the GBRs.

Taken together, our sequence and structural analysis as well as our assay results indicate that we have isolated gold-binding RNA aptamers that utilize double-stranded G regions to confer a secondary structure that allows for the “display” of single-stranded A binding motifs. Previous studies have aimed to understand the binding of adenine to various metal surfaces, including gold. Early surface-enhanced raman spectroscopy (SERS) studies and density functional theory (DFT) calculations suggest that single adenine molecules interact with metal surfaces utilizing the endocyclic N7 and the exocyclic N6 amine.²⁵ Recent infrared (IR) spectroscopy and x-ray photoelectron spectroscopy (XPS) studies of homo-oligomeric adenine indicate similar interactions.²¹

Electrochemical studies of adenine binding to gold electrodes suggest that surface features and defects of the gold, such as steps and kinks, play a role in determining the stability of adenine films on gold.²⁶ Though there have been studies of both single molecules of adenine and homo-oligomers, very little work has focused upon the binding of structured RNAs to metal and other surfaces. For example, it is currently unknown whether the secondary structure of our isolated RNAs provides greater access for N6 and N7 in adenine to the gold surface. Our gold binding aptamers provide a convenient access point for such studies, and future work using electrochemical, SERS and IR techniques may help to further elucidate the interactions between structured RNAs and surfaces. Such studies will be valuable for tailoring aptamers isolated using ISOS for materials applications.

Conclusion

To summarize, we have developed a novel approach, *in vitro* selection on surfaces or ISOS, for the discovery of aptamers that bind to planar substrates and surface bound targets. In comparison to previously reported methods, ISOS allows for a greater degree of accuracy for surface targets and greater control over target surface concentration, leading to an overall increase in the stringency of selection. As an example of ISOS, we have isolated gold binding RNA aptamers (GBRs) from an initial library of 10^{14} candidates that show an increased affinity for gold surfaces. Sequence analysis of the isolated aptamers revealed a high purine (A and G) content as a conserved feature. Consistent with previously reported results, our GBRs contained a high concentration of single-stranded adenine regions, known to be a gold-binding motif. Structural analysis

based upon sequencing and predictive modeling indicated that G residues form stem-loops that assist in “displaying” adenine for facile binding. Assay results showed that our gold-binding aptamers are effective gold binders and can compete against polyA. It is further shown that polyU is an effective competitor as well and that this is likely the result of the polyU binding to the ssA binding sites in our selected GBRs, disrupting binding. In our initial experiments, we have shown that ISOS is a useful tool for the selection of aptamers for surfaces. Ongoing work is focused upon the selection of aptamers that bind to single crystal surfaces, polymers and surface bound targets using both RNA and phage displayed peptides. It is expected that the versatility and control offered by ISOS will make it invaluable for future research in bioinspired materials.

Experimental

Gold Substrate Preparation. Circular glass windows (20 mm × 3.3 mm, Edmund Optics) were cleaned in piranha solution and stored in distilled ethanol prior to use. A 50 Å adhesion layer of chromium metal was evaporated onto the glass surface followed by a 1000 Å layer of gold. Prior to performing a selection, the substrates were sonicated with methylene chloride (2 × 5 m), acetone (2 × 5 m), water (2 × 5 m) and finally distilled ethanol (2 × 5 m). Following the solvent washes, the substrates were UV/ozone cleaned and rinsed with distilled ethanol, and dried under N₂ or Ar gas.

PCR. The protocol used to make the DNA template was carried out as previously described with modifications.^{27,28} 25 pmoles (1.5×10^{13}) of the template 5'-GGGAATGGATCCACATCTACGAATTC(N30)TTCAC-TGCAGACTTGACGAAGCTT-3 was amplified using 12 cycles of PCR with forward

and reverse primers reported previously using standard PCR reaction conditions.²⁷ The PCR product was phenol/chloroform extracted and ethanol precipitated. The template was resuspended in 50µl of Tris-HCl pH 7.5 and cleaned using a Bio-Spin 6 size exclusion column (Biorad). DNA template concentration was carried out using standard spectrophotometric techniques.

Transcription. 1×10^{14} molecules of PCR product was used in the in vitro transcription reaction. Standard transcription reaction conditions were performed.²⁷ The RNA was treated with 10 µl RQ1-DNase (Promega) and then phenol/chloroform extracted and ethanol precipitated. The RNA was run on a 6% denaturing acrylamide gel (37.5:1 acrylamide:bisacrylamide, 8 M urea, 1× TBE). The radioactive band was imaged on STORM (Amersham), cut out and eluted in 0.3 M NaOAc pH 5.2 overnight at 4°C. The RNA was then precipitated in ethanol, resuspended in 50µl water and passed over a Bio-Spin 6 column to remove impurities.

ISOS Selection. Six rounds of ISOS were performed with details described in Table 1. Gold concentration was controlled using the appropriate ISOS insert. The radio-labelled RNA was heated at 95°C for 5 min in 200 µL of reaction buffer (20 mM Hepes, 5 mM MgCl₂, 30 mM NaCl, 0.5 mM ascorbic acid) and then snap cooled on ice for 5 min. The ISOS chamber was washed with 200 µL of water twice and once with reaction buffer and then heated to the appropriate temperature. RNA in buffer (preheated) was added to the ISOS and reacted for 15 min with stirring. The supernatant was then removed and the ISOS reaction vessel was washed with 200 µL of preheated buffer three times for 5 minutes each. Bound RNA was eluted from the surface with 200 µL of

formamide heated to 100°C for 10 minutes. The supernatant was removed and the gold insert was checked for radioactivity to ensure all RNA had been eluted. The supernatant was precipitated using ethanol and resuspended in 10 μ L water. In addition to the formal ISOS selection, negative selections to remove binders to the Kel-F insert and to the spinvane were carried out at rounds 1, 5 and 6.

RT-PCR. AMV (Promega) and Superscript (SS, Gibco-BRL) reverse transcriptions were carried out with 15 μ L of 20 μ M reverse primer, 6 μ L 10 mM dNTP, 6 μ L 5 RT buffer, 1 μ L reverse transcription enzyme and incubated at 42°C for 1 hr. 1 μ L RNase A was added and the reaction was further incubated for 1 hr at 37°C. A negative control was also run to check for contamination. PCR was performed by adding the forward primer as described above and the reaction product was confirmed using a 3% agarose gel.

Cloning and Sequence Analysis. After the sixth round, the PCR fragments were ligated into TOPO TA-2.1 vector and then transformed into Novablue competent cells. 48 individual colonies were picked and sequenced. Sequencing was carried out on an Applied Biosystems 3130XL Genetic Analyzer using a BigDye Terminator v3.1 sequencing kit. Sequences were formatted and then run through ClustalW²⁹ using standard methods. 41 out of 48 sequences were found to be usable and there were no repeated sequences. The randomized area of the sequences were then analyzed using MEME/MAST²¹ and further analyzed for base composition. Complete sequences with random and non-random regions were run through mfold^[23] to look at structural

similarity of the sequences and base composition of the single and double stranded regions of the randomized region.

Gold Dot Preparation. A physical mask (7.6 cm × 2.5 cm) containing 54 evenly spaced 2 mm holes was clamped to a piranha cleaned SiO₂ substrate. A 50 Å adhesion layer of chromium metal was evaporated onto the SiO₂ surface followed by a 1000 Å layer of gold. Following deposition, the dots were cut from the substrate and stored in distilled ethanol. Prior to performing an assay, the gold dots were sonicated with methylene chloride (2 × 5 m), acetone (2 × 5 m), water (2 × 5 m) and finally distilled ethanol (2 × 5 m). Following the solvent washes, the gold dots were UV/ozone cleaned and rinsed with distilled ethanol, and dried under N₂ or Ar gas.

Gold Dot Assay. The reaction conditions were the same as the ISOS conditions except where variation is noted. RNA was mixed with buffer, heated to 95°C for 5 minutes and then snap cooled for 5 minutes on ice. If polyNTPs were used in the assay, they were mixed with the RNA prior to addition of the gold dot. The gold dot was then placed into the tube with the RNA and incubated for 15 minutes. Following incubation, the dot was washed with buffer (3 × 5 m). To quantify the binding, the gold dots were either imaged using phosphor autoradiography (STORM, Amersham) and analyzed using ImageQuant (Amersham) or quantified using scintillation counting.

Bridge

In this chapter, the identification of gold binding RNA aptamers was detailed. In the next chapter, the use of these aptamers as well as similar gold binding peptide aptamers for gold nanocrystal synthesis will be discussed.

CHAPTER VI
SCREENING OF GOLD BINDING RNA AND PEPTIDE APTAMERS FOR GOLD
NANOPARTICLE FORMATION

Introduction

Anisotropic gold nanoparticles have garnered significant attention due to their intriguing shape dependent optical properties, including multi-modal plasmon resonance¹ as well as photoluminescence², which have made them promising candidates for a number of applications ranging from biotagging agents² to surface-enhanced raman scattering substrates.³ Preparations of nanoscale metal rods,^{4,5} prisms,⁶ plates,⁷ cubes⁸ and stars⁹ have been previously described. Although a number of methods, including electrochemical¹⁰ and templated growth,¹¹ have been used for their synthesis, shaped gold nanoparticles are synthesized most commonly using seeded growth methods.^{4,5,12}

In the seeded growth of gold nanorods, a previously synthesized “seed” nanoparticle is introduced to a growth solution containing a Au (III) salt, a weak reducing agent and a directing agent (most commonly a surfactant). Initially, the seed particles grow through the slow-diffusion of gold atoms onto their surface. After an initial period, the seeds have grown into isometric crystals with well-defined Au (111) and Au (100) crystal faces. These enlarged seeds aggregate along these well-defined faces to formed

pentatwinned species that serve as the starting material for rod growth. Simultaneous with the twinning events, the surfactant begins to associate and assemble on the Au (100) faces acting as a directing agent and preventing further growth on the (100) face. As a result, further growth occurs on the Au (111) faces and along the (110) axis, leading to an elongation of the crystal to form a nanorod. Slight changes in reactant ratio, the use of different seeds, variations in pH or the use of dopants can be used to modify the interactions of the directing agent with the growing crystal or otherwise affect the growth, leading to changes in morphology.⁹ Despite much progress, the ability to obtain uniform shaped nanoparticles in high yields remains elusive. For this reason, alternative synthesis methods that do not rely on the use of surfactants are being sought.

Recently, the use of biological reagents for the synthesis of shaped nanoparticles has been proposed. In 2002, Naik et al. reported the discovery of peptides that could mediate the growth of prismatic silver nanoparticles.¹³ Followup work by Slocik showed that one of these peptides could also be used for the synthesis of spherical gold nanoparticles.¹⁴ It was postulated by Slocik that tyrosine residues in the peptide were responsible for reducing and nucleating the gold, while the remainder of the peptide was responsible for stabilizing the particle.¹⁴ In 2004, Gugglioti et al. reported the identification of RNA aptamers that could catalyze the formation of variously shaped Pd crystals.¹⁵ Followup work by Feldheim's group showed that these aptamers could be assembled onto surfaces, allowing for both the synthesis and self assembly of both Pd and Pt crystals.¹⁶ Although the exact mechanism by which these biomolecules mediate

crystal growth is not known, it is likely they act similar to interfacial growth agents as seen in biomineralization reactions.¹⁷

In order to discover these peptide and RNA molecules or *aptamers* useful for nanoparticle synthesis, a process known as *in vitro* selection was used (Figure 6.1). The two most common methods of *in vitro* selection are phage display¹⁸ for identifying peptide aptamers and Systematic Evolution of Ligands via EXponential Enrichment (SELEX) for identifying oligonucleotide aptamers.¹⁹ Though the specifics of phage

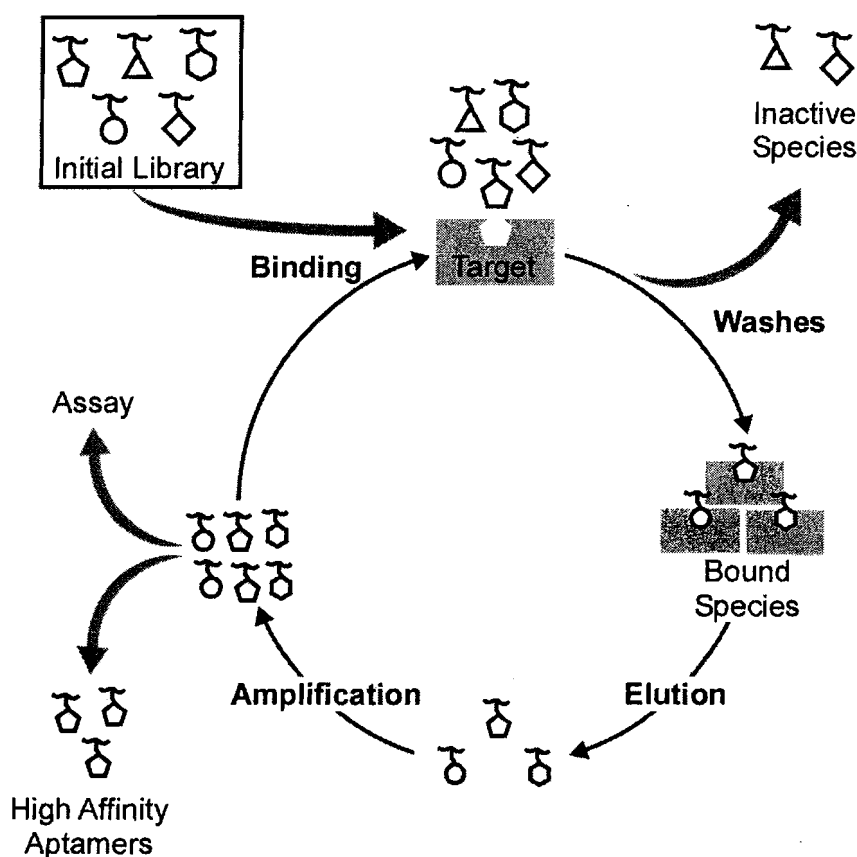


Figure 6.1. Schematic of the *in vitro* selection cycle. The library is incubated with the target. Following incubation, inactive species are washed from the target. Bound species are eluted, amplified and then incubated with the target again. Following a number of rounds, high affinity aptamers are isolated.

display and SELEX are different, the same general principles of *in vitro* selection apply. Shown in Figure 6.1 is a typical *in vitro* selection cycle. In the first step, an initial library (typically containing 10^9 - 10^{14} individual candidates) is mixed with the intended target. The candidate pool is given a chance to interact with the target under specific conditions as determined by the experimenter. In the second step, non-binders and poorly bound species are washed away from the bound species, which are subsequently eluted away from the target. The eluted target binders are amplified via suitable biochemical methods generating a new library that is enriched with target binders. The cycle of incubation, washes/elution and amplification are repeated several times until appropriate assays indicate that the desired aptamers have been isolated.

Although a number of approaches have been demonstrated for the identification of aptamers that bind to the surfaces of materials, we sought to identify methods by which we could isolate aptamers that could be used as interfacial growth agents in the formation of shaped gold nanoparticles. That is, we sought aptamers that would identify and bind to specific crystal planes and inhibit their growth, similar to the seed mediated approach described above. To this end, we developed a novel approach known as *in vitro* selection on surfaces or ISOS, described in detail in Chapter V. In comparison to traditional methods, it was anticipated that ISOS would give access to aptamers with a higher degree of specificity for the surfaces of growing crystals.

Reported herein are initial investigations into the formation of gold nanocrystals using RNA and peptide aptamer interfacial growth agents discovered using *in vitro*

selection on surfaces. Specifically, we describe: (i) the use of gold binding RNA aptamers (GBRs, Chapter V) for the seed-mediated growth of gold nanocrystals, (ii) the use of GBRs for the formation of surface bound gold crystals, (iii) the use of ISOS to discover gold binding peptides and (iv) the use of ISOS derived peptides for the formation of gold nanocubes. The results of these investigations indicate that the use of aptamers as interfacial growth agents in the seed mediated synthesis of gold nanocrystals is a promising area for continued research.

Results and Discussion

RNA Mediated Gold Nanocrystal Synthesis

In order to identify gold binding RNA aptamers (GBRs), a SELEX experiment using ISOS was carried out. Following six rounds of selection, sequence and structural analysis as well as binding assays indicated that structured GBRs containing single-stranded polyadenine binding motifs were isolated (see Chapter V for full details).

Following four rounds of SELEX, the Round 4 (R4) gold binding RNAs were compared to the initial Round 0 (R0) RNAs for their ability to act as interfacial growth agents in the synthesis of shaped gold nanoparticles. As a simple test, the R4 RNA was mixed with HAuCl_4 (0.025 mM) in a salt/buffer solution (5 mM MgCl_2 , 20 mM KOH/HEPES and 100 mM NaCl) in order to determine if the R4 RNAs could directly reduce the Au (III) species to form nanoparticles. Visual, as well as UV-vis confirmation indicated that R4 RNA could not directly reduce the gold. R0 RNA was similarly unable to reduce the gold ions.

Based upon this observation, a seeded growth route⁴ was pursued for RNA mediated gold nanocrystal synthesis, as described in the introduction. While citrate stabilized nanoparticles have typically been used as seeds, earlier testing showed that these immediately precipitated in the salt/buffer solution required to confer stable secondary and tertiary structure to the RNA. For this reason, 4-dimethylaminopyridine (DMAP) stabilized nanoparticles²⁰ have been employed instead, as these have been shown to be similarly useful in seeded growth reactions. To carry out the seeded growth, DMAP were added to a growth solution containing salt/buffer, RNA and HAuCl₄. Immediately following seed addition, ascorbic acid was added. Within 1 min, the solution had turned from clear to light pink, indicating the formation of nanoscale gold species in solution. An aliquot of this solution was added to a second growth solution, followed by the addition of ascorbic acid, again yielding a pink solution. This process was repeated a final time, yielding the final R4 aptamer mediated gold nanoparticles. Identical experiments were carried out with R0 RNA, CTAB and no growth agent as a control.

TEM analysis (Figure 6.2) of the resultant products allowed for determination of nanoparticle size and shape, as well as determination of the distribution of differently shaped nanoparticles in solution. In the case of the no growth agent control, the products were uniformly spherical nanoparticles of varying size as expected for a multiple step seeded growth process. In the case of the CTAB control, the products were enlarged, amorphous particles likely resulting from the disruption of the expected CTAB micelle by the salts in the solution. Interestingly, the R4 aptamer mediated gold nanoparticles

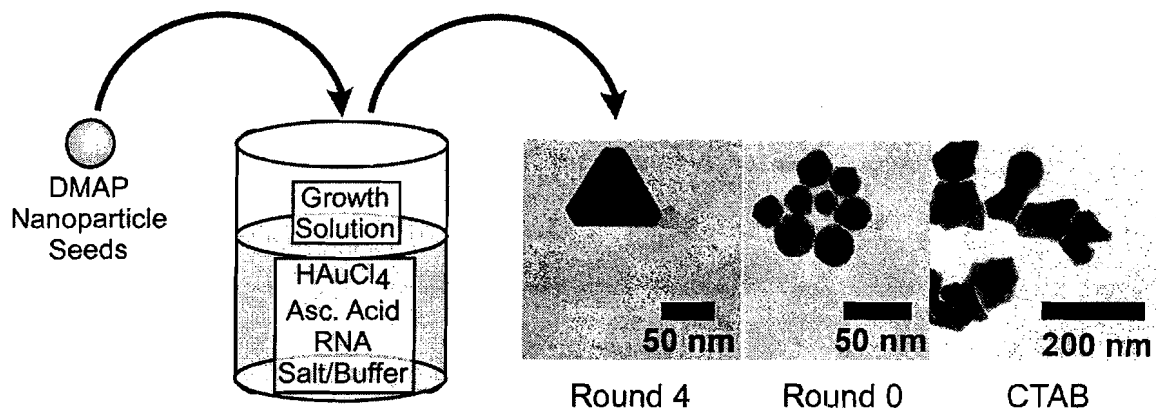


Figure 6.2. Synthetic method for producing nanocrystals using RNA, and resultant products. Note that for Round 4 and Round 0 similar products were found in both samples.

contained a distribution of spherical particles, hexagonal plates, triangular prisms and rods. The R0 sample contained a similar distribution of gold nanoparticles. To determine the extent to which the R4 samples were enriched with the different shapes of nanoparticles versus R0 samples, ~500 particles from each sample were counted by hand at random and sorted by crystal morphology. Despite an apparent enrichment in the R4 sample versus R0, the samples were the same within experimental error.

After the sixth round of selection yielding the final gold binding RNA aptamers (GBRs) a similar series of experiments were carried out. R0 RNA and GBRs as well as single-stranded polyNTPS (polyA, G, C and U) were tested for their ability to form gold nanoparticles. Because the isolated GBRs were enriched with polyA binding sites, it was expected that a polyA homopolymer may have similar activity. In all cases, the majority of products were aggregates of spherical nanoparticles with a similar distribution of shaped nanoparticles as seen in the R4 versus R0 comparison.

One explanation for this lack of activity on the part of the RNAs was that the gold nanoparticle seeds, even after some initial growth, were too small to be recognized by the gold binding aptamers. To test this theory, we chose to investigate the growth of gold islands (~75 nm diameter) on an SiO₂ substrate. The gold islands were patterned onto SiO₂ via a process known as shadow nanosphere lithography.²¹ 1 cm² sections of the patterned surface were incubated under identical conditions as those used to investigate the growth of gold nanoparticles in solution. As an additional parameter, the effect of GBR concentration on gold island growth was also considered. SEM was used to observe the effects of the RNA on both the morphology and growth rate of the gold islands. Although no changes in morphology could be detected (within the limits of the microscope), it was found that island growth could be decreased through the use of increasing RNA concentration.

The results of our initial RNA-mediated gold nanoparticle growth studies have shown that the isolated GBRs do not have a significant effect on the formation of

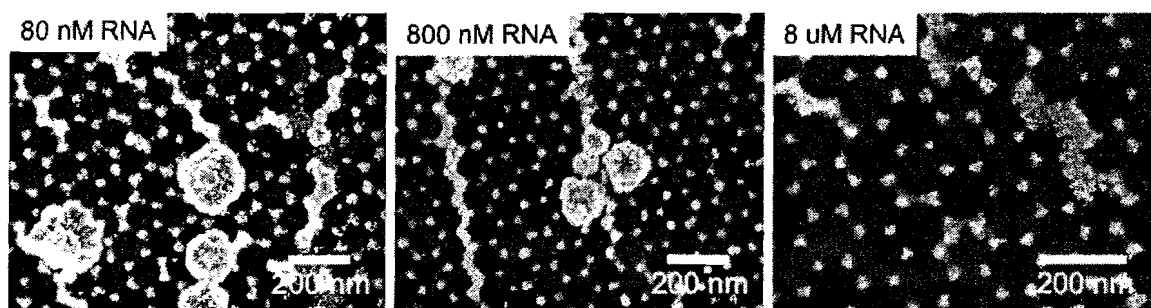


Figure 6.3. SEM images of gold island growth on surfaces. Increased RNA concentration leads to a decrease in gold island size.

differently shaped gold nanoparticles. A few possible reasons for this are (i) the size mismatch between the seeds and the RNA may be too great to confer preferential binding, (ii) the kinetics of the seeded growth process may preclude the bulky RNA molecules from participating, (iii) the evaporated gold surface may not sufficiently mimic the surface of the growing crystal or (iv) RNA may not be ideal for the identification of surfaces, since much of the activity of RNA is a result of its three-dimensional character. For many of these reasons, current efforts are focused upon identifying RNA aptamers that can act as three-dimensional templates by directly using gold nanorods as the template.

Peptide Mediated Gold Nanocrystal Synthesis

To identify peptides that would bind to evaporated gold surfaces, the Ph.D. 12 phage display kit (New England Biolabs) was used. Five rounds of selection were carried out using ISOS, with increasing surfactant concentration and increasing temperature as methods for increasing stringency during selection (see Appendix C for details). Following the five rounds of selection, sequencing was carried out to determine if any consensus sequences were present within the sample. One consensus motif comprised of two peptide aptamers was isolated (Figure 6.4). Comparison of this motif to previously identified gold binding peptides²² indicate that, using ISOS, unique gold binding peptides could be isolated. Functionally, these peptides contain a central polar region flanked by nonpolar regions and calculations of the pI indicate that the GBPs will carry a negative charge at neutral pH. Of the two isolated GBPs within the consensus motif, GBP1 was synthesized individually for further investigation.

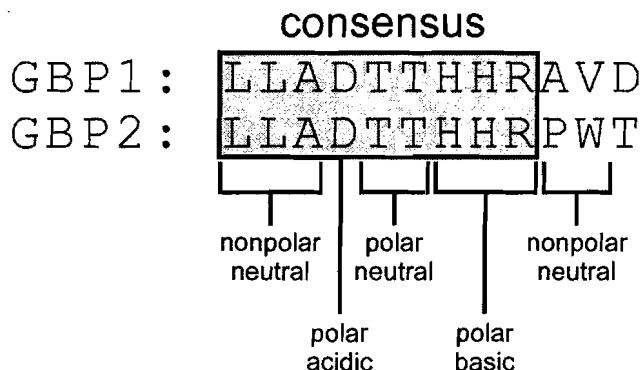


Figure 6.4. Two gold binding peptides that were isolated using phage display, with consensus sequence and properties labeled.

In previous work by Slocik et al.,¹⁴ a silver binding peptide was mixed with HAuCl₄ in KOH/HEPES pH 7.2, yielding spherical nanoparticles. To determine whether or not the GBPs were similarly active, an identical experiment was carried out using GBP1, with no nanoparticle formation. For this reason, a seeded growth process, similar to that used for the RNA experiments, was used. In this case, citrate stabilized gold nanoparticles were added to a growth solution containing KOH/HEPES, HAuCl₄, AgNO₃ and GBP1, followed by ascorbic acid addition as above. Several concentrations of GBP1 were screened including 0 mg/mL, 1 mg/mL, 0.2 mg/mL, 0.1 mg/mL and 0.02 mg/mL. In the case of no added GBP1, the solution immediately turned pink. However, in cases where GBP1 was added (at all tested concentrations), the solutions slowly became light orange in color. TEM inspection of these samples indicated the formation of small (1 to 2-nm) gold nanoparticles with a small population of gold nanocubes. Interestingly, no other shaped nanocrystals were formed (i.e. rods, prisms). Because of the slow evolution of color, it is likely that GBP1 is binding to the growing gold species and limiting growth

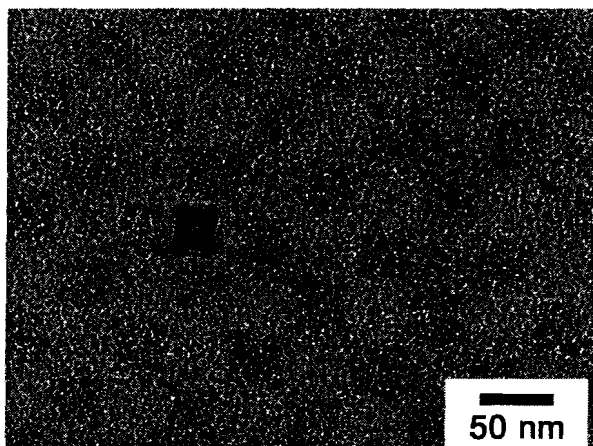


Figure 6.5. TEM image of small nanoparticles and a nanocube obtained during peptide mediated synthesis.

to very small gold nanoparticles. Further manipulations of peptide concentration along with changes in reaction conditions may assist in improving the synthesis of gold nanocrystals using gold binding peptides isolated using ISOS.

Conclusions and Future Directions

The use of biomolecules in the synthesis of nanomaterials is an area of active research. A biomimetic approach offers the ability to control the size, shape and crystallinity of nanomaterials under benign conditions. Using in vitro selection on surfaces, we have identified gold binding RNA and peptide aptamers. These aptamers were screened for their ability to form shaped gold nanoparticles via a seeded growth approach. Although a small population of unique crystal morphologies (hexagonal plates, prisms, cubes and rods) were seen, results thus far indicate that further study of the isolated aptamers will be required before the true promise of the aptamer mediated approach is realized.

Further areas of study include:

(1) Screening of more individual peptide and RNA gold binders from the isolated pools. Although the aptamers chosen for study thus far were chosen judiciously, often times the best aptamers aren't the most represented in the pool.

(2) Combinatorial screening of reaction conditions. The conditions used thus far have all been based roughly on preexisting literature seeded growth preparations. Identification of the right conditions, given the complexity of the growth solutions, may require large scale screening of solution composition.

(3) Selection for single crystals instead of evaporated gold. Although evaporated gold is a convenient target, the use of single crystalline targets may be a better representation of the growing nanocrystal.

(4) Selection of biomolecules as templates. Due to the inherent structural component of biomolecules, their use as templates rather than surface active agents may be more appropriate for nanocrystal synthesis.

Experimental

Selection of Gold Binding RNA Aptamers (GBRs). The selection of gold binding RNA aptamers is comprehensively covered in Chapter V. Aptamers isolated in that work were used, unmodified, for the studies here.

Seeded Growth Using GBRs. Three 90 μL growth solutions (A-C) containing 1 mM MgBr_2 , 20 mM KOH/HEPES pH 8.1, 20 μg RNA and .025 mM HAuCl_4 were prepared. To growth solution A, 10 μL of DMAP stabilized nanoparticles ($[\text{Au}] = .025$

mM) was added, followed immediately by 10 μL of Ascorbic Acid (0.5 mM). Once a pink color was noted in the solution, a 10 μL aliquot of the growing crystals was transferred to growth solution B. After a similar growth period, a 10 μL L aliquot of solution B was transferred to growth solution C. Following growth, the samples were spray-cast onto SiO TEM grids and inspected via TEM. This procedure was used for all RNA samples. In the case of CTAB, 0.1 M CTAB was used instead of RNA.

Shadow Nanosphere Lithography. Gold islands on SiO₂ substrates were formed via shadow nanosphere lithography.²⁰ Briefly, 16 mL of water was added to a 10 cm piranha cleaned petri dish. A piranha cleaned SiO₂ substrates (4 cm²) was placed in the water, near the top edge. 15 μL of 50% ethanol was added near the bottom right edge, forming a “hole” in the water. As the hole slowly closed in, 30 μL of a 5% solution of 240-nm polystyrene beads in 50% ethanol were added to the hole. The beads spread evenly over the surface of the water, forming a monolayer. Carefully, the top edge of the petri dish was lifted, allowing for a monolayer of styrene nanoparticles to form on the surface of the SiO₂ substrate. Following ample drying, 50 Å of Cr and 400 Å of Au were deposited onto the substrates. The polystyrene beads were dissolved from the surface via sonication in toluene. SEM inspection of the resultant surface indicated the formation of gold islands.

RNA Mediated Growth of Islands. A 90 μL growth solution containing 1 mM MgBr₂, 20 mM KOH/HEPES pH 8.1, 20 μg RNA and 0.025 mM HAuCl₄ was prepared. To this, a 1 mm² gold island substrate was added, followed immediately by 10 μL of

Ascorbic Acid (0.5 mM). After a 2 minute incubation, the substrate was removed from the growth solution, rinsed with nanopure water and dried under N₂. The substrate was then inspected via SEM.

Selection of Gold Binding Peptide Aptamers. Gold binding peptide aptamers (GBPs) were identified using the methods described in Appendix C. Aside from an increase in surfactant concentration, an increase in temperature and decrease in gold concentration (via ISOS insert changes) were used to increase the stringency of selection. Five rounds of selection total were completed. Isolation of phage DNA was completed as described in Appendix C and submitted for sequencing. GBP1 was purchased from Sigma/Genosys and used as received.

Seeded Growth Using GBPs. Three 90 uL growth solutions (A-C) containing 100 mM KOH/HEPES pH 7.2, 0.025 .M HAuCl₄, 0.005 mM AgNO₃ and the peptide GBP1. To growth solution A, 10 μL of citrate stabilized gold nanoparticles ([Au] = 0.025 mM) was added, followed immediately by 10 μL of ascorbic acid (0.5 mM). Following a color change to light orange, a 10 μL aliquot of growth solution A was added to growth solution B. After a similar growth period, a 10 μL of solution B was transferred to solution C. Following growth, the samples were spray-cast onto SiO TEM grids and inspected via TEM. This procedure was used for peptide concentrations of 0 mg/mL, 1 mg/mL, 0.2 mg/mL, 0.1 mg/mL and 0.02 mg/mL.

CHAPTER VII

CONCLUDING SUMMARY

Access to well-defined gold nanoparticles will pave the way for their use in a wide variety of emerging technologies. Recent successes in the synthesis of both spherical and shaped gold nanoparticles have opened access to the study of their fundamental optical, electronic and catalytic properties. Even with this progress, access to gold nanoparticles that are sufficiently pure and monodisperse in terms of size and shape remains a significant challenge. In this dissertation, two routes to well-defined gold nanoparticles have been discussed, specifically diafiltration and aptamer mediated synthesis.

Diafiltration

The most immediately useful and practical approach developed here is the use of diafiltration for the removal of small molecules from gold nanoparticle samples. In Chapter II, the use of diafiltration for the removal of excess thiol ligand as well as salts from nanoparticle samples was described. We showed that diafiltration was far better at removing these common impurities than any other method. Furthermore, diafiltration is efficient and convenient for routine use and produces far less waste than other described

methods. For these reasons, diafiltration has become the “gold” standard method for purifying water-soluble gold nanoparticles in the Hutchison lab.

Our use of diafiltration, and the access to highly pure nanoparticles it has provided, has allowed us to achieve new milestones in gold nanoparticle research. Evan Foster and Shuji Goto were able to form highly ordered arrays of phosphonate stabilized 1.5-nm gold nanoparticles on hafnium modified SiO₂ substrates.¹ Greg Kearns reported that highly pure gold nanoparticles allowed for access to gold nanoparticles that retained their useful electronic properties following assembly into linear arrays on DNA.² Our collaborators at OSU, Robert Tanguay and Stacey Harper, have recently reported the results of studies aimed at understanding the effects of impurities on the interactions of gold nanoparticles in biological systems.³ This work in particular is extremely important because no other research group has been able to provide similar structure activity relationships with regards to bio-nano interactions. Aside from issues of purity, the ability to remove small molecules from nanoparticle samples allowed Jenny Dahl to do some groundbreaking work on the functionalization of citrate-stabilized gold nanoparticles.⁴ Diafiltration has been an important enabling tool for all of these advances, and is expected to continue playing a role in future gold nanoparticle research.

Another area we have investigated using diafiltration is for the size separation of gold nanoparticles. We were successful in separating a bimodal mixture of 1.5 and 3-nm gold nanoparticles, suggesting the utility of diafiltration for the separation of nanoscaled materials of disparate core size. As an extension of this, the isolation of trimeric species from other monomers and aggregates was attempted. Although modest enrichment of

trimeric species was seen, our success was ultimately limited by the stability of the trimers in solution. While diafiltration has been promising for the isolation of nanomaterials of disparate core size, high-resolution fractional separations have thus far been limited by the pore dispersity of the membranes. It is expected that further improvements in membrane technology will allow for this type of separation.

Aptamer Mediated Synthesis

The second approach described in this dissertation, aptamer mediated synthesis, is not immediately practical, but provides an excellent framework for continued, interdisciplinary research. In chapter IV, the challenges and future prospects of the use of in vitro selection for identifying aptamers useful for materials were laid out. In the past decade, initial progress has been made in the identification of aptamers useful for materials. Building upon this initial work, future efforts should be focused upon the use of better display techniques and functional libraries, the use of targets that better represent the eventual aptamer need and the use of selection conditions that better mimic the environment in which the aptamers will be used. Consideration of these factors, along with continued advances in the characterization of the interactions between biomolecules and materials will allow for the realization of the promises of a bioinspired approach.

Our contribution to this burgeoning field has been the development of in vitro selection on surfaces (ISOS). ISOS is a powerful platform for displaying planar substrates to in vitro selection libraries. Our work in Chapter V showed that ISOS could be used to identify gold binding RNA aptamers. Although evaporated gold was a convenient first target for our beginning research in this field, the true power of ISOS will

be realized with the selection of aptamers (both peptides and RNA) that bind to single-crystal faces, chiral surfaces or polymeric surfaces, amongst others. Further work with ISOS and aptamer mediated synthesis will surely yield well-defined gold nanomaterials in time.

Taken together, diafiltration and aptamer mediated synthesis offer both short-term access and long term prospects for the convenient and routine access to well-defined nanomaterials. It is with great anticipation that I wait to see how these contributions to well-defined nanomaterials preparation will affect our ability to study the properties of nanomaterials and utilize them in a responsible fashion.

APPENDIX A
SUPPORTING INFORMATION TO CHAPTER II

TGA Traces for Purification Experiment

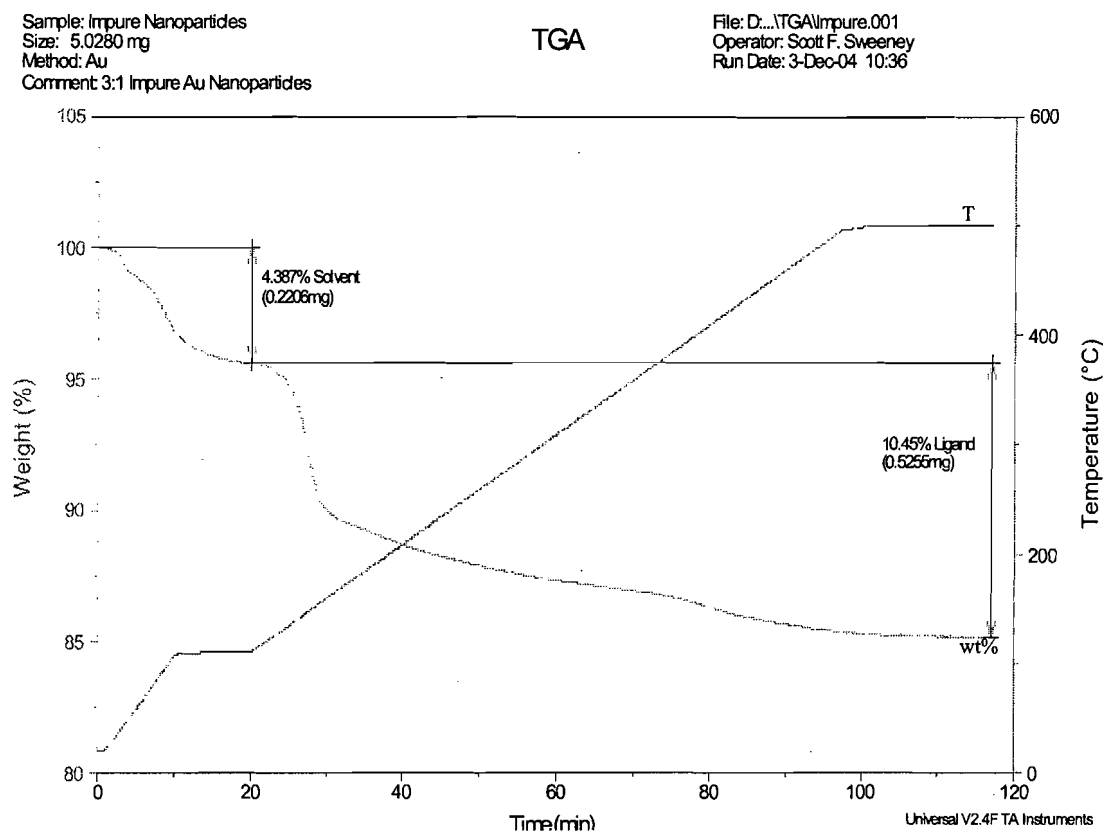


Figure A.1. TGA trace for the impure sample Au₂S-Crude.

Sample: ECC Nanoparticles
Size: 1.9980 mg
Method: Au
Comment: 3:1 ECC Au Nanoparticles

TGA

File: D:\...0299-Data\TGA\ECC.001
Operator: Scott F. Sweeney
Run Date: 5-Dec-04 13:35

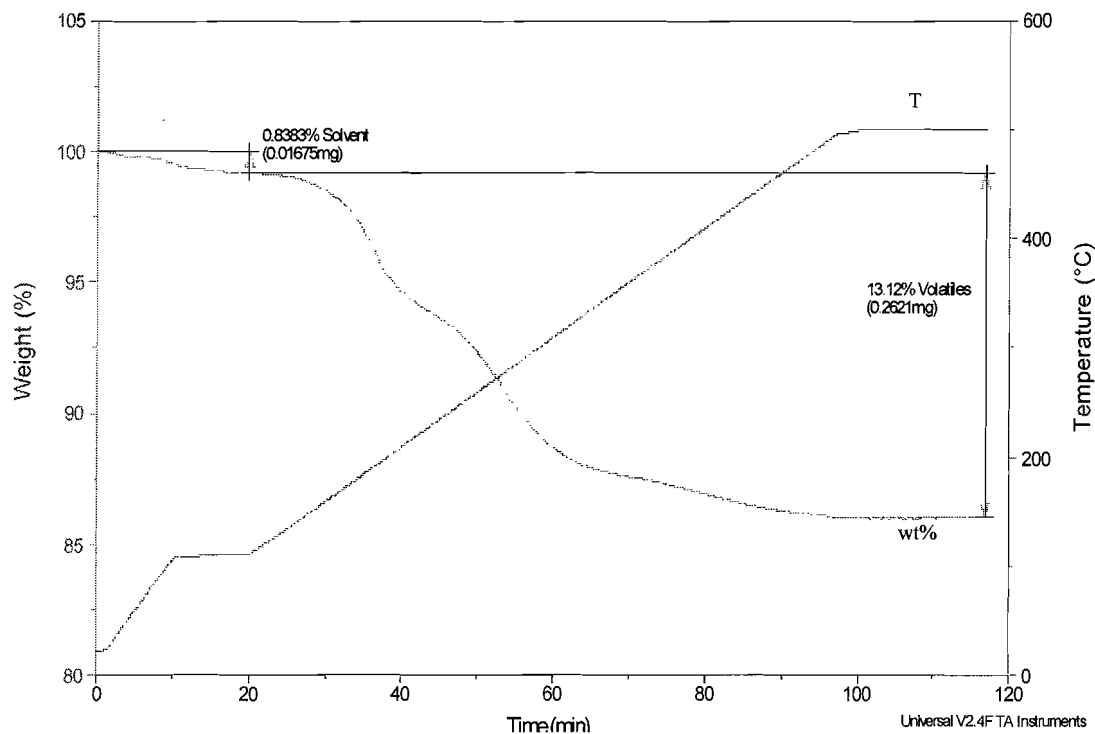


Figure A.2. TGA trace for the sample $Au_{2.8}$ -ECC.

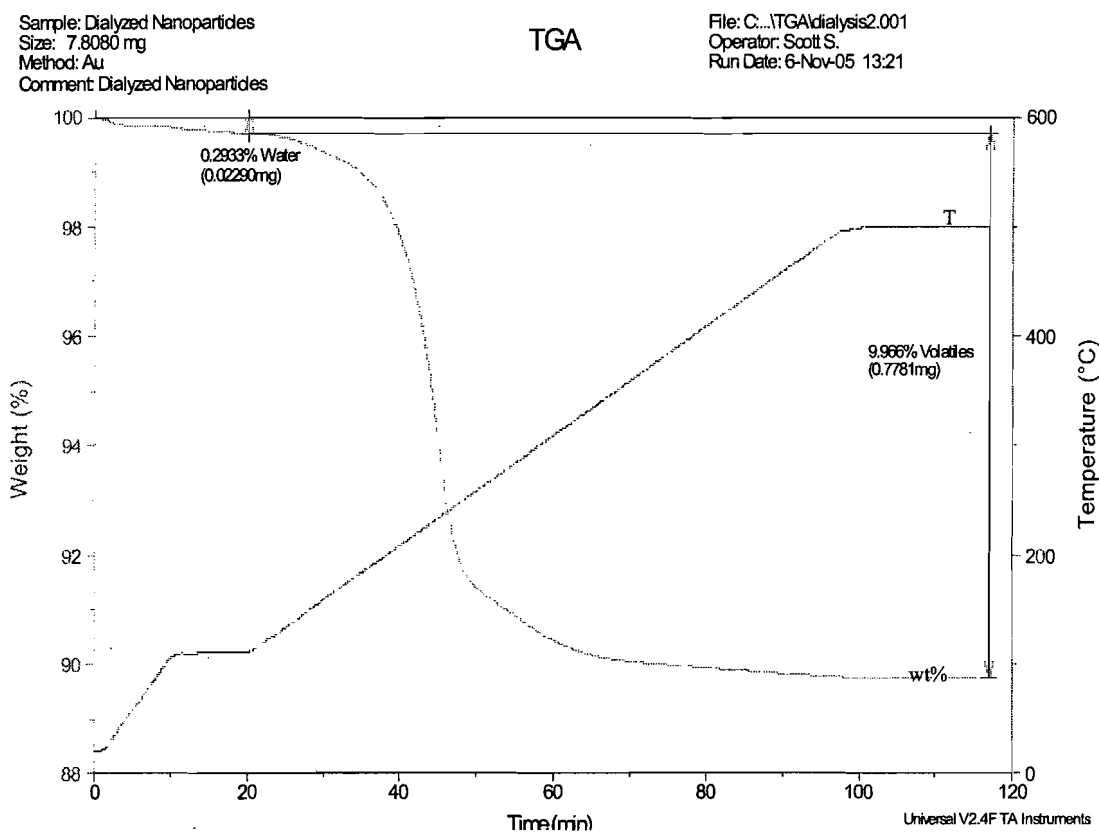


Figure A.3. TGA trace for dialyzed sample Au_{2.7}-D.

Sample: 70 kD Nanoparticles
Size: 2.6570 mg
Method: Au
Comment: 3:1 70 kD Au Nanoparticles

TGA

File: D:\TGA\70kD.001
Operator: Scott F. Sweeney
Run Date: 5-Dec-04 18:05

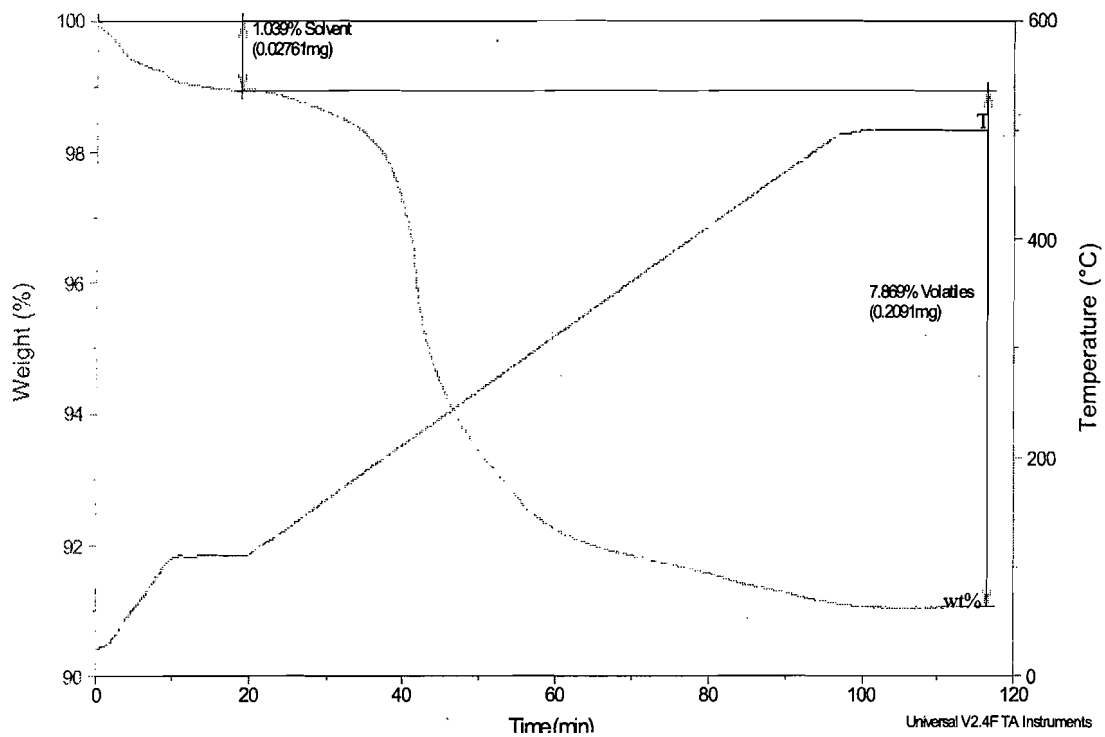


Figure A.4. TGA trace for sample Au_{2.9}-70R.

UV-vis Spectra

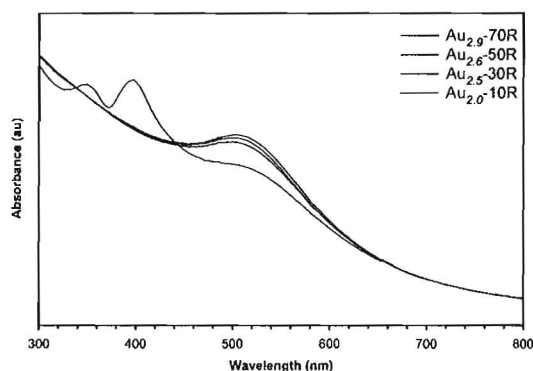


Figure A.5. Normalized UV/vis spectra for each of the retentate fractions. Blue trace is of Au_{2.9}-70R with $\lambda_{MAX} = 527$ nm. Red trace is of Au_{2.6}-50R with $\lambda_{MAX} = 522$ nm. Black trace is of Au_{2.5}-30R with $\lambda_{MAX} = 521$ nm. Each of these fractions has a distinct plasmon resonance, and a flat baseline. Green trace is of Au_{2.0}-10R. The two peaks at 350 and 410 nm are consistent with small ~1-nm gold nanoparticles, and the plasmon resonance has been significantly broadened as a result of the increased concentration of small nanoparticles.

TEM Analysis

Size analysis of the TEM images was performed by first increasing the image contrast through levels adjustment and unsharp mask in Adobe Photoshop CS. Next, the images were opened in ImageJ¹, and a size analysis was performed. The resultant data was filtered by aspect ratio and minimum particle size. In order to exclude aggregates or overlapping particles, particles with an aspect ratio of less than 0.75 were rejected. Similarly, in order to eliminate “false-particles” as a result of background noise, particles less than 0.8-nm (the particle size limit at the magnifications used) in diameter were rejected. In all cases, more than 1000 particles were counted in determining mean particle diameters and size distributions.²

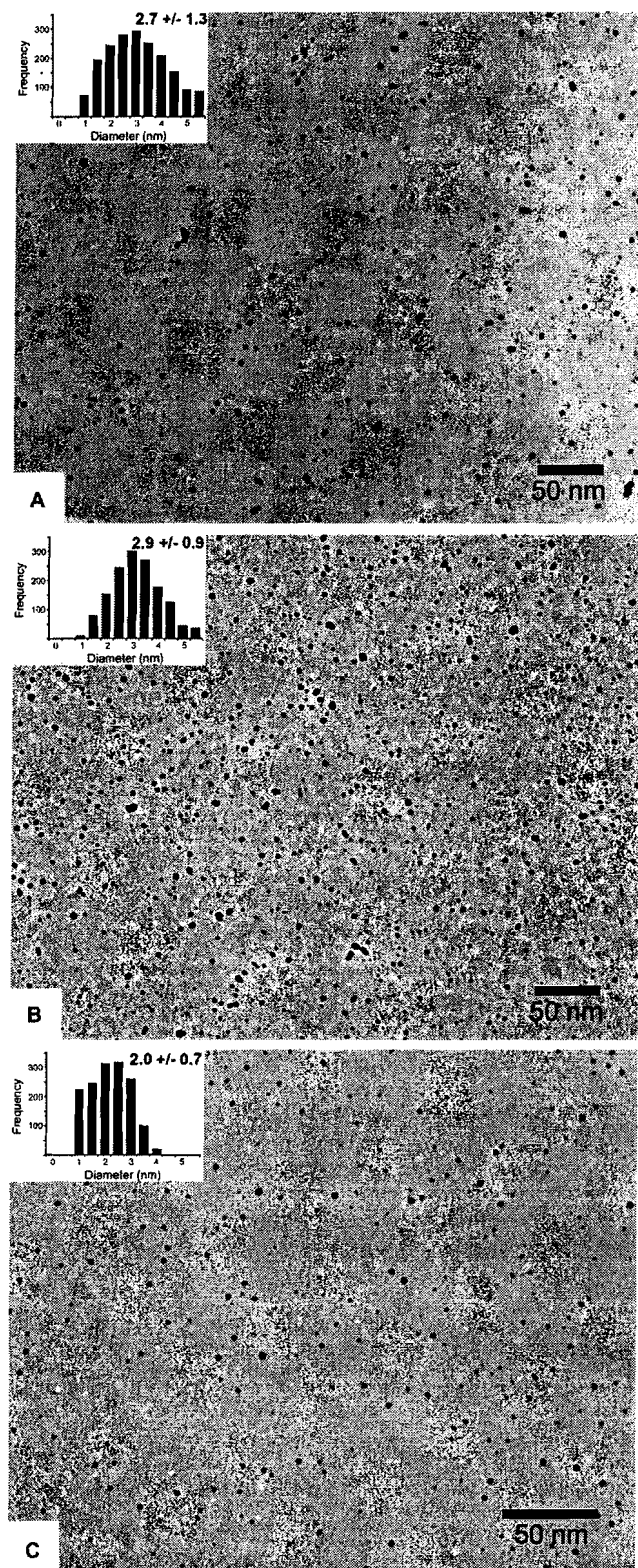


Figure A.6. Sample TEM images from fractionation of Au₃-Crude, Au_{2.9}-70R and Au_{2.0}-10R.

APPENDIX B

SYNTHETIC SCHEMES FOR CHAPTER III

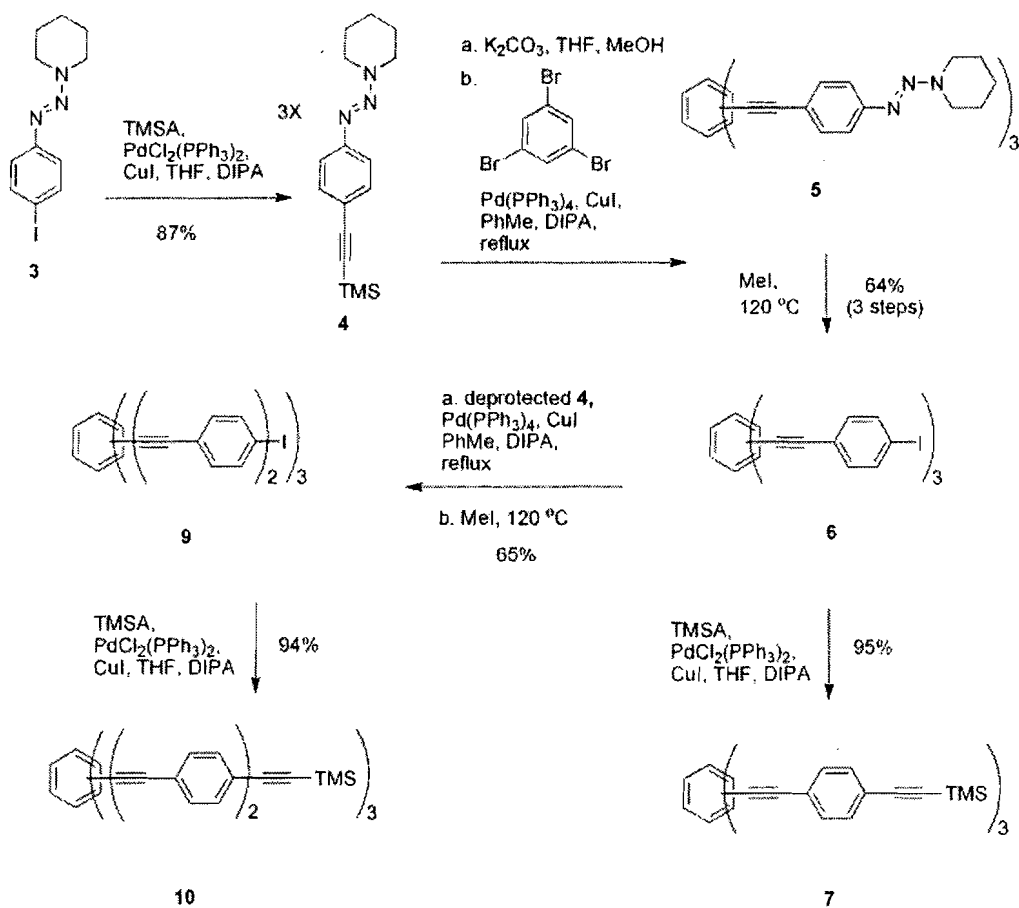


Figure B.1. Synthesis of Trifold Symmetrical TMS-ethynyl Preligands

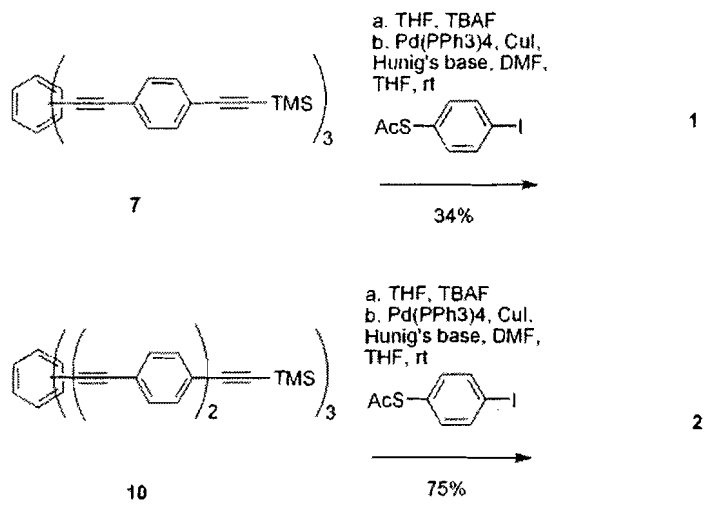


Figure B.2. Synthesis of Protected Thiol Capped Ligands

APPENDIX C

PHAGE DISPLAY USING IN VITRO SELECTION ON SURFACES

Introduction

In vitro selection on surfaces (ISOS) allows for the selection of biomolecules (RNA, DNA or peptides) with a high affinity for targets on planar substrates. Targets can include metals, semiconductors, organics and polymers. ISOS is unique in that selection is carried out *only* for the target that is defined by the area located within the Kel-F inserts. Because of this, ISOS can offer a higher degree of selectivity than other systems.

General Considerations

Inspection of ISOS microreactor

1. Handle Kel-F inserts with extreme care. The bottom of the inserts must remain highly polished. Any damage or imperfection may lead to leaks and loss of selectivity.
Inspect the Kel-F inserts before each use for damage (i.e. scratches, pits, etc.) Do not use insert if damaged.
2. Inspect the ISOS microreactor before using. Inspect wires for thermocouple and heater to ensure that they are not frayed.

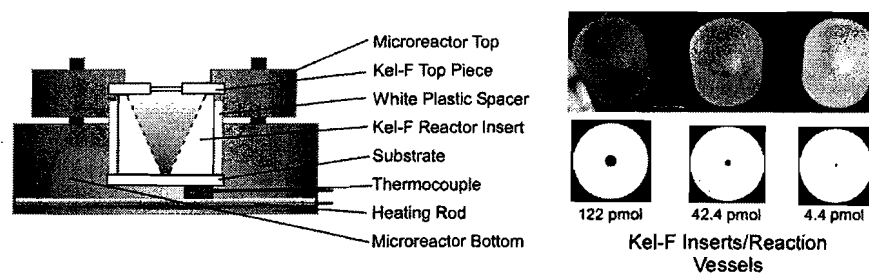


Figure C.1. (Right) Schematic of the ISOS microreactor, indicating important components. (Left) Kel-F Inserts that define access to the planar substrates. Concentrations are pmols of Au surface atoms.

Substrates

1. Substrates for the ISOS microreactor should be disks 20 mm in diameter and 3.3 mm in height. Borosilcate windows available from Edmund Scientific (NT45-461) make good substrates for evaporation of metals and coating with organics, polymers, biomolecules, etc. Off size materials can be mounted on these substrates using double sided tape, or sample holders can be fabricated.
2. **Caution!** Care must be taken to ensure that the substrates are planar and large enough to cover the majority of the Kel-F insert. Non-planar substrates will lead to leaking, and substrates that are too small will lead to damage of the Kel-F inserts.

Cleaning

1. The Kel-F insert and Kel-F top piece (Kel-F disk with small hole) should be cleaned prior to use. Clean with detergent and rinse thoroughly with DI and Ultrapure water. Finally, clean with appropriate solvents to disinfect.
2. Substrates should be rinsed with appropriate solvents to ensure there are no environmental contaminants on the surface.
3. Dry insert, Kel-F top piece and substrate with N₂ or compressed air.

Assembly

1. After inspecting and cleaning the ISOS microreactor and substrate, the microreactor can be assembled for use. Insert the substrate into the base of the microreactor, target side up. Use the spacer insert (white plastic cylinder) to press the substrate firmly to the bottom of the microreactor.
2. Place the Kel-F insert into the center of the spacer insert and press flush against substrate. Choice of Kel-F insert is based upon the amount of substrate needed for selection. Smaller apertures allow for limited access, giving more strigency to the selection.
3. Press the Kel-F top piece in the ISOS microreactor top, then place the whole top assembly onto the base as shown in Figure 1.
4. Using the three screws supplied with the microreactor, very carefully tighten the top to the bottom. First finger tighten the screws, then tighten using an allen wrench $\sim 3/8$ of a turn. Overtightening can result in the substrate breaking, undertightening can lead to leaking.
5. If using the heater, insert the heating rod into the appropriate hole on the side of the microreactor. Plug thermocouple and heating rod into temperature controller.

Phage Handling

1. Typically, phage should be stored in TBS, TBST or LB, chilled at 4°C. Do not store phage in PEG/NaCl more than overnight. Plan experiments accordingly.

General Selection Procedure

This general procedure is based upon the instruction manual for the Ph.D. 12™ Phage Display Peptide Library Kit as well as phage display selection experiments on sputtered gold substrates using the ISOS microreactor.

Day 1

Counterselection or “preclearing” of the phage library to the materials of the ISOS microreactor. Setup of overnight E. coli culture.

1. Clean and assemble ISOS microreactor using a glass substrate and an appropriate Kel-F insert. Wash with 3x500 uL TBST 0.2% for 2 minutes with shaking. Remove all remaining TBST using pipette.
2. Pipette 190 uL TBST 0.2% and 10 uL phage from the Ph.D. 12 kit into the ISOS microreactor. Place on shaker for 1 hour.
3. Pipette off the supernatant from the microreactor and transfer to a autoclaved 1.5 mL centrifuge tube. Wash microreactor with 2x200 uL TBST 0.2% and combine with original supernatant. Add 100 uL PEG/NaCl to the combined washes and place into refrigerator overnight.
4. Disassemble and clean microreactor.
5. In an autoclaved test tube, place 3 mL of LB broth. To this, add a small amount of K12 *E. coli* using a toothpick. Shake at 37°C overnight.

Day 2

Round 1 of phage display on the intended target. Amplification of phage using K12 E. coli. Removal of E. coli from amplified phage. Setup of overnight E. coli culture.

1. Centrifuge pre-cleared phage (Day 1 Step 3) at 14000 RPM at 4°C for 15 minutes.
Pipette off supernatant and centrifuge again at 14000 RPM at 4°C for 2 minutes.
Pipette off remaining supernatant.
2. Meanwhile, inspect, clean and assemble ISOS microreactor with the intended target substrate and an appropriate Kel-F insert. Wash with 3x500 uL TBST 0.2% for 2 minutes with shaking.
3. Pipette 200 uL of TBST 0.2% into the centrifuge tube and resuspend phage pellet.
4. Add the 200 uL of phage to the ISOS microreactor. Place on shaker for 1 hour.
5. Pipette off and discard the supernatant from the microreactor. Rinse with 2x200 uL TBST 0.2% for 2 minutes with shaking.
6. Add 200 uL glycine/HCl pH 2.2 and shake for 7 minutes. Meanwhile, pipette 20 mL of LB broth into a 250 mL autoclaved Erlenmeyer flask. To this, add 200 uL of the overnight *E. coli* culture.
7. Pipette off glycine/HCl from the ISOS microreactor and transfer into a 1.5 mL autoclaved centrifuge tube. Add 30 uL Tris-HCl pH 9.1 and vortex gently for a few moments.
8. Add 200 uL of the selected phage (Step 7) to the 250 mL Erlenmeyer flask. Cover flask and shake vigorously at 37°C for 4.5 hours.
9. Meanwhile, disassemble, inspect and clean the ISOS microreactor.

10. Transfer liquid from the 250 mL Erlenmeyer flask to an autoclaved 50 mL plastic centrifuge tube. Centrifuge at 10000 RPM for 15 minutes. Transfer the supernatant to a new autoclaved 50 mL plastic centrifuge tube. Add 3.3 mL PEG/NaCl and place into a refrigerator overnight.
11. In an autoclaved test tube, place 3 mL of LB broth. To this, add a small amount of K12 *E. coli* using a toothpick. Shake at 37°C overnight.

Day 3

Isolation of Round 1 phage and preparation for Round 2. Round 2 of phage display with higher stringency on the intended target. Amplification of phage using K12 E. coli. Removal of E. coli from amplified phage. Setup of overnight E. coli culture.

1. Centrifuge Round 1 phage at 10000 RPM at 4°C for 15 minutes. Pour off supernatant and centrifuge again at 10000 RPM at 4°C for 2 minutes. Pipette off remaining supernatant. Resuspend pellet in 1 mL TBS and transfer to an autoclaved 1.5 mL centrifuge tube. Add 150 uL of PEG/NaCl and allow to precipitate in the refrigerator for 20 minutes.
2. Carry out second round of phage display: Repeat Steps 2-11 from Day 2 using TBST 0.3%.

Day 4

Isolation of Round 2 phage and preparation for Round 3. Round 3 of phage display with higher stringency on the intended target. Amplification of phage using K12 E. coli. Removal of E. coli from amplified phage. Setup of overnight E. coli culture.

1. Isolate Round 2 phage: Carry out Step 1 from Day 3.

2. Carry out third round of phage display: Repeat Steps 2-11 from Day 2 using TBST 0.4%

Day 5 and Beyond

Isolation of previous round's phage and preparation for the next round of phage

display. Next round of phage display with higher stringency on the intended target.

Amplification of phage using K12 E. coli. Removal of E. coli from amplified phage. Setup of overnight E. coli culture.

1. Repeat steps as for Day 4 with increasing stringency until final round of phage display is complete (4-5 rounds is typically sufficient).
2. Stringency can be increased by: (i.) Increasing Tween concentration in order to decrease nonspecific peptide/target interactions; (ii.) Decreasing target concentration by decreasing Kel-F insert aperture size; (iii.) Increasing the temperature.

Phage Titering

Isolation of individual phage and preparation for sequencing.

Day 1

1. Isolate Final Round phage: Carry out Step 1 Day 3, resuspending final pellet in 200 uL TBS.
2. Prepare a day culture by diluting 30 uL of overnight culture in 3 mL of LB broth. Shake vigorously at 37°C for 4 hours.
3. Carry out 12 serial dilutions of isolated phage in LB broth. Label 12 PCR tubes 1-12. To each tube add 90 uL LB broth. To first tube, add 10 uL of the isolated phage and

- vortex quickly. To second tube, add 10 uL of Tube 1 and vortex quickly. Continue until all dilutions are completed, then place PCR tubes into refrigerator until needed.
4. Place 8 LB plates into the 37°C oven to prewarm them.
 5. Approximately 1 hour before *E. coli* culture is completed, heat top agar in microwave for ~1.5 minutes. Pipette 4 mL aliquots of top agar into 8 15 mL tubes and place into 60°C water bath.
 6. To each of 8 autoclaved 1.5 mL centrifuge tubes pipette 200 uL of *day* culture. *The following steps must be completed rapidly, otherwise top agar will harden.*
 7. Choose 8 dilutions to titer (typically 5-12).
 8. Pipette 10 uL of a dilution into a tube from Step 6. Vortex quickly.
 9. Remove an LB plate from the oven and label. Turn over so that agar is on the bottom.
 10. Remove a tube containing top agar from the 60°C water bath. To this add 4 uL IPTG and 40 uL Xgal. Transfer the contents of the tube from Step 8 into the 15 mL tube and vortex quickly.
 11. Pour contents of 15 mL tube onto the prewarmed LB plate. Spread evenly over the top by moving plate in a figure 8 motion.
 12. Set plate aside for 5 minutes, invert and incubate overnight at 37°C.
 13. Repeat steps 8-12 for all dilutions.
 14. In an autoclaved test tube, pipette 3 mL LB broth. To this, pipette in 30 uL *day* culture. Shake at 37°C overnight.

Day 2

15. Inspect the plates. Look for a plate with ~100 well separated spots.

16. Pipette 25 mL of LB broth into a 50 mL autoclaved centrifuge tube. This, add 250 uL of overnight culture.
17. Pipette 1 mL of the diluted overnight culture into each of 20 autoclaved test tubes.
18. Identify twenty good spots on the chosen plate.
19. Using a 1-200 uL pipette tip, stab an individual spot and transfer into a test tube containing overnight culture. Repeat for each of the twenty spots.
20. Place tubes into incubator at 37°C for 4.5 hours.
21. In the meantime, label 3x20 autoclaved 1.5 mL centrifuge tubes. Label the first two sets 1-20 and label the last set with an appropriate name, ie. "ISOS-Au-1."
22. Transfer contents of test tubes to one set of 1-20 labeled autoclaved 1.5 mL centrifuge tubes. Centrifuge at 14000 RPM for 3 minutes.
23. Pipette 500 uL of each supernatant into second set of 1-20 labeled autoclaved 1.5 mL centrifuge tubes. Pipette 200 uL of each supernatant into the named centrifuge tubes, and set aside.
24. Pipette 200 uL of PEG/NaCl to the second set of 1-20 centrifuge tubes. Invert 10 times. Incubate 10 minutes. Centrifuge at 14000 RPM for 10 minutes. Remove supernatant. Centrifuge at 14000 RPM for 2 minutes. Remove remaining supernatant.
25. Resuspend pellet in 100 uL NaI buffer and mix gently with pipette. Add 250 uL ethanol. Invert 10 times. Incubate 10 minutes. Centrifuge at 14000 RPM for 10 minutes. Remove supernatant. Centrifuge at 14000 RPM for 2 minutes. Remove remaining supernatant.

26. Resuspend pellet in 500 uL 70% ethanol. Vortex briefly. Centrifuge at 14000 RPM for 3 minutes. Remove supernatant. Remove remaining supernatant. Speed-vac to dryness. If pellet is white (from salts) repeat Step 26. Resuspend DNA in 20 uL of TE buffer.

REFERENCES

Chapter I

- (1) Pan, L.; Shoji, T.; Nagataki, A.; Nakayama, Y. *Adv. Eng. Mat.* **2007**, *9*, 584.
- (2) Xiao, R.; Cho, S.; Liu, R.; Lee, S. B. *J. Am. Chem. Soc.* **4483**, *129*, 4483.
- (3) Yan, Y. M.; Zheng, W.; Su, L.; Mao, Q. *Adv. Mater.* **2006**, *18*, 2639.
- (4) Hooker, S. A.; Geiss, R.; Schilt, R. and Kar, A. In Proceedings of the 31st International Cocoa Beach Conference & Exposition on Advanced Ceramics and Composites, American Ceramics Society, **1997**, 58
- (5) Liu, Y.; Fu, Q.; Flyntzani-Stephanopoulos, M. *Catal. Today* **2004**, *93-95*, 241.
- (6) Suh, D. J.; Kwak, C.; Kim, J. H.; Kwon, S. M.; Park, T. J. *Power Sources* **2005**, *142*, 70.
- (7) Song, C. *Catal. Today* **2002**, *77*, 17; Rodriguez, J. A.; Liu, P.; Hrbek, J.; Evans, J. S.; Perez, M. *Ang. Chem. Int. Ed.* **2007**, *46*, 1329; Liu, P.; Rodriguez, J. A. *J. Chem. Phys.* **2007**, *126*, 8.
- (8) Pan, X. Q.; Wang, H. Q.; Lee, R. J. *Pharm. Res.* **2003**, *20*, 417.
- (9) Yang, Z.; Huck, W. T. S.; Clarke, S. M.; Tajbakhsh, A. R.; Terentjev, E. M. *Nat. Mater.* **2005**, *4*, 486.
- (10) Lee, C. C.; Mackay, J. A.; Frechet, J. M. J.; Snoka, F. C. *Nat. Biotech.* **2005**, *23*, 1517.
- (11) Jongnam-Park, E. L.; Hwang, N. M.; Kang, M.; Kim, S. C.; Hwang, Y.; Park, J. G.; Noh, H. J.; Kim, J. Y.; Park, J. H.; Hyeon, T. *Angew. Chem. Int. Ed.* **2005**, *44*, 2872.

- (12) Rolland, J. P.; Hagberg, E. C.; Denison, G. M.; Carter, K. R.; DeSimone, J. M. *Ang. Chem. Int. Ed.* **2004**, *43*, 5796.
- (13) Kalyuzhny, G.; Murray, R. W. *J. Phys. Chem B* **2005**, *109*, 7012.
- (14) Cumberland, S. L.; Hanif, K. M. J., A.; Khitrov, G. A.; Strouse, G. F.; Woessner, S. M.; Yun, C. S. *Chem. Mater* **2002**, *14*(4), 1576; Hines, M. A.; Guyot-Sionnest, P. *J. Phys. Chem.* **1996**, *100*, 468.
- (15) Faraday, M. *Philos. Trans.* **1857**, *147*, 145.
- (16) Mie, G. *Ann. Phys.* **1908**, *25*, 377.
- (17) Gans, R. *Ann. Phys.* **1912**, *37*, 881.
- (18) Alivisatos, A. P. *J. Phys. Chem.* **1996**, *100*, 13226.
- (19) Amman, M.; Mullen, K.; Ben-Jacob, E. *J. Appl. Phys.* **1989**, *65*, 339; Barner, J. B.; Ruggiero, S. T. *Phys. Rev. Lett.* **1987**, *59*, 807; Giaever, I.; Zeller, H. R. *Phys. Rev. Lett.* **1968**, *20*, 1504; Schonenberger, C.; van Houten, H.; Beenakker, C. W. J. *Phys B* **1993**, *189*, 218.
- (20) Grabert, H.; Devoret, M. H. In NATO ASI Series, Series B, Physics, v. 294; Plenum Press: New York, **1992**.
- (21) Schmid, G. *Chem. Rev.* **1992**, *92*, 1709.
- (22) Jana, N. R.; Gearheart, L.; Murphy, C. J. *J. Phys. Chem. B* **2001**, *105*, 4065.
- (23) J. E. Millstone, C. A. Mirkin, *Adv. Funct. Mater.* **2006**, *16*, 1209.
- (24) Huang, C. J.; Chiu, P. H.; Wang, Y. H.; Chen, W. R.; Meen, T. H. *J. Electrochem. Soc.* **2006**, *153*, D129.
-
- (25) Hao, F.; Nehl, C. L.; Hafner, J. H.; Nordlander, P. *Nano Lett.* **2007**, *7*, 729.
- (26) Feldheim, D. L.; Keating, C. D. *Chem. Soc. Rev.* **1998**, *27*, 1.
- (27) Lu, Y.; Yin, Y. D.; Li, Z. Y.; Xia, Y. N. *Nano Lett.* **2002**, *2*, 785.

- (28) Lee, J. S.; Han, M. S.; Mirkin, C. A. *Angew. Chem., Int. Ed.* **2007**, *46*, 4093.
- (29) Hong, R.; Han, G.; Fernandez, J. M.; Kim, B. j.; Forbes, N. S.; Rotello, V. M. *J. Am. Chem. Soc.* **2006**, *128*, 1078.
- (30) Kouwenhoven, L. P.; Schon, G.; Sohn, L. L. in *Mesoscopic Electron Transport*; Kouwenhoven, L. P., Schon, G., Sohn, L. L., Eds.; Kluwer Academic Publishers: Dordrecht, The Netherlands, 1997, 1.
- (31) Brust, M.; Bethell, D.; Schiffrin, D. J.; Kiely, C. J. *Adv. Mater.* **1995**, *7*, 795.
- (32) Ingram, R. S.; Hostetler, M. J.; Murray, R. W.; Schaaf, T. G.; Khoury, J. T.; Whetten, R. L.; Bigioni, T. P.; Guthrie, D. K.; First, P. N. *J. Am. Chem. Soc.* **1997**, *119*, 9279.
- (33) Curie, D. *Luminescence in Crystals*; John Wiley and Sons: New York, 1963.
- (34) Feldheim, D. L.; Eaton, B. E. *ACS Nano* **2007**, ASAP Article.
- (35) Liu, J. W.; Lu, Y. *Analytical Chemistry* **2004**, *76*, 1627.
- (36) Daniel, M.-C.; Astruc, D. *Chem. Rev.* **2004**, *104*, 293; Link, S.; El-Sayed, M. A. *Int. Rev. Phys. Chem.* **2000**, *19*, 409.
- (37) Liu, J. W.; Lu, Y. *Chem. Mater.* **2004**, *16*, 3231.
- (38) Millstone, J. E.; Métraux, G. S.; Mirkin, C. A. *Adv. Funct. Mater.* **2006**, *16*, 1209.
- (39) Perez-Juste, J.; Pastoriza-Santos, I.; Liz-Marzan, L. M.; Mulvaney, P. *Coord. Chem. Rev.* **2005**, *249*, 1870.
- (40) Wang, H. F.; Huff, T. B.; Zweifel, D. A.; He, W.; Low, P. S.; Wei, A.; Cheng, J. X. *Roc. Natl. Acad. Sci. U. S. A.* **2005**, *102*, 15752.
- (41) Richardson, H. H.; Hickman, Z. N.; Govorov, A. O.; Thomas, A. C.; Zhang, W.; Kordesch, M. E. *Nano Lett.* **2006**, *6*, 783.
- (42) LaMer, V. K.; Dinegar, R. H. *J. Am. Chem. Soc.* **1950**, *72*, 4847.
- (43) Wu, C.; Zeng, T. *Chem. Mater.* **2007**, *19*, 123.

- (44) Turkevitch, J.; Stevenson, P. C.; Hillier, J. *Discuss. Faraday Soc.* **1951**, *11*, 55.
- (45) Frens, G. *Nature: Phys. Sci.* **1973**, *241*, 20.
- (46) Dahl, J.; Maddux, B.; Hutchison, J. *Chem. Rev.* **2007**, *107*, 2228.
- (47) Brust, M.; Walker, M.; Bethell, D.; Schiffrin, D. J.; Whyman, R. J. *J. Chem Soc., Chem. Commun.* **1994**, *5*, 801.
- (48) Gandubert, V. J.; Lennox, R. B. *Langmuir* **2005**, *21*, 6532.
- (49) Rucareanu, S.; Gandubert, V. J.; Lennox, R. B. *Chem. Mater.* **2006**, *18*, 4674.
- (50) Woehrle, G. H.; Brown, L. O.; Hutchison, J. E. *J. Am. Chem. Soc.* **2005**, *127*, 2172; Woehrle, G. H.; Warner, M. G.; Hutchison, J. E. *J. Phys. Chem. B* **2002**, *106*, 9879.
- (51) Cariati, F.; Naldini, L. *Inorg. Chim. Act.* **1971**, *5*, 172; Malatesta, L.; Naldini, L.; Simonetta, G.; Cariati, F. *Chem. Commun.* **1965**, 212; McPartlin, M.; Malatesta, L.; Mason, R. *J. Chem. Soc., Chem. Commun.* **1969**, 334; Teo, B. K.; Shi, X.; Zhang, H. *J. Am. Chem. Soc.* **1992**, *114*, 2743.
- (52) Schmid, G.; Pfeil, R.; Boese, R.; Brandermann, F.; Meyer, S.; Calis, G. H. M.; Van der Velden, J. W. A. *Chem. Ber.* **1981**, *114*, 3634.
- (53) Weare, W. W.; Reed, S. M.; Warner, M. G.; Hutchison, J. E. *J. Am. Chem. Soc.* **2000**, *122*, 12890.
- (54) Brust, M.; Fink, J.; Bethell, D.; Schiffrin, D. J.; Kiely, C. J. *J. Chem Soc., Chem. Commun.* **1995**, *6*, 1655.
- (55) Kanaras, A. G.; Kamounah, F. S.; Schaumburg, K.; Kiely, C. J.; Brust, M. *J. Chem Soc., Chem. Commun.* **2002**, 2294.
- (56) Schaaf, T. G.; Shafigullin, M. N.; Khoury, J. T.; Vezmar, I.; Whetten, R. L.; Cullen, W. G.; First, P. N.; Gutierrez-Wing, C.; Ascensio, J.; Jose-Yacaman, M. J. *J. Phys. Chem B* **1997**, *101*, 7885.
- (57) Hostetler, M. J.; Wingate, J. E.; Zhong, C.-J.; Harris, J. E.; Vachet, R. W.; Clark, M. R.; Londono, J. D.; Green, S. J.; Stokes, J. J.; Wignall, G. D.; Glish, G. L.; Porter, M. D.; Evans, N. D.; Murray, R. W. *Langmuir* **1998**, *14*, 17.

- (58) Shon, Y. S.; Cutler, E. *Langmuir* **2004**, *20*, 6626-6630; Shon, Y. S.; Wuelfing, W. P.; Murray, R. W. *Langmuir* **2001**, *17*, 1255-1261; Shon, Y. S.; Gross, S. M.; Dawson, B.; Porter, M.; Murray, R. W. *Langmuir* **2000**, *16*, 6555.
- (59) Lohse, S. E.; Dahl, J. A.; Hutchison, J. E. *Langmuir*, **2007**, *Manuscript in Preparation*.
- (60) Millstone, J. E.; Park, S.; Shuford, K. L.; Qin, L. D.; Schatz, G. C.; Mirkin, C. A. *J. Am. Chem. Soc.* **2005**, *127*, 5312.
- (61) Kim, F.; Connor, S.; Song, H.; Kuykendall, T.; Yang, P. D. *Angew. Chem., Int. Ed.* **2004**, *43*, 3673.
- (62) Sun, Y. G.; Xia, Y. N. *Science* **2002**, *298*, 2176.
- (63) Chang, S. S.; Shih, C. W.; Chen, C. D.; Lai, W. C.; Wang, C. R. *C. Langmuir* **1999**, *15*, 701.
- (64) Lim, I. I. S.; Maye, M. M.; Luo, J.; Zhong, C. J. *J. Phys. Chem B* **2005**, *109*, 2578.
- (65) Murphy, C. J.; San, T. K.; Gole, A. M.; Orendorff, C. J.; Gao, J. X.; Gou, L.; Hunyadi, S. E.; Li, T. *J. Phys. Chem. B* **2005**, *109*, 13857.
- (66) Perez-Juste, J.; Liz-Marzan, L. M.; Carnie, S.; Chan, D. Y. C.; Mulvaney, P. *Adv. Funct. Mater.* **2004**, *14*, 571.
- (67) Templeton, A. C.; Hostetler, M. J.; Kraft, C. T.; Murray, R. W. *J. Am. Chem. Soc.* **1998**, *120*, 1906.
- (68) Templeton, A. C.; Hostetler, M. J.; Warmoth, E. K.; Chen, S.; Hartshorn, C. M.; Krishnamurthy, V. M.; Forbes, M. D. E.; Murray, R. W. *Langmuir* **1998**, *120*, 4845.
- (69) Li, D.; Jones, G. L.; Dunlap, J. R.; Hua, F.; Zhao, B. *Langmuir* **2006**, *22*, 3344.
- (70) Hua, F.; Swihart, M. T.; Ruckenstein, E. *Langmuir* **2005**, *21*, 6054.
- (71) Niemeyer, C. M.; Ceyhan, B.; Gao, S.; Chi, L.; Peschel, S.; Simon, U. *Colloid Polym. Sci.* **2005**, *283*, 783; Xie, H.; Tkachenko, A. G.; Glomm, W. R.; Ryan, J. A.; Brennaman, M. K.; Papanikolas, J. M.; Franzen, S.; Feldheim, D. L. *Anal. Chem.* **2003**, *75*, 5797.

- (72) Lin, S. Y.; Tsai, Y. T.; Chen, C. C.; Lin, C. M.; Chen, C. H. *J. Phys. Chem. B* **2004**, 2134.
- (73) Brown, L. O.; Hutchison, J. E. *J. Am. Chem. Soc.* **1999**, 121, 882.
- (74) Hostetler, M. J.; Templeton, A. C.; Murray, R. W. *Langmuir* **1999**, 15, 3782.
- (75) Badia, A.; Cuccia, L.; Demers, L.; Morin, F.; Lennox, R. B. *J. Am. Chem. Soc.* **1997**, 119, 2682.

Chapter II

- (1) Peng, Z. Q.; Walther, T.; Kleinermanns, K., *Langmuir* **2005**, 21, 4249.
- (2) Lim, I. I. S.; Maye, M. M.; Luo, J.; Zhong, C. J., *J. Phys. Chem B* **2005**, 109, 2578.
- (3) Wei, Z. Q.; Zamborini, F. P., *Langmuir* **2004**, 20, 11301-11304.
- (4) Goodman, C. A.; Frankamp, B. L.; Cooper, B. A.; Rotello, V. A., *Colloids Surf. B Biointerfaces* **2004**, 39, 123.
- (5) Alivisatos, A. P., *J. Phys. Chem.* **1996**, 100, 13239.
- (6) Bartz, M.; Kuther, J.; Seshadri, R.; Tremel, W., *Angew. Chem. Int. Ed.* **1998**, 37, 2466.
- (7) Boal, A. K.; Rotello, V. M., *J. Am. Chem. Soc.* **2000**, 122, 735.
- (8) Frey, P. A.; Frey, T. G., *J. Struct. Biol.* **1999**, 127, 100.
- (9) Hainfeld, J. F., *Science* **1987**, 236, 453.
- (10) Huang, D.; Liao, F.; Molesa, S.; Redinger, D.; Subramanian, V., *J. Electrochem. Soc.* **2003**, 157(7), 412.
- (11) Jahn, W., *J. Struct. Biol.* **1999**, 127, 106.
- (12) Neiman, B.; Grushka, E.; Lev, O., *Anal. Chem.* **2001**, 73, 5220.
- (13) Wohltjen, H.; Snow, A. W., *Anal. Chem.* **1998**, 70, 2856.

- (14) Kearns, G. J.; Foster, E. W.; Hutchison, J. E. *Anal. Chem.* **2006**, *78*, 298.
- (15) Foster, E. W.; Kearns, G. J.; Goto, S.; Hutchison, J. E., *Adv. Mater.* **2005**, *17*, 1542.
- (16) Brust, M.; Bethell, D.; Schiffrin, D. J.; Kiely, C. J., *Adv. Mater.* **1995**, *7*, 795.
- (17) Brust, M.; Fink, J.; Bethell, D.; Schiffrin, D. J.; Kiely, C. J., *J. Chem Soc., Chem. Commun.* **1995**, *6*, 1655.
- (18) Foos, E. E.; Snow, A. W.; Twigg, M. E.; Ancona, M. G., *Chem. Mater.* **2002**, *14*, 2401.
- (19) Hostetler, M. J.; Wingate, J. E.; Zhong, C.-J.; Harris, J. E.; Vachet, R. W.; Clark, M. R.; Londono, J. D.; Green, S. J.; Stokes, J. J.; Wignall, G. D.; Glish, G. L.; Porter, M. D.; Evans, N. D.; Murray, R. W., *Langmuir* **1998**, *14*, 17.
- (20) Kanaras, A. G.; Kamounah, F. S.; Schaumburg, K.; Kiely, C. J.; Brust, M., *J. Chem Soc., Chem. Commun.* **2002**, 2294.
- (21) Weare, W. W.; Reed, S. M.; Warner, M. G.; Hutchison, J. E., *J. Am. Chem. Soc.* **2000**, *122*, 12890.
- (22) Yonezawa, T.; Sutoh, M.; Kunitake, T., *Chem. Lett.* **1997**, 619.
- (23) Cumberland, S. L.; Berrettini, M. G.; Javier, A.; Strouse, G. F., *Chem. Mater.* **2003**, *15*, 1047.
- (24) Wang, D.; Jibao, H.; Rosenzweig, N.; Rosenzweig, Z., *Nano Lett.* **2004**, *4*(3), 409.
- (25) Kalyuzhny, G.; Murray, R. W., *J. Phys. Chem. B* **2005**, *109*, 7012.
- (26) Xie, H.; Gu, Y. L.; Ploehn, H. J., *Nanotechnology* **2005**, *16*, S492.
- (27) Woehrle, G. H.; Brown, L. O.; Hutchison, J. E., *J. Am. Chem. Soc.* **2005**, *127*, 2172.
- (28) Brust, M.; Walker, M.; Bethell, D.; Schiffrin, D. J.; Whyman, R. J., *J. Chem Soc., Chem. Commun.* **1994**, *5*, 801.
- (29) Sang-Keun, O.; Kim, Y.; Ye, H.; Crooks, R. M., *Langmuir* **2003**, *19*, 10420.

- (30) Kim, Y.; Sang-Keun, O.; Crooks, R. M., *Chem. Mater.* **2004**, *16*, 167.
- (31) Crooks, R. M.; Zhao, M.; Sun, L.; Chechik, V.; Yeung, L. K., *Acc. Chem. Res.* **2001**, *34*(3), 181.
- (32) Novak, J. P.; Nickerson, C.; Franzen, S.; Feldheim, D. L., *Anal. Chem.* **2001**, *73*, 5758.
- (33) Smith, J., *Bull. Kor. Chem Soc.* **2003**, *24*, 684.
- (34) Templeton, A. C.; Cliffler, D. E.; Murray, R. W., *J. Am. Chem. Soc.* **1999**, *121*, 7081.
- (35) Chemseddine, A.; Weller, H., *Ber. Bunsenges. Phys. Chem.* **1993**, *97*, 636.
- (36) Al-Somali, A. M.; Krueger, K. M.; Falkner, J. C.; Colvin, V. L., *Anal. Chem.* **2004**, *76*, 5903.
- (37) Krueger, K. M.; Al-Somali, A. M.; Falkner, J. C.; Colvin, V. L., *Anal. Chem.* **2005**.
- (38) Song, Y.; Heien, M. L.; Jimenez, V.; Wightman, R. M.; Murray, R. W., *Anal. Chem.* **2004**, *76*, 4911.
- (39) Akthakul, A.; Hochbaum, A. I.; Stellacci, F.; Mayes, A. M., *Adv. Mater.* **2005**, *17*, 532.
- (40) Clarke, N. Z.; Waters, C.; Johnson, K. A.; Satherly, J.; Schiffrin, D. J., *Langmuir* **2001**, *17*, 6048.
- (41) Ebersold, M. F.; Zydney, A. L., *Biotechnol. Prog.* **2004**, *20*, 543.
- (42) Lajmi, A. R.; Schwartz, L.; Sanghvi, Y. S., *Org. Process Res. Dev.* **2004**, *8*, 651.
- (43) Tishchenko, G.; Luetzow, K.; Schauer, J.; Albrecht, W.; Bleha, M., *Sep. Pur. Tech.* **2001**, *22-23*, 403.
- (44) Limayem, I.; Charcosset, C.; Fessi, H., *Sep. Pur. Tech.* **2004**, *38*, 1.
- (45) McKenzie, L. C.; Hutchison, J. E., *Chim. Oggi-Chem. Today* **2004**, *22*, 30.

- (46) Anastas, P. T.; Warner, J. C. *Green Chemistry Theory and Practice*; Oxford University Press: Oxford, 1998.
- (47) Woehrlé, G. H.; Hutchison, J. E.; Ozkar, S.; Finke, R. G. *Turk. J. of Chem.* 2006, 30, 1.
- (48) Stoner, M. R.; Fischer, N.; Nixon, L.; Buckel, S.; Benke, M.; Austin, F.; Randolph, T. W.; Kendrick, B. S., *J. Pharm. Sci.* 2004, 93, 2332.
- (49) Shao, J. H.; Zydney, A. L., *Biotech. Bio.* 2004, 87, 286.
- (50) Cheryan, M. *Ultrafiltration Handbook*; Technomic: Lancaster, PA, 1986.
- (51) Brock, T. D. *Membrane Filtration: A User's Guide and Reference Manual*; Science Tech, Inc.: Madison, WI, 1983.
- (52) Link, S.; El-Sayed, M. A., *Int. Rev. Phys. Chem.* 2000, 19, 409.
- (53) Schaaf, T. G.; Shafigullin, M. N.; Khoury, J. T.; Vezmar, I.; Whetten, R. L.; Cullen, W. G.; First, P. N.; Gutierrez-Wing, C.; Ascensio, J.; Jose-Yacaman, M. J., *J. Phys. Chem B* 1997, 101, 7885.
- (54) Gutierrez, E.; Powell, R. D.; Furuya, F. R.; Hainfeld, J. F.; Schaaf, T. G.; Shafigullin, M. N.; Stephens, P. W.; Whetten, R. L., *Eur. Phys. J. D* 1999, 9, 647.

Chapter III

- (1) Novak, J. P.; Brousseau, L. C.; Vance, F. W.; Johnson, R. C.; Lemon, B. I.; Hupp, J. T.; Feldheim, D. L. *J. Am. Chem. Soc.* 2000, 122, 12029; McConnell, W. P.; Novak, J. P.; Brousseau, L. C.; Fuierer, R. R.; Tenent, R. C.; Feldheim, D. L. *J. Phys. Chem. B* 2000, 104, 8925.
- (2) Reinhard, B. M.; Siu, M.; Agarwal, H.; Alivisatos, A. P.; Liphardt, J. *Nano Lett.* 2005, 5, 2246.
- (3) Nikoobakht, B.; Burda, C.; Braun, M.; Hun, M.; El-Sayed, M. A. *Photo. Chem. Photo. Bio.* 2004, 75(6), 591.
- (4) Novak, J. P.; Feldheim, D. L. *J. Am. Chem. Soc.* 2000, 122, 3979-3980; Brousseau, L. C.; Novak, J. P.; Marinakos, S. M.; Feldheim, D. L. *Adv. Mater.* 1999, 11, 447.

- (5) Sung, K.-M.; Mosley, D. W.; Peelle, B. R.; Zhang, S.; Jacobson, J. M. *J. Am. Chem. Soc.* **2004**, *126*, 5064.
- (6) Alivisatos, A. P.; Johnsson, K. P.; Peng, X.; Wilson, T. E.; Loweth, C. J.; Bruchez, M. P.; Schultz, P. G. *Nature* **1996**, *382*, 609-611; Loweth, C. J.; Caldwell, W. B.; Peng, X.; Alivisatos, A. P.; Schultz, P. G. *Ang. Chem. Int. Ed.* **1999**, *38*, 1808.
- (7) Cumberland, S. L.; Berrettini, M. G.; Javier, A.; Strouse, G. F. *Chem. Mater.* **2003**, *15*, 1047-1056; Mirkin, C. A.; Letsinger, R. L.; Mucic, R. C.; Storhoff, J. J. *Nature* **1996**, *382*, 607-609; Mitchell, G. P.; Mirkin, C. A.; Letsinger, R. L. *J. Am. Chem. Soc.* **1999**, *121*, 8122-8123; Park, S. Y.; Lee, J. S.; Georganopoulou, D.; Mirkin, C. A.; Schatz, G. C. *J. Phys. Chem. B* **2006**, *110*, 12673.
- (8) Novak, J. P.; Nickerson, C.; Franzen, S.; Feldheim, D. L. *Anal. Chem.* **2001**, *73*, 5758.
- (9) Taher, D.; Walfort, B.; Lang, H. *Inorg. Chim. Act.* **2006**, *359*, 1899; Hortholary, C.; Coudret, C. *J. Org. Chem.* **2003**, *68*, 2167.
- (10) Brust, M.; Walker, M.; Bethell, D.; Schiffrin, D. J.; Whyman, R. J. *J. Chem. Soc., Chem. Commun.* **1994**, *5*, 801.
- (11) Rucareanu, S.; Gandubert, V. J.; Lennox, R. B. *Chem. Mater.* **2006**, *18*, 4674.
- (12) Tour, J.; Jones, L.; Pearson, D.; Lamba, J.; Burgin, T.; Whitesides, G.; Allara, D.; Parikh, A.; Atre, S. *J. Am. Chem. Soc.* **1995**, *117*, 9529.
- (13) Hostetler, M. J.; Templeton, A. C.; Murray, R. W. *Langmuir* **1999**, *15*, 3782; Montalti, M.; Prodi, L.; Zaccheroni, N.; Baxter, R.; Teobaldi, G.; Zerbetto, F. *Langmuir* **2003**, *19*(12), 5172.

Chapter IV

- (1) Nam, K. T.; Kim, D. W.; Yoo, P. J.; Chiang, C. Y.; Meethong, N.; Hammond, P. T.; Chiang, Y. M.; Belcher, A. M. *Science* **2006**, *312*, 885.
- (2) Pender, M.; Sowards, L.; Hartgerink, J.; Stone, M.; Naik, R. *Nano Lett* **2006**, *6*, 40.
- (3) Ball, P. *Nanotechnology* **2005**, *16*, R1.

- (4) Anastas, P. T.; Warner, J. C. *Green Chemistry Theory and Practice*; Oxford University Press: Oxford, **1998**.
- (5) Bauerlein, E. *Angew. Chem., Int. Ed.* **2003**, *42*, 614.
- (6) Mann, S. *Biomaterialization: Principles and Concepts in Bioinorganic Materials Chemistry*; Oxford University Press: Oxford, New York, **2001**.
- (7) Young, J. R.; Davis, S. A.; Bown, P. R.; Mann, S. *Journal of Structural Biology* **1999**, *126*, 195.
- (8) Gardea-Torresdey, J. L.; Parsons, J. G.; Gomez, E.; Peralta-Videa, J.; Troiani, H. E.; Santiago, P.; Yacaman, M. J. *Nano Lett.* **2002**, *2*, 397.
- (9) Benyus, J. M. *Biomimicry: Innovation Inspired by Nature*, 1st ed.; Morrow: New York, **1997**.
- (10) Dahl, J.; Maddux, B.; Hutchison, J. *Chem. Rev.* **2007**, *107*, 2228; McKenzie, L. C.; Hutchison, J. E. *Chimica Oggi-Chemistry Today* **2004**, *22*, 30.
- (11) Smith, G. P.; Petrenko, V. A. *Chem. Rev.* **1997**, *97*, 391.
- (12) Ellington, A. D.; Szostak, J. W. *Nature* **1990**, *346*, 818-822; Tuerk, C.; Gold, L. *Science* **1990**, *249*, 505.
- (13) Conrad, R. C.; Bruck, F. M.; Bell, S.; Ellington, A. D. in *RNA:Protein Interactions, A Practical Approach*; Smith, C. W. J., Ed. **1998**, 285.
- (14) Bowser, M. T. *Analyst* **2005**, *130*, 128.
- (15) Jenison, R. D.; Gill, S. C.; Pardi, A.; Polisky, B. *Science* **1994**, *263*, 1425.
- (16) Minunni, M.; Tombelli, S.; Gullotto, A.; Luzi, E.; Mascini, M. *Biosens. Bioelectron.* **2004**, *20*, 1149-1156; Radi, A. E.; Sanchez, J. L. A.; Baldrich, E.; O'Sullivan, C. K. *J. Am. Chem. Soc.* **2006**, *128*, 117.
- (17) Tarasow, T. M.; Tarasow, S. L.; Eaton, B. E. *Nature* **1997**, *389*, 54; Tarasow, T. M.; Tarasow, S. L.; Eaton, B. E. *J. Am. Chem. Soc.* **2000**, *122*, 1015.
- (18) Gugliotti, L. A.; Feldheim, D. L.; Eaton, B. E. *Science* **2004**, *304*, 850.

- (19) Liu, D. G.; Gugliotti, L. A.; Wu, T.; Dolska, M.; Tkachenko, A. G.; Shipton, M. K.; Eaton, B. E.; Feldheim, D. L. *Langmuir* **2006**, *22*, 5862.
- (20) Slocik, J. M.; Naik, R. R.; Stone, M. O.; Wright, D. W. *J. Mat. Chem.* **2005**, *15*, 749; Slocik, J. M.; Wright, D. W. *Biomacromolecules* **2003**, *4*, 1135; Tomczak, M. M.; Glawe, D. D.; Drummy, L. F.; Lawrence, C. G.; Stone, M. O.; Perry, C. C.; Pochan, D. J.; Deming, T. J.; Naik, R. R. *J. Am. Chem. Soc.* **2005**, *127*, 12577.
- (21) Slocik, J. M.; Stone, M. O.; Naik, R. R. *Small* **2005**, *1*, 1048.
- (22) Tamerler, C.; Duman, M.; Oren, E. E.; Gungormus, M.; Xiong, X. R.; Kacar, T.; Parviz, B. A.; Sarikaya, M. *Small* **2006**, *2*, 1372.
- (23) Smith, G. P.; Petrenko, V. A. *Chem. Rev.* **1997**, *97*, 391.
- (24) Jana, N. R.; Gearheart, L.; Murphy, C. J. *J. Phys. Chem. B* **2001**, *105*, 4065; Johnson, C. J.; Dujardin, E.; Davis, S. A.; Murphy, C. J.; Mann, S. *J. Mat. Chem.* **2002**, *12*, 1765.
- (25) Whaley, S. R.; English, D. S.; Hu, E. L.; Barbara, P. F.; Belcher, A. M. *Nature* **2000**, *405*, 665.
- (26) Zuo, R. J.; Ornek, D.; Wood, T. K. *Appl. Microbiol. and Biotechnol.* **2005**, *68*, 505.
- (27) Naik, R. R.; Jones, S. E.; Murray, C. J.; McAuliffe, J. C.; Vaia, R. A.; Stone, M. O. *Adv. Funct. Mater.* **2004**, *14*, 25.
- (28) Gupta, A.; Oppenheim, A. B.; Chaudhary, V. K. In *Phages: Their Role in Bacterial Pathogenesis and Biotechnology*; Waldor, M. K., Friedman, D. I., Adhya, S. L., Eds.; ASM Press: Washington, D.C., **2005**.
- (29) Golden, M. C.; Collins, B. D.; Willis, M. C.; Koch, T. H. *J. Biotechnol.* **2000**, *81*, 167.
- (30) Sandman, K.; Benner, J.; Noren, C. *J. Am. Chem. Soc.* **2000**, *122*, 960.
- (31) Tian, F.; Tsao, M.; Schultz, P. *J Am Chem Soc* **2004**, *126*, 15962.
- (32) Bugaut, A.; Toulme, J. J.; Rayner, B. *Org. Biomol. Chem.* **2006**, *4*, 4082; Bugaut, A.; Toulme, J. J.; Rayner, B. *Angew. Chem., Int. Ed.* **2004**, *43*, 3144; Bugaut, A.; Bathany, K.; Schmitter, J. M.; Rayner, B. *Tet. Lett.* **2005**, *46*, 687.

- (33) Zuker, M. *Nucleic Acids Res.* **2003**, *31*, 3406.
- (34) Braun, R.; Sarikaya, M.; Schulten, K. *J. Biomater. Sci., Polym. Ed.* **2002**, *13*, 747.
- (35) Peelle, B. R.; Krauland, E. M.; Wittrup, K. D.; Belcher, A. M. *Langmuir* **2005**, *21*, 6929.
- (36) Tamerler, C.; Oren, E. E.; Duman, M.; Venkatasubramanian, E.; Sarikaya, M. *Langmuir* **2006**, *22*, 7712.
- (37) Brown, S. *Nat. Biotechnol.* **1997**, *15*, 269.
- (38) Naik, R. R.; Stringer, S. J.; Agarwal, G.; Jones, S. E.; Stone, M. O. *Nat. Mater.* **2002**, *1*, 169.
- (39) Thai, C. K.; Dai, H. X.; Sastry, M. S. R.; Sarikaya, M.; Schwartz, D. T.; Baneyx, F. *Biotech. Bioeng.* **2004**, *87*, 129.
- (40) Nygaard, S.; Wendelbo, R.; Brown, S. *Adv. Mater.* **2002**, *14*, 1853.
- (41) Serizawa, T.; Sawada, T.; Matsuno, H.; Matsubara, T.; Sato, T. *J. Am. Chem. Soc.* **2005**, *127*, 13780.
- (42) Shiba, K. *J. Drug Targeting* **2006**, *14*, 512-518; Kase, D.; Kulp, J. L.; Yudasaka, M.; Evans, J. S.; Iijima, S.; Shiba, K. *Langmuir* **2004**, *20*, 8939.
- (43) Calendar, R.; Inman, R. In *Phages: Their Role in Bacterial Pathogenesis and Biotechnology*; Waldor, M. K., Friedman, D. I., Adhya, S. L., Eds.; ASM Press: Washington, D.C., **2005**.
- (44) Brown, S. *Proc. Natl. Acad. Sci. U. S. A.* **1992**, *89*, 8651.
- (45) Brown, S.; Mehmet, S.; Johnson, E. *J. Mol. Biol.* **2000**, *299*, 725.
- (46) Schnirman, A. A.; Zahavi, E.; Yeger, H.; Rosenfeld, R.; Benhar, I.; Reiter, Y.; Sivan, U. *Nano Lett.* **2006**, *6*, 1870.
- (47) Slocik, J. M.; Naik, R. R.; Stone, M. O.; Wright, D. W. *J. Mat. Chem.* **2005**, *15*, 749.

- (48) Legiewicz, M.; Lozupone, C.; Knight, R.; Yarus, M. *RNA* **2005**, *11*, 1701.
- (49) Gugliotti, L. A.; Feldheim, D. L.; Eaton, B. E. *J. Am. Chem. Soc.* **2005**, *127*, 17814.

Chapter V

- (1) Farokhzad, O.; Cheng, J.; Teply, B.; Sherifi, I.; Jon, S.; Kantoff, P.; Richie, J.; Langer, R. *Proc Natl Acad Sci USA* **2006**, *103*, 6315.
- (2) Guo, K.; Wendel, H. P.; Scheideler, L.; Ziemer, G.; Scheule, A. M. *Journal of Cellular and Molecular Medicine* **2005**, *9*, 731.
- (3) Pavlov, V.; Xiao, Y.; Shlyahovsky, B.; Willner, I. *J. Am. Chem. Soc.* **2004**, *126*, 11768-11769; Radi, A. E.; Sanchez, J. L. A.; Baldrich, E.; O'Sullivan, C. K. *J. Am. Chem. Soc.* **2006**, *128*, 117.
- (4) Slocik, J. M.; Naik, R. R.; Stone, M. O.; Wright, D. W. *J. Mat. Chem.* **2005**, *15*, 749.
- (5) Slocik, J. M.; Stone, M. O.; Naik, R. R. *Small* **2005**, *1*, 1048.
- (6) Flynn, C. E.; Lee, S. W.; Peelle, B. R.; Belcher, A. M. *Acta Mater.* **2003**, *51*, 5867-5880; Flynn, C. E.; Mao, C. B.; Hayhurst, A.; Williams, J. L.; Georgiou, G.; Iverson, B.; Belcher, A. M. *J. Mat. Chem.* **2003**, *13*, 2414.
- (7) Dahl, J.; Maddux, B.; Hutchison, J. *Chem. Rev.* **2007**, *107*, 2228-69; McKenzie, L. C.; Hutchison, J. E. *Chimica Oggi-Chemistry Today* **2004**, *22*, 30.
- (8) Schnirman, A. A.; Zahavi, E.; Yeger, H.; Rosenfeld, R.; Benhar, I.; Reiter, Y.; Sivan, U. *Nano Lett.* **2006**, *6*, 1870.
- (9) Whaley, S. R.; English, D. S.; Hu, E. L.; Barbara, P. F.; Belcher, A. M. *Nature* **2000**, *405*, 665.
- (10) Bauerlein, E. *Angew. Chem., Int. Ed.* **2003**, *42*, 614.
- (11) Naik, R. R.; Stringer, S. J.; Agarwal, G.; Jones, S. E.; Stone, M. O. *Nat. Mater.* **2002**, *1*, 169.
- (12) Serizawa, T.; Sawada, T.; Matsuno, H.; Matsubara, T.; Sato, T. *J. Am. Chem. Soc.* **2005**, *127*, 13780.

- (13) Shiba, K. *J. Drug Targeting* **2006**, *14*, 512; Wang, S. Q.; Humphreys, E. S.; Chung, S. Y.; Delduco, D. F.; Lustig, S. R.; Wang, H.; Parker, K. N.; Rizzo, N. W.; Subramoney, S.; Chiang, Y. M.; Jagota, A. *Nat. Mater.* **2003**, *2*, 196.
- (14) Ahmad, G.; Dickerson, M. B.; Church, B. C.; Cai, Y.; Jones, S. E.; Naik, R. R.; King, J. S.; Summers, C. J.; Kroger, N.; Sandhage, K. H. *Adv. Mater.* **2006**, *18*, 1759; Dickerson, M. B.; Naik, R. R.; Stone, M. O.; Cai, Y.; Sandhage, K. H. *Chem. Comm.* **2004**, 1776; Slocik, J. M.; Naik, R. R.; Stone, M. O.; Wright, D. W. *J. Mat. Chem.* **2005**, *15*, 749.
- (15) Sengle, G.; Eisenfuhr, A.; Arora, P. S.; Nowick, J. S.; Famulok, M. *Chem. Biol.* **2001**, *8*, 459-473; Tarasow, T. M.; Tarasow, S. L.; Eaton, B. E. *Nature* **1997**, *389*, 54-57; Tarasow, T. M.; Tarasow, S. L.; Eaton, B. E. *J. Am. Chem. Soc.* **2000**, *122*, 1015.
- (16) Bloomfield, V. A.; Crothers, D. M.; Tinoco, I. *Nucleic Acids: Structures, Properties and Functions*, University Science Books, Sausalito, CA (USA), **2000**.
- (17) Gugliotti, L. A.; Feldheim, D. L.; Eaton, B. E. *Science* **2004**, *304*, 850.
- (18) Liu, D. G.; Gugliotti, L. A.; Wu, T.; Dolska, M.; Tkachenko, A. G.; Shipton, M. K.; Eaton, B. E.; Feldheim, D. L. *Langmuir* **2006**, *22*, 5862.
- (19) Kumar, A.; Jakhmola, A. *Langmuir* **2007**, *23*, 2915-8; Ma, N.; Dooley, C. J.; Kelley, S. O. *J. Am. Chem. Soc.* **2006**, *128*, 12598.
- (20) Ellington, A. D.; Szostak, J. W. *Nature* **1990**, *346*, 818; Tuerk, C.; Gold, L. *Science* **1990**, *249*, 505.
- (21) Kimura-Suda, H.; Petrovykh, D. Y.; Tarlov, M. J.; Whitman, L. J. *J. Am. Chem. Soc.* **2003**, *125*, 9014.
- (22) Bailey, T. L.; Elkan, C. In *Proceedings of the Second International Conference on Intelligent Systems for Molecular Biology*; Altman, R. B., Brutlag, D. L., Karp, P. D., Lathrop, R. H., Searls, D. B., Eds.; AAAI Press: Menlo Park, CA (USA), **1994**, 28.
- (23) Khvorova, A.; Kwak, Y.; Tamkun, M.; Majerfeld, I.; Yarus, M. *Proc. Natl. Acad. Sci. U. S. A.* **1999**, *96*, 10649.

- (24) Zuker, M. *Nucleic Acids Res.* **2003**, *31*, 3406.
- (25) Giese, B.; McNaughton, D. *J. Phys. Chem. B* **2002**, *106*, 101.
- (26) Martins, A.; Queiros, A.; Silva, F. *Chemphyschem* **2005**, *6*, 1056.
- (27) Conrad, R. C.; Bruck, F. M.; Bell, S.; Ellington, A. D. In *RNA:Protein Interactions, A Practical Approach*; Smith, C. W. J., Ed. **1998**, 285.
- (28) Garrey, S. M.; Voelker, R.; Berglund, J. A. *J. Biol. Chem.* **2006**, *281*, 27443.
- (29) Thompson, J. D.; Higgins, D. G.; Gibson, T. J. *Nucleic Acids Res.* **1994**, *22*, 4673.

Chapter VI

- (1) Perez-Juste, J.; Pastoriza-Santos, I.; Liz-Marzan, L. M.; Mulvaney, P. *Coord. Chem. Rev.* **2005**, *249*, 1870.
- (2) Wang, H. F.; Huff, T. B.; Zweifel, D. A.; He, W.; Low, P. S.; Wei, A.; Cheng, J. X. *Roc. Natl. Acad. Sci. U. S. A.* **2005**, *102*, 15752.
- (3) Suzuki, M.; Nakajima, K.; Kimura, K.; Fukuoka, T.; Mori, Y. *Anal. Sci.* **2007**, *23*, 829.
- (4) Jana, N. R.; Gearheart, L.; Murphy, C. J. *J. Phys. Chem. B* **2001**, *105*, 4065.
- (5) Perez-Juste, J.; Liz-Marzan, L. M.; Carnie, S.; Chan, D. Y. C.; Mulvaney, P. *Adv. Funct. Mater.* **2004**, *14*, 571-579.
- (6) J. E. Millstone, G. S. M., C. A. Mirkin, *Adv. Funct. Mater.* **2006**, *16*, 1209.
- (7) Kim, F.; Connor, S.; Song, H.; Kuykendall, T.; Yang, P. D. *Angew. Chem., Int. Ed.* **2004**, *43*, 3673.
- (8) Huang, C. J.; Chiu, P. H.; Wang, Y. H.; Chen, W. R.; Meen, T. H. *J. Electrochem. Soc.* **2006**, *153*, D129.
- (9) Hao, F.; Nehl, C. L.; Hafner, J. H.; Nordlander, P. *Nano Lett.* **2007**, *7*, 729.
- (10) Chang, S. S.; Shih, C. W.; Chen, C. D.; Lai, W. C.; Wang, C. R. *Langmuir* **1999**, *15*, 701.

- (11) Foss, C. A.; Hornyak, G. K.; Stockert, J. A.; Stockert, C. R. *Adv. Mater.* **1993**, *5*, 135.
- (12) Johnson, C. J.; Dujardin, E.; Davis, S. A.; Murphy, C. J.; Mann, S. *J. Mat. Chem.* **2002**, *12*, 1765; Wei, Z. Q.; Mieszawska, A. J.; Zamborini, F. P. *Langmuir* **2004**, *20*, 4322-4326; Wei, Z. Q.; Zamborini, F. P. *Langmuir* **2004**, *20*, 11301.
- (13) Naik, R. R.; Stringer, S. J.; Agarwal, G.; Jones, S. E.; Stone, M. O. *Nat. Mater.* **2002**, *1*, 169.
- (14) Slocik, J. M.; Stone, M. O.; Naik, R. R. *Small* **2005**, *1*, 1048.
- (15) Gugliotti, L. A.; Feldheim, D. L.; Eaton, B. E. *Science* **2004**, *304*, 850.
- (16) Liu, D. G.; Gugliotti, L. A.; Wu, T.; Dolska, M.; Tkachenko, A. G.; Shipton, M. K.; Eaton, B. E.; Feldheim, D. L. *Langmuir* **2006**, *22*, 5862.
- (17) Bauerlein, E. *Angew. Chem., Int. Ed.* **2003**, *42*, 614.
- (18) Smith, G. P.; Petrenko, V. A. *Chem. Rev.* **1997**, *97*, 391.
- (19) Ellington, A. D.; Szostak, J. W. *Nature* **1990**, *346*, 818; Tuerk, C.; Gold, L. *Science* **1990**, *249*, 505.
- (20) Gandubert, V. J.; Lennox, R. B. *Langmuir* **2005**, *21*, 6532.
- (21) Kosiorek, A.; Kandulski, W.; Chudzinski, P.; Kempa, K.; Giersig, M. *Nano Lett.* **2004**, *4*, 1359.
- (22) Brown, S. *Nat. Biotechnol.* **1997**, *15*, 269; Woodbury, R. G.; Wendin, C.; Clendenning, J.; Melendez, J.; Elkind, J.; Bartholomew, D.; Brown, S.; Furlong, C. E. *Biosens. Bioelectr.* **1998**, *13*, 1117; Brown, S.; Mehmet, S.; Johnson, E. *J. Mol. Biol.* **2000**, *299*, 725; Soh, N.; Tokuda, T.; Watanabe, T.; Mishima, K.; Imato, T.; Masadome, T.; Asano, Y.; Okutani, S.; Niwa, O.; Brown, S. *Talanta* **2003**, *60*, 733.

Chapter VII

- (1) Foster, E. W.; Kearns, G. J.; Goto, S.; Hutchison, J. E. *Adv. Mater.* **2005**, *17*, 1542.
- (2) Kearns, G. J.; Foster, E. W.; Hutchison, J. E. *Anal. Chem.* **2006**, *78*, 298.

- (3) Harper, S.; Lee, S.; Miller, J.; Hutchison, J. E.; Tanguay, R. *Manuscript in Preparation*
- (4) Dahl, J.; Maddux, B.; Hutchison, J. *Chem. Rev.* **2007**, *107*, 2228.

Appendix A

- (1) ImageJ is a freely available image analysis program written in Java. ImageJ is available for all popular operating systems and can be obtained from <http://rsb.info.nih.gov/ij/>.
- (2) Woehrle, G. H.; Hutchison, J. E.; Ozkar, S.; Finke, R. G. *Turk. J. Chem.* **2006**, *30*, 1-13.